Surface waves and seismic noise

S. Parolai

UNIVERSITÀ
DEGLI STUDI
DI TRIESTE

Phase velocity

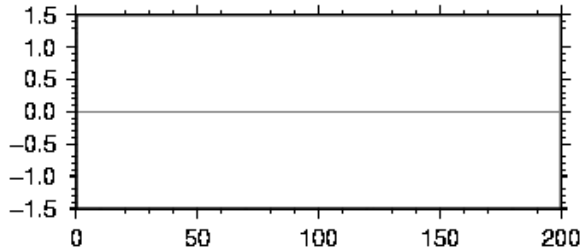

Phase velocity

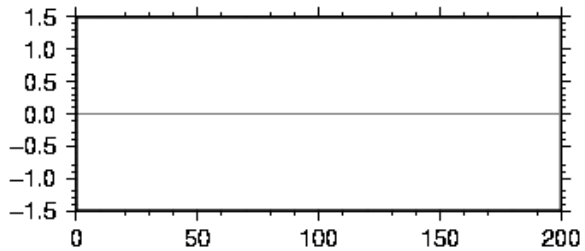

Phase velocity

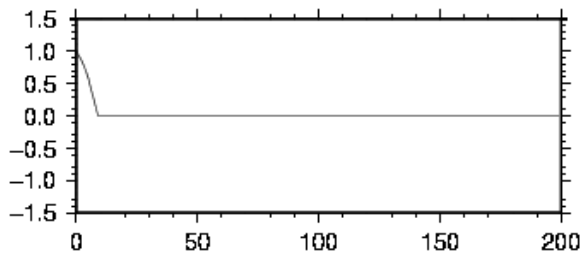

Group velocity

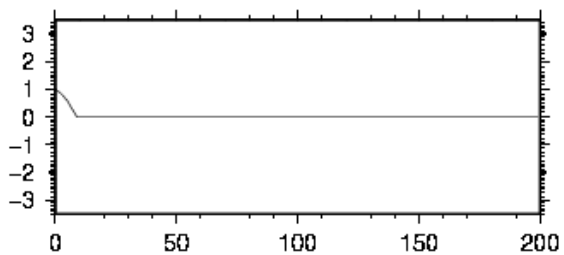

Seismic noise analysis

Single station noise measurements: H/V

Array measurements

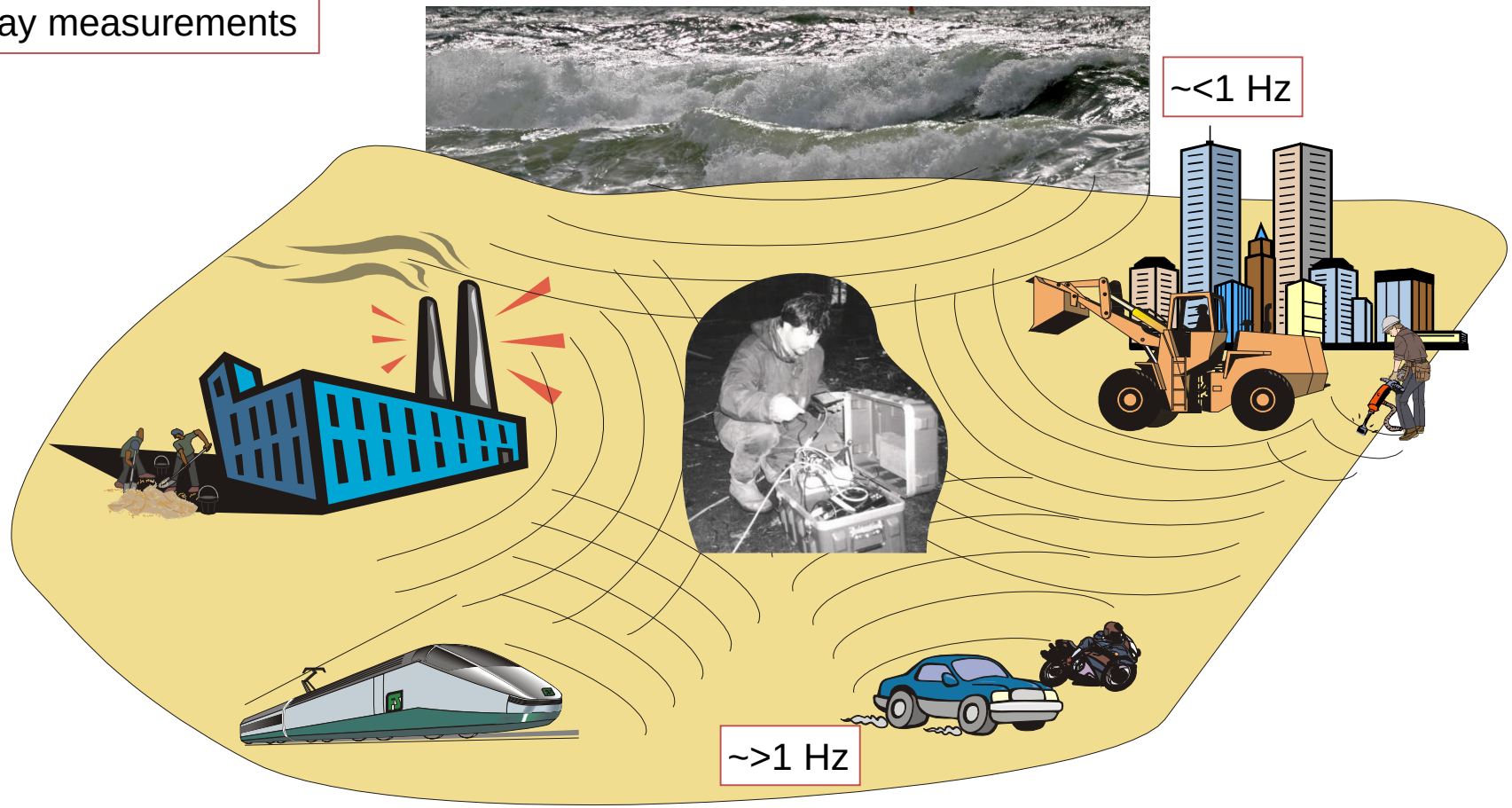

Influence of local geology on seismic ground motion: seismic noise

With seismic noise we mean all the seismic signal that is recorded by the instruments while they are working (passive acquisition)

In the high frequency range (> 1-2 Hz) it is mainly related to human activity (although local meteorological conditions may play a role)

In the low frequency range (<1 Hz) it is mainly dominated by wave generated by tides, water waves striking coast, large scale meteorological conditions)

Power spectral density of 1 year of recording

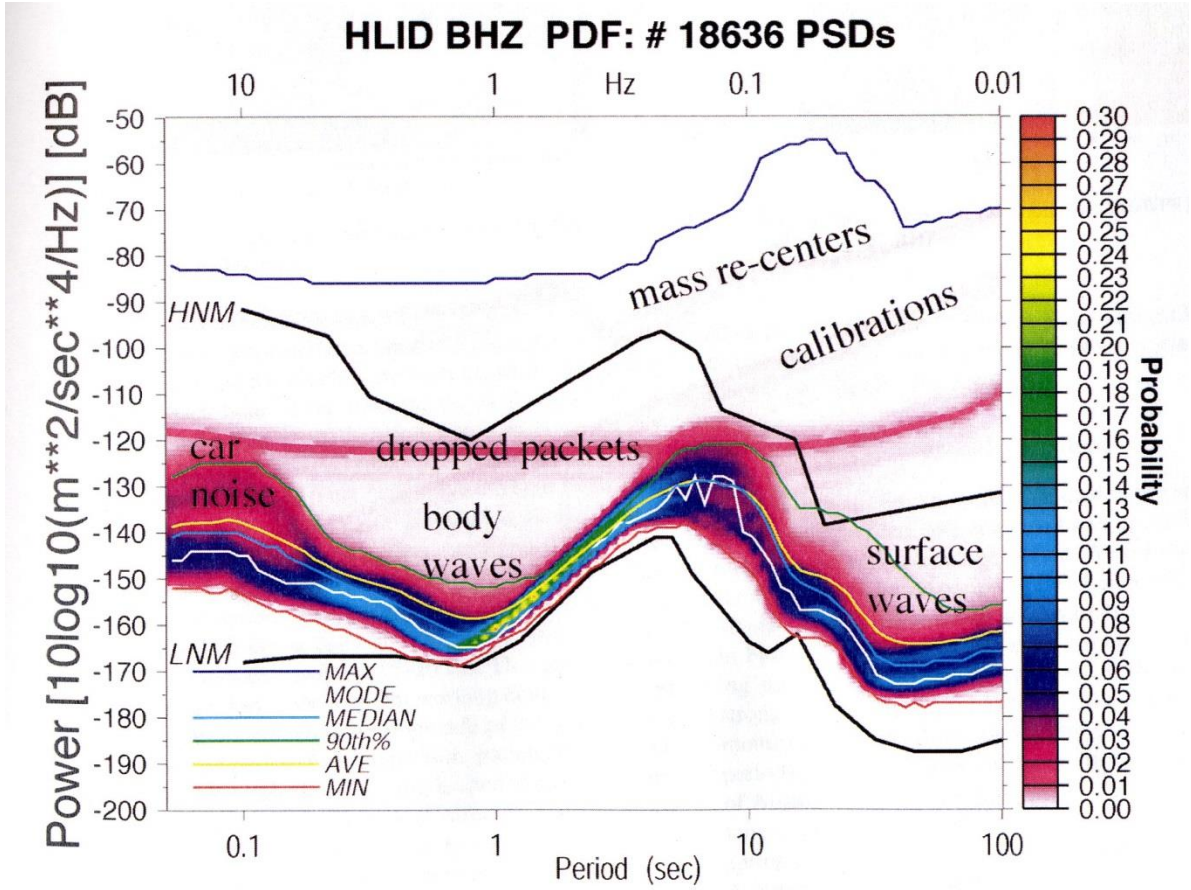

Figure 8. PDF for station HLID BHZ, constructed using 18,636 PSDs during the period from September 2000 to September 2003. Recording system transients and earthquakes are observable in the PDF.

After McNamara and Buland (2004)

Power spectral density: comparison with earthquake data

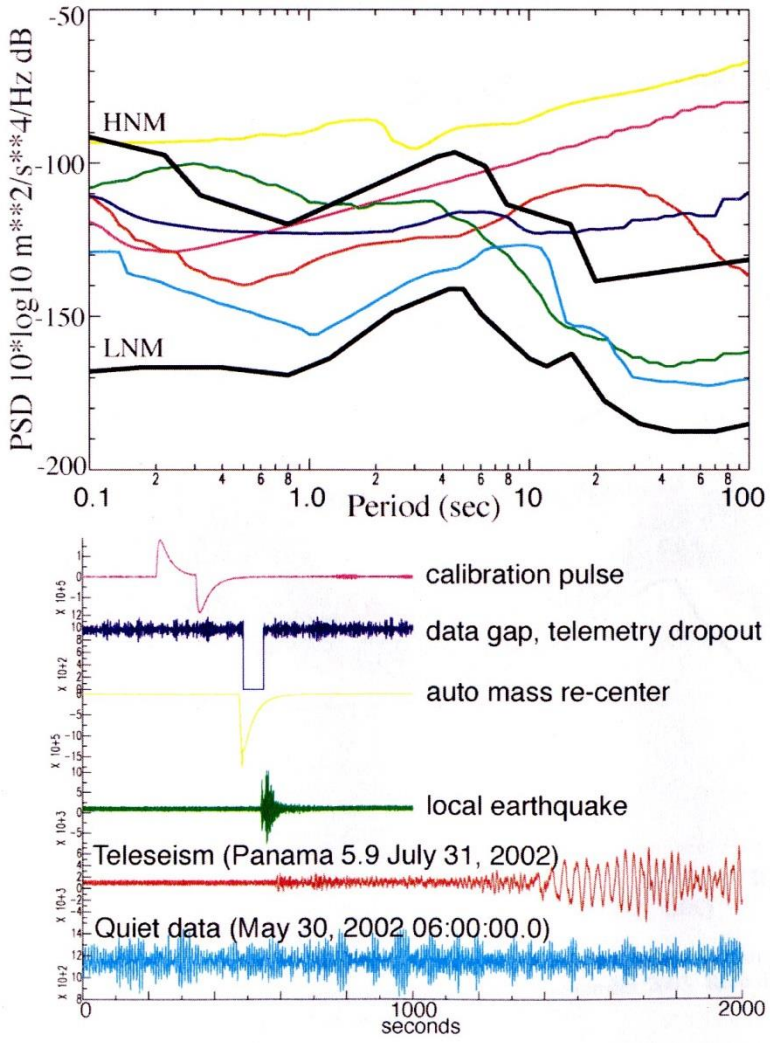

Local and teleseimic events show PDS affecting different frequency bands

After McNamara and Buland (2004)

Power spectral density : spatial variability

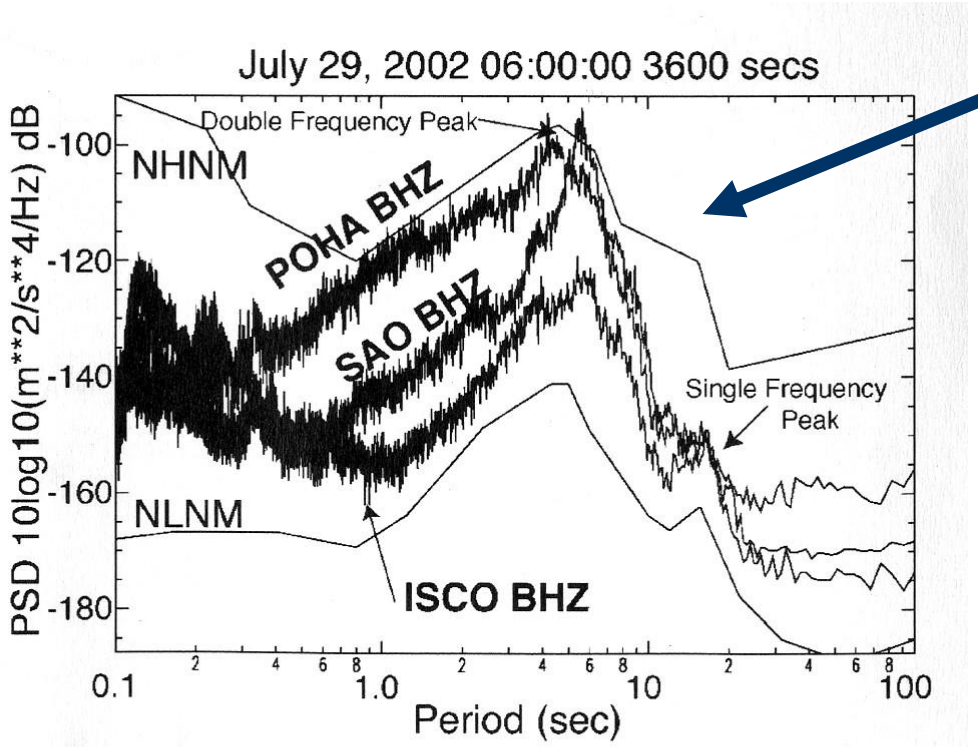

Figure 6. Microseismic noise at island coastal and continental interior sites, 29 May 2002 06:00:00 3600 sec. Island of Hawaii, POHA BHZ, northern California, SAO BHZ, continental interior, Colorado ISCO. Note increasing microseism noise from Colorado to California to Hawaii.

Moving away from the Ocean the spectral amplitudes are strongly reduced (especially between 2 and 10 s)!

After McNamara and Buland (2004)

Power spectral density : influence of human activity

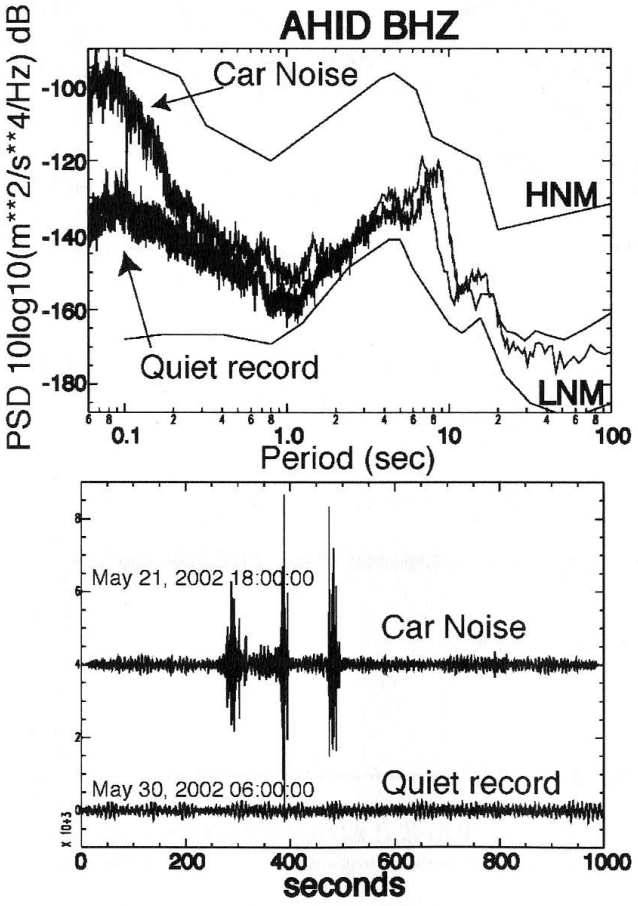

Figure 5. AHID car traffic noise PSD and time series. Car noise record 21 May 2002 18:00:00. Quiet record 30 May 2002 06:00:00. Note the increased power at 5–10 Hz for the car noise record.

Cars are mainly affecting high frequencies (low periods)

After McNamara and Buland (2004)

Power spectral density : influence of human activity

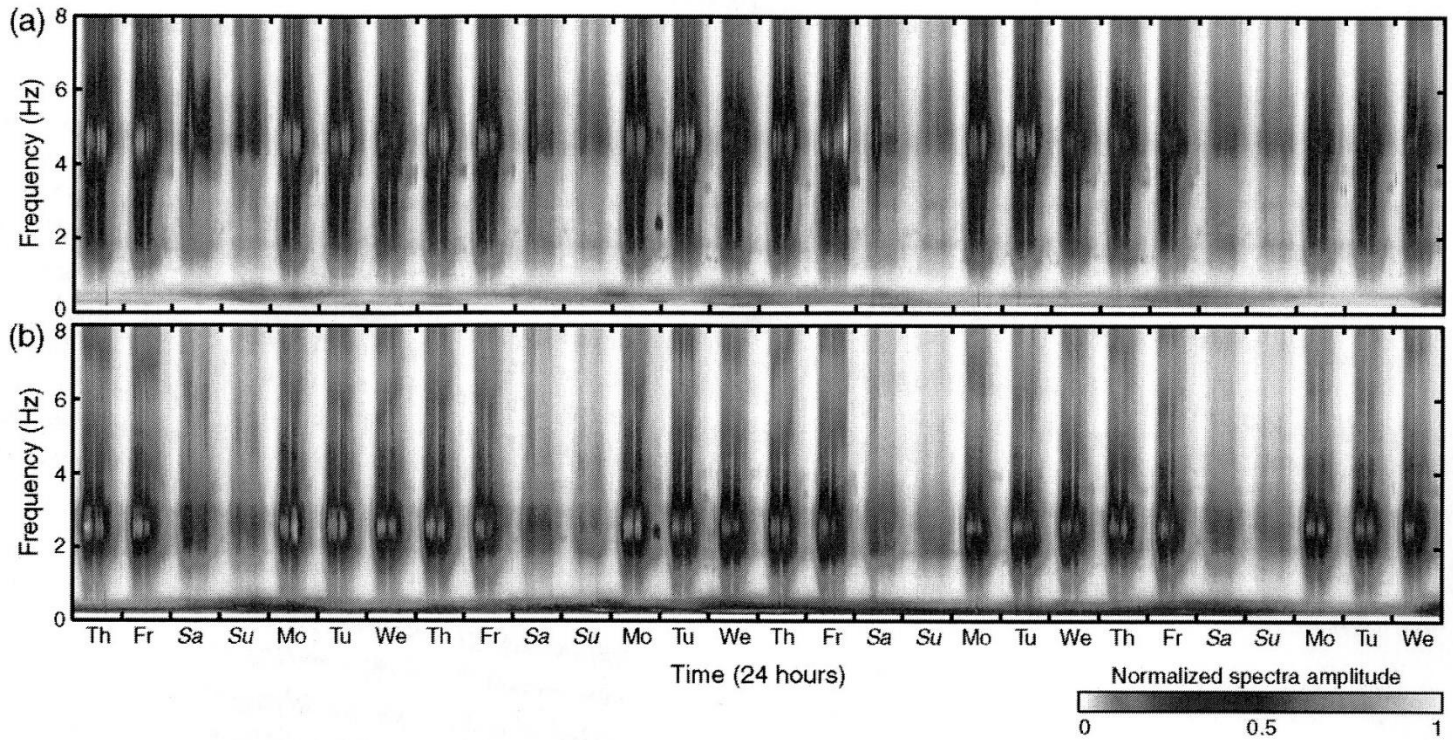

Fig. 4. Normalized Fourier spectra amplitude continuously recorded in urban area (Grenoble, French Alps) from 10.06.2004 midnight to 22.07.2004 midnight, a) vertical component, and b) north-east component. Modified from Bonnefoy-Claudet (2004). At frequency higher than 1 Hz microtremor exhibit clearly daily and weekly variations linked with cultural activities, and at low frequency microseism shows variations over time not linked to cultural activities.

After Bonnefoy-Claudet. (2004)

Power spectral density : influence of human activity

The life-style is clearly mapped into the noise variations!

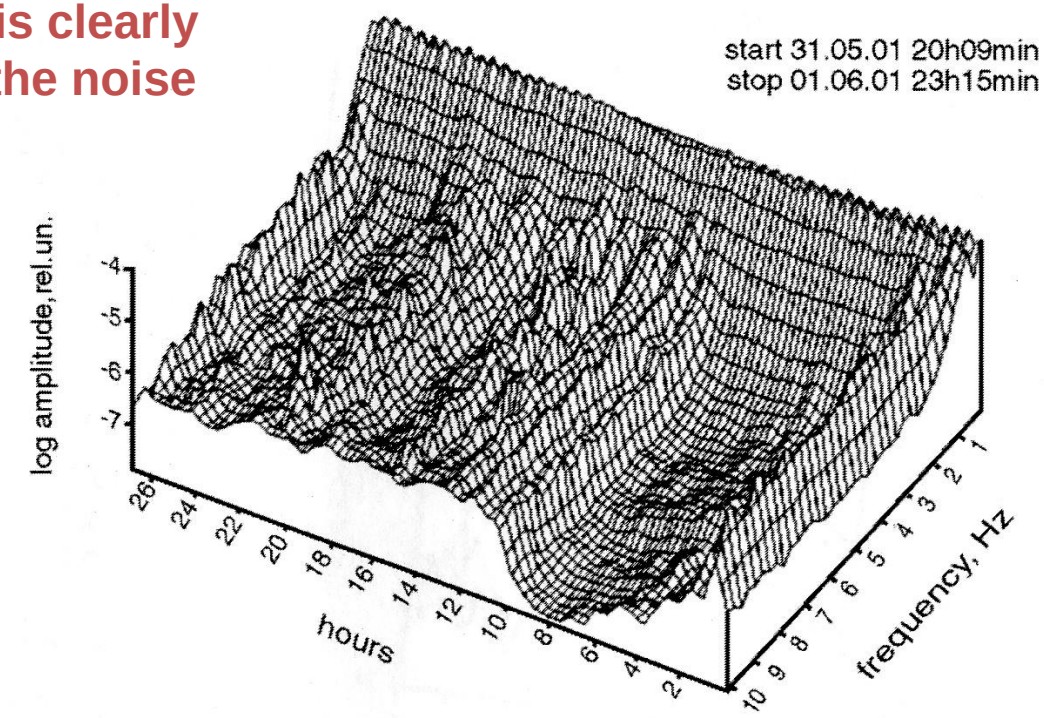

Fig. 5. Continuous seismic noise recorded at Lanzarote island (Canary, Spain). The resulting spectra amplitude are displayed according to frequency (*X* axis) and time (*Y* axis). Experiment started on 31.05.2001 at 20:09 local time and concluded late evening the next day. After Gorbatikov et al. (2004).

After Gorbatikov et al. (2004)

Seismic noise : time variability

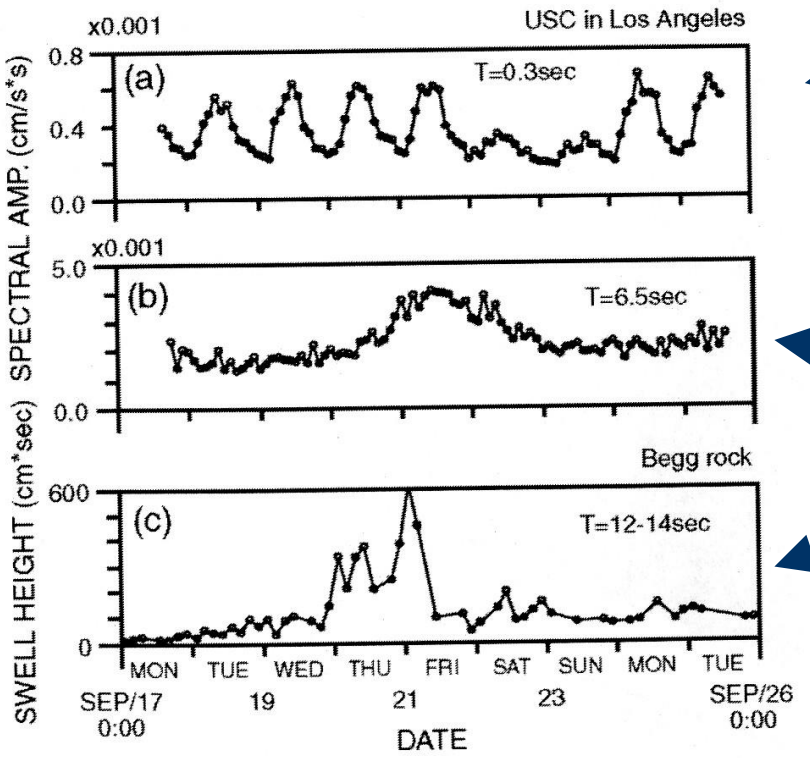

Fig. 3. Fourier spectra amplitude variations of seismic noise (Los Angeles) over time (horizontal components) at (a) 0.3 and (b) 6.5 s. (c) Recordings of swell height variations over time about a hundred kilometers from Los Angeles, after Yamanaka et al. (1993). At 0.3 s a good correlation between microtremor and cultural activities is shown, while at 6.5 s microseism variation is linked to ocean disturbances.

At 0.3 s the variation of seismic noise amplitude correlates well with human activity!

At 6.5 s the variation of seismic noise amplitude correlates well with ocean disturbance!

After Yamanaka et al. (1993)

Influence of local geology on seismic ground motion: seismic noise

Although the source of seismic noise are not yet well known and the composition of the noise wave field is not yet clear (body waves? surface waves? what a percentage? only fundamental or higher modes?)

Seismic noise was found to be a useful tool for site effect investigation.

Horizontal-to-vertical (H/V) spectral ratio or Nakamura method

The method was proposed already in 1971 by Nogoshi and Igarashi.

They showed the relationship between this ratio and the ellipticity of Rayleigh waves.

Since the lowest frequency maximum of the ellipticity coincide with the resonance frequency of a site they use the H/V spectral ratio as an indicator of the underground structure.

Only in 1989 Nakamura made the method popular but he claimed that the H/V spectral ratio was a reliable estimation of the site response!

Horizontal-to-vertical (H/V) spectral ratio or Nakamura method

The Nogoshi interpretation of the method is based on surface waves and was followed by many authors

- H/V is related to ellipticity of Rayleigh waves

- The ellipticity is frequency dependent and exibits a sharp peak around the fundamental frequency of the site when the impedance contrast is high enough. The peak is due to the vanishing of the vertical component, corresponding to a reversal of the rotation sense of the fundamental mode Rayleigh wave.

Horizontal-to-vertical (H/V) spectral ratio or Nakamura method

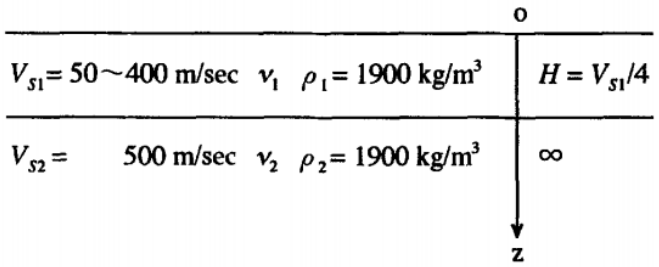

Figure 1. Model of an elastic layer over a half-space. Poisson's ratios, ν, were determined from V_S as follows: $\nu = 0.499$, for $V_S < 150$ m/sec; $\nu = 0.499 - 1.16 \cdot 10^{-4}(V_S - 150)$, for $V_S \geqq 150$ m/sec.

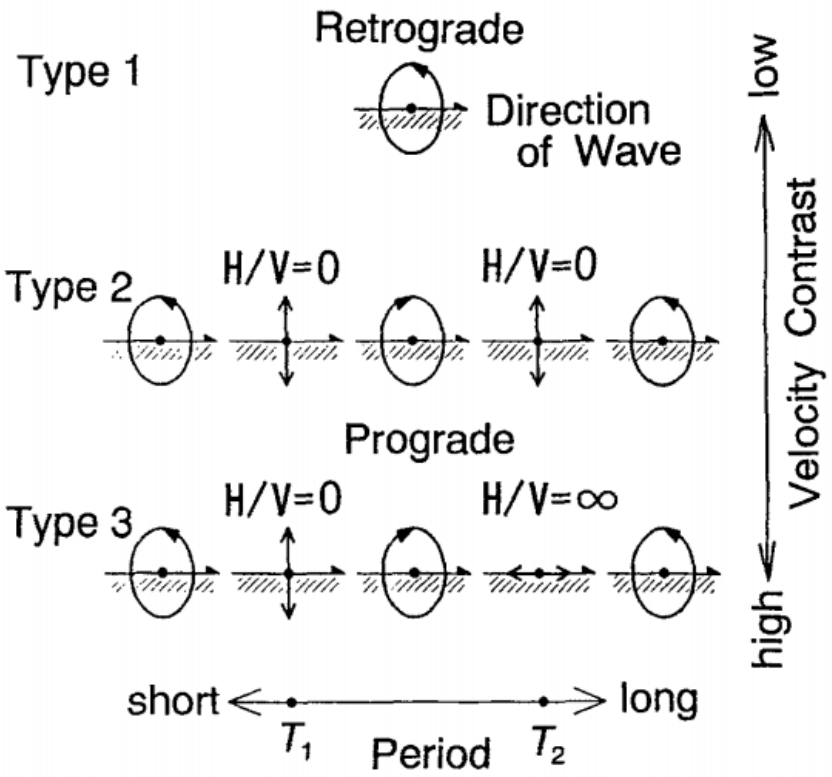

Figure 2. Particle orbit of three types of fundamental-mode Rayleigh waves for the models in Figure 1.

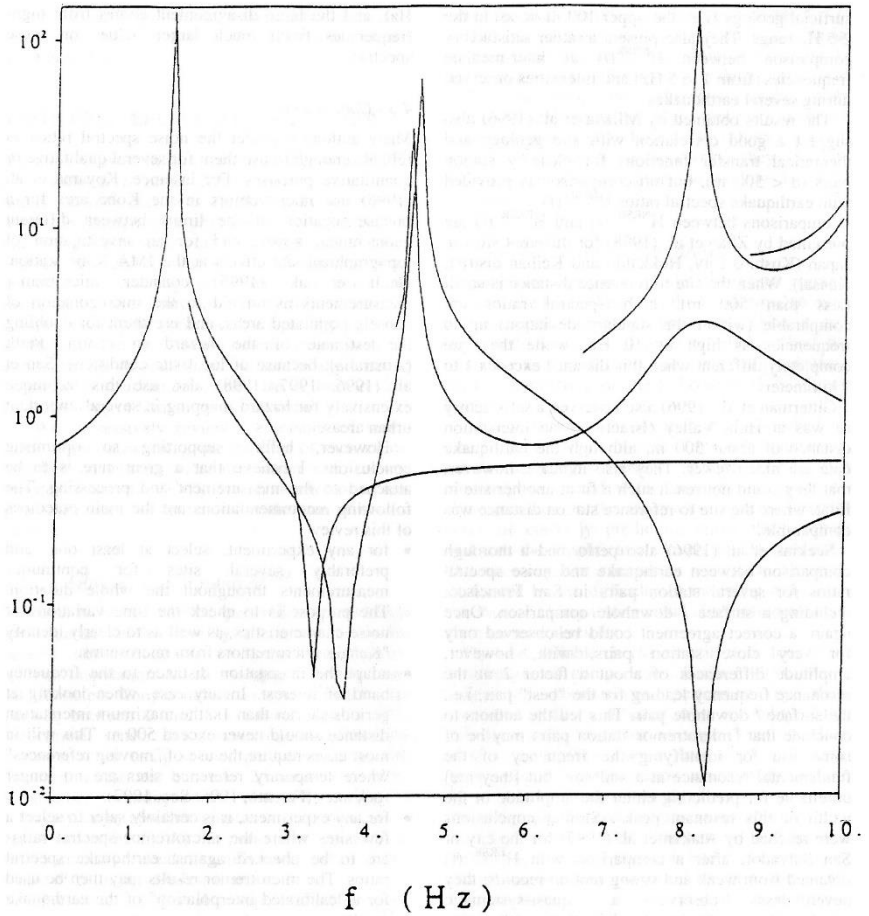

Figure 1 : *An exemple of ellipticity curves for Rayleigh waves in a stratified half-space, displaying the H/V ratio (log scale) as a function of frequency, for the 5 first Rayleigh modes. The infinite peaks correspond to a vanishing of the vertical component, while the sharp troughs correpsond to a vanishing of the horizontal component.*

After Konno and Ohmachi (1998)

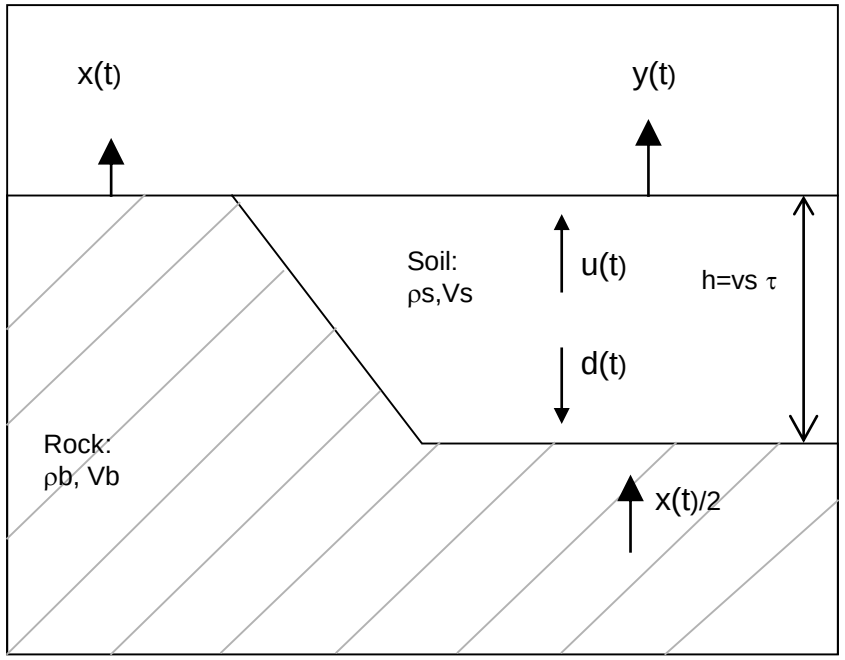

$C=(\rho_b V_v/\rho_s V_s)$ is the impedance contrast

$$r=\frac{pbVb-psVs}{pbVb+psVs}=\frac{c-1}{1+c}$$

$$u(t)=-rd(t-\tau)+(1+r)\frac{x(t-\tau)}{2}$$

$$d(t)=u(t-\tau) \quad y(t)=2u(t)$$

Assuming that the free surface amplification is equal to 2 and eliminating u(t) and d(t) we obtain:

$$y(t)=-ry(t-2\tau)+(1+r)x(t-\tau)$$

Some properties of the Fourier Transform $\mathfrak{I}$

-Linearity: $\mathfrak{I}[a_1 f_1(t) + a_2 f_2(t)] = a_1 \mathfrak{I} f_1(\omega) + a_2 \mathfrak{I} f_2(\omega)$

-Derivative: $\mathfrak{I}[f^{(n)}(t)] = (i\omega)^n \mathfrak{I} f(\omega)$

-Shift: $\mathfrak{I}[f(t-a)] = e^{-i\omega a} \mathfrak{I} f(\omega)$

-Convolution: $\mathfrak{I}[f_1(t) * f_2(t)] = \mathfrak{I} \int_0^t f_1(\tau) f_2(t-\tau) d\tau = \mathfrak{I} f_1(\omega) \mathfrak{I} f_2(\omega)$

Applications: linear system (source*path*site*instrument), time-delay of propagation (e.g. array analysis), solving differential equations, etc…

Parseval identity
(sum of the square values)

$$\| f(t) \|_2 = \| \mathfrak{I} f(\omega) \|_2$$

If X(f) is the Fourier transform of x(t) and Y(f) is the Fourier transform of y(t)

The Fourier transform of $x(t-\tau)$ is $X(f)e^{-i2\pi f\tau}$ and the Fourier transform of $y(t-2\tau)$ is $Y(f)e^{-i4\pi f\tau}$

The time delay τ correspond in the frequency domain to a phase shift $2\pi f\tau$

Multiplying the spectrum for the phasor $e^{-i2\pi f\tau}$ only modifies the phase but not the amplitude of the spectrum in fact:

$$e^{-i2\pi f\tau} = \cos(2\pi f\tau) - i\sin(2\pi f\tau)$$

$$\sqrt{\left(\cos(2\pi f\tau)\right)^2 + \left(\sin(2\pi f\tau)\right)^2} = 1$$

$$\phi(f) = \tan^{-1}\left(\frac{-\sin(2\pi f\tau)}{\cos(2\pi f\tau)}\right)$$

The Fourier trasform of Y(f) is then:

$$Y(f) = -rY(f)e^{-i4\pi f\tau} + (1+r)X(f)e^{-i2\pi f\tau}$$

If we define the transfer function H(f) as Y(f)/X(f) we obtain:

$$H(f) = \frac{(1+r)e^{-i2\pi f\tau}}{1+re^{-i4\pi f\tau}}$$

The modulus of H(f) can be simply calculated by computing the modulus of the numerator and of the denominator

The modulus of the numerator is:

$$\left|(1+r)e^{-i2\pi f\tau}\right| = \left|(1+r)\left(\cos\left(2\pi f\tau\right)-i\sin\left(2\pi f\tau\right)\right)\right| =$$

$$\sqrt{(1+r)^2\left(\left(\cos\left(2\pi f\tau\right)\right)^2+\left(\sin\left(2\pi f\tau\right)\right)^2\right)} = 1+r$$

The modulus of the denominator is:

$$\left|1+re^{-i4\pi f\tau}\right| = \left|\left(1+r\cos\left(4\pi f\tau\right)\right)-ir\sin\left(4\pi f\tau\right)\right| =$$

$$\sqrt{\left(1+r\cos\left(4\pi f\tau\right)\right)^2+\left(r\sin\left(4\pi f\tau\right)\right)^2} =$$

$$\sqrt{1+r^2\cos^2\left(4\pi f\tau\right)+2r\cos\left(4\pi f\tau\right)+r^2\sin^2\left(4\pi f\tau\right)} =$$

$$\sqrt{1+r^2+2r\cos\left(4\pi f\tau\right)}$$

A simple model: site effects due to the seismic impedance contrast

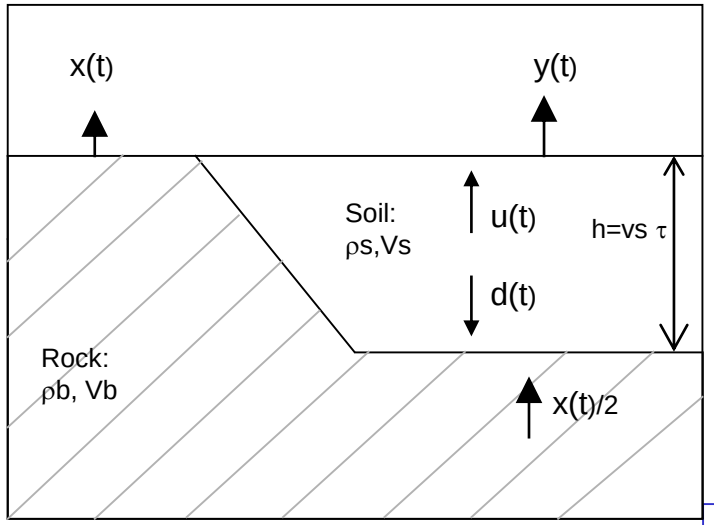

$$|H(f)| = \left(\frac{(1+r)^2}{1+2r\cos(4\pi f \tau)+r^2} \right)^{1/2}$$

$$r = \frac{p_b V_b - p_s V_s}{p_b V_b + p_s V_s} = \frac{c-1}{1+c}$$

$\tau = h/V_s$

f_o=400/(4*100)=1Hz

$C = \left(\frac{2800*1200}{2600*400}\right)$ ~3.23

$|H(f)|$ maximum for f=f_o such that cos(4πfτ)=-1 ➡ $f_o = \frac{1}{4\tau} = \frac{V_s}{4h}$

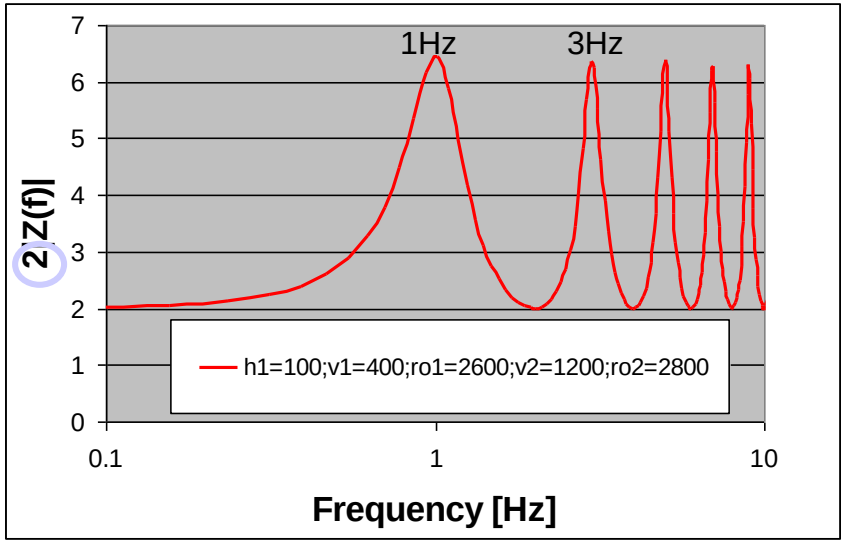

indeed we have a set of maximums at frequencies

$$f_n = \frac{V_s}{4h}(2n+1) \quad \text{with } n = 0,1,2,3,\ldots$$

(n=0 fundamental mode
n>0 higher modes)

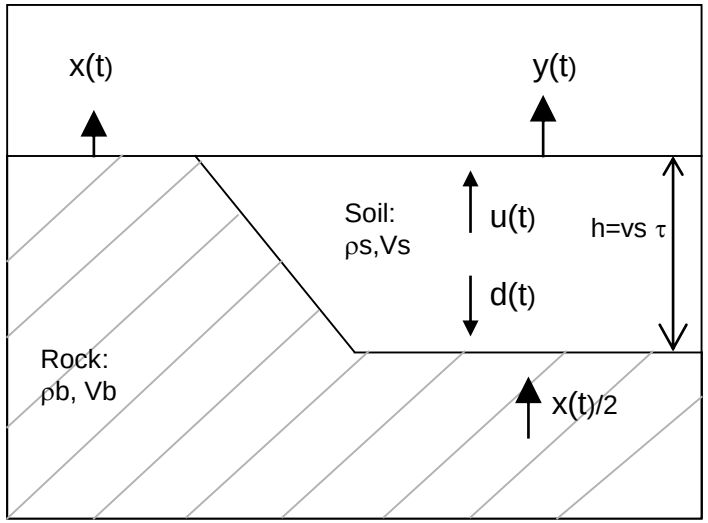

$$|H(f)| = \left(\frac{(1+r)^2}{1+2r\cos(4\pi ft)+r^2} \right)^{1/2}$$

For f=f_n $|H(f)|$ values

f_o=400/(4*100)=1Hz

$$C = \left(\frac{2800*1200}{2600*400}\right) \sim 3.23$$

$$|H(f_n)| = \left(\frac{(1+r)^2}{1-2r+r^2} \right)^{1/2} = \frac{1+r}{1-r} = c$$

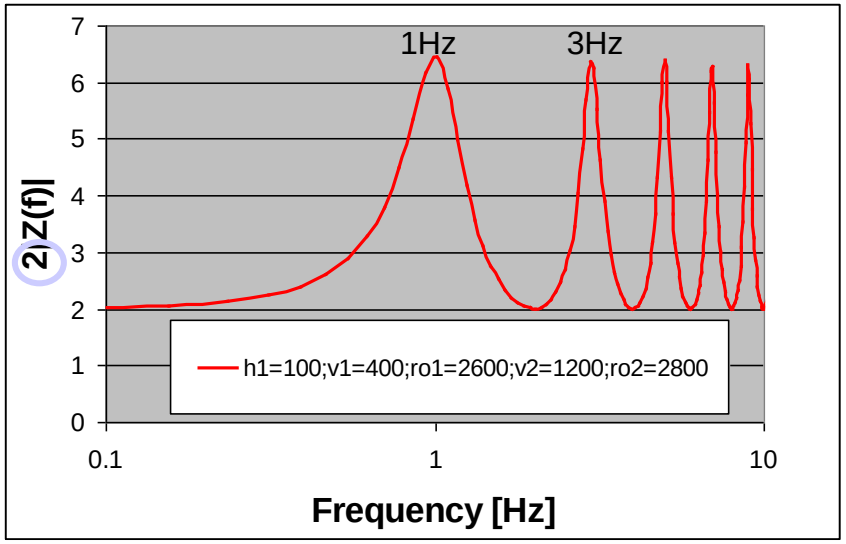

the impedance contrast determines the amplitude of the peaks (elastic layers)

Horizontal-to-vertical (H/V) spectral ratio or Nakamura method

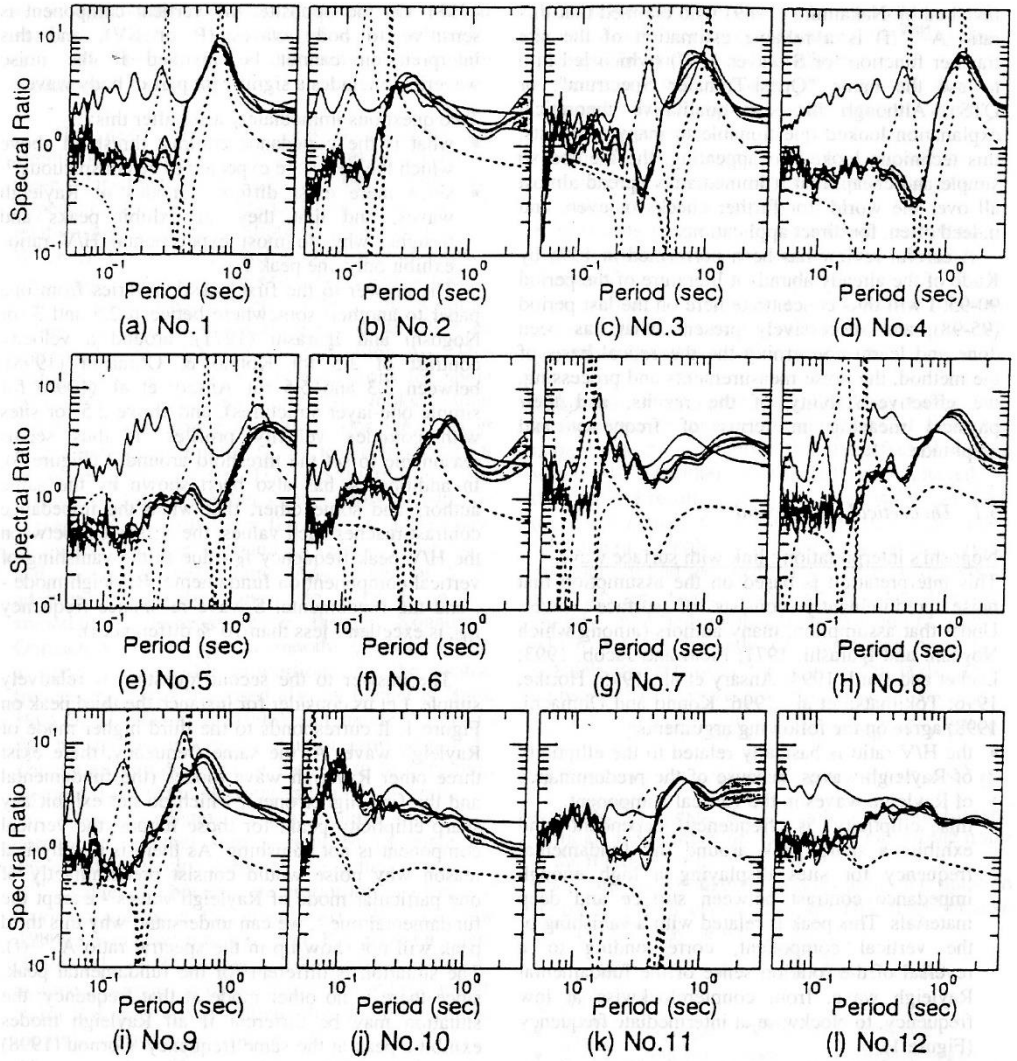

Figure 2 : *Examples of Rayleigh ellipticity curves for a collection of realistic profiles (fundamental mode: thick dotted line; first higer mode: thin dotted line). Also shown are the corresponding transfer functions for S-waves (thin solid line) and observed microtremor H/V ratio (thick solid line ± one standard deviation). Reproduced from Konno & Ohmachi, 1998.*

Good agreement between the lowest frequency peak in the H/V spectral ratio, the theoretical ellipticity and the S-wave transfer function

After Konno and Ohmachi (1998)

Horizontal-to-vertical (H/V) spectral ratio or Nakamura method

-Is the H/V peak a good estimate of site amplification?

Since ellipticity tend to become infinitive for large impedance contrast this might be a shorthcoming.

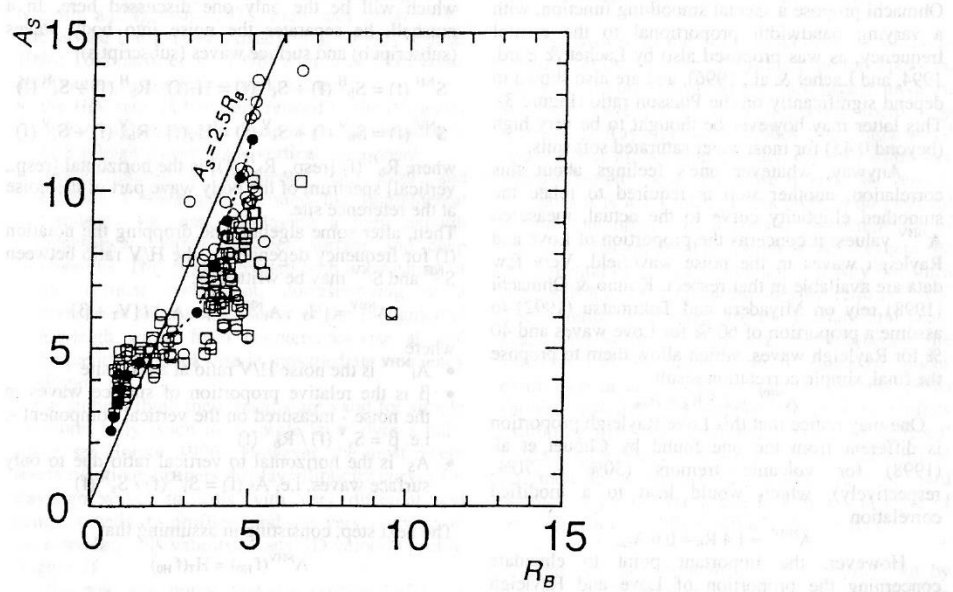

Figure 4 : *Relation between the peak spectral amplification for vertically incident S waves, and the amplitude of the smoothed Rayleigh ellipticity curve (abscissa), as computed for a collection of 85 different velocity profiles. Reproduced from Konno & Ohmachi, 1998.*

After Konno and Ohmachi (1998)

Horizontal-to-vertical (H/V) spectral ratio or Nakamura method

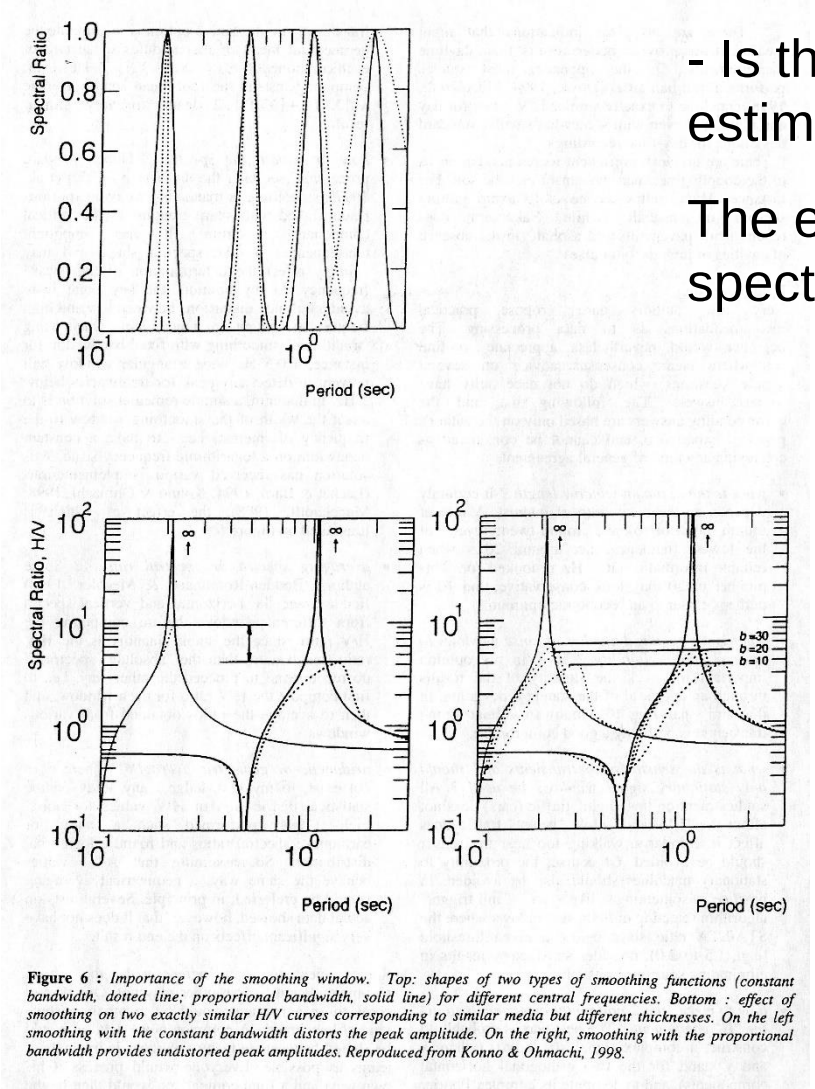

Figure 6 : *Importance of the smoothing window. Top: shapes of two types of smoothing functions (constant bandwidth, dotted line; proportional bandwidth, solid line) for different central frequencies. Bottom : effect of smoothing on two exactly similar H/V curves corresponding to similar media but different thicknesses. On the left smoothing with the constant bandwidth distorts the peak amplitude. On the right, smoothing with the proportional bandwidth provides undistorted peak amplitudes. Reproduced from Konno & Ohmachi, 1998.*

- Is the H/V peak a good estimate of site amplification?

The effect of smoothing the spectra should be considered

After Konno and Ohmachi (1998)

Horizontal-to-vertical (H/V) spectral ratio or Nakamura method

-Are only Rayleigh waves determining the shape of H/V?

The effect of Love wave cannot be neglected but it varies depending on the relative proportion between Rayleigh and Love waves.

Two assumptions are generally made:

The ratio between Love and Rayleigh wave is frequency independent (most of the time the Rayleigh and Love wave contribution are considered identical)

The ratio between vertical and horizontal forces at the noise sources are identical (the ratio betwen Love and Rayleigh wave is frequency dependent)

Horizontal-to-vertical (H/V) spectral ratio or Nakamura method

Nakamura assumes that surface waves are eliminated in the spectral ratio and therefore H/V is related to the S-wave transfer function

Main assumptions are:

1)The vertical component is not amplified at the fundamental resonance frequency

2)The H/V on rock is equal to 1

3) the ratio *b* between surface wave and body waves in the vertical noise wavefield is much smaller than 1

4) The product of *b* and the H/V ratio due only to the surface wave part of the wavefield is much smaller than the true horizontal transfer function

Horizontal-to-vertical (H/V) spectral ratio or Nakamura method

1) and 2) can be easily accepted based on experience

However:

3) is valid only for high impedance contrasts but then 4) cannot be accepted because the ellipticity in these cases tend to infinitive!

Most of seismological community prefers the explanation based on surface waves although the importance of body waves cannot be ruled out (see Parolai et al., 2008)!

Horizontal-to-vertical (H/V) spectral ratio : Northwestern Turkey

Comparison of fundamental resonance frequency estimates carried out by noise H/V, earthquake H/V and GIT

Very good agreement!

Comparison of amplification estimates at the fundamental resonance frequency carried out by noise H/V, earthquake H/V and GIT

Poor consistency!

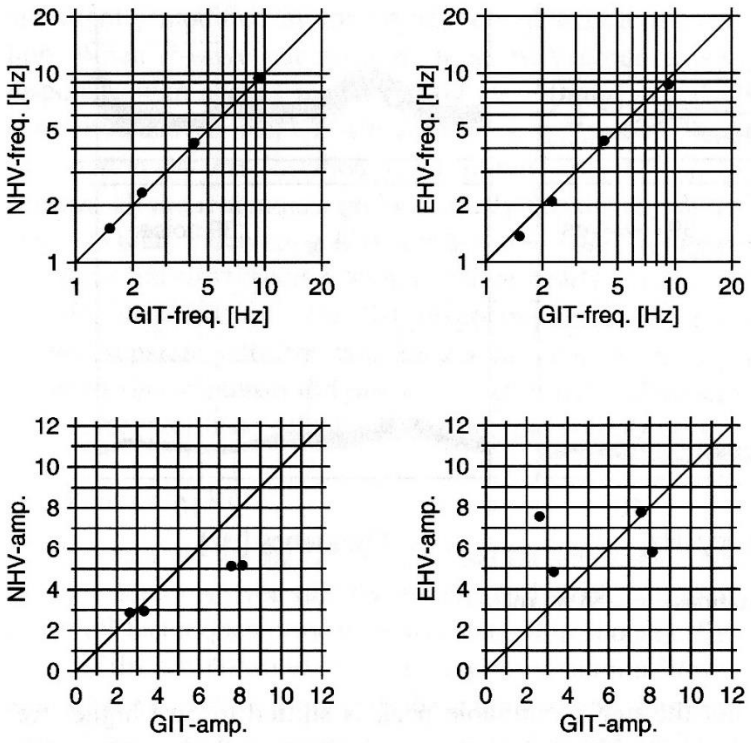

Figure 9. (Top panels) GIT fundamental resonance frequencies versus NHV (left) and EHV (right) resonance frequencies using soil stations. (Bottom panels) Comparisons between the amplification at the fundamental resonance frequency as derived by GIT, NHV (left), and EHV (right).

Horizontal-to-vertical (H/V) spectral ratio or Nakamura method

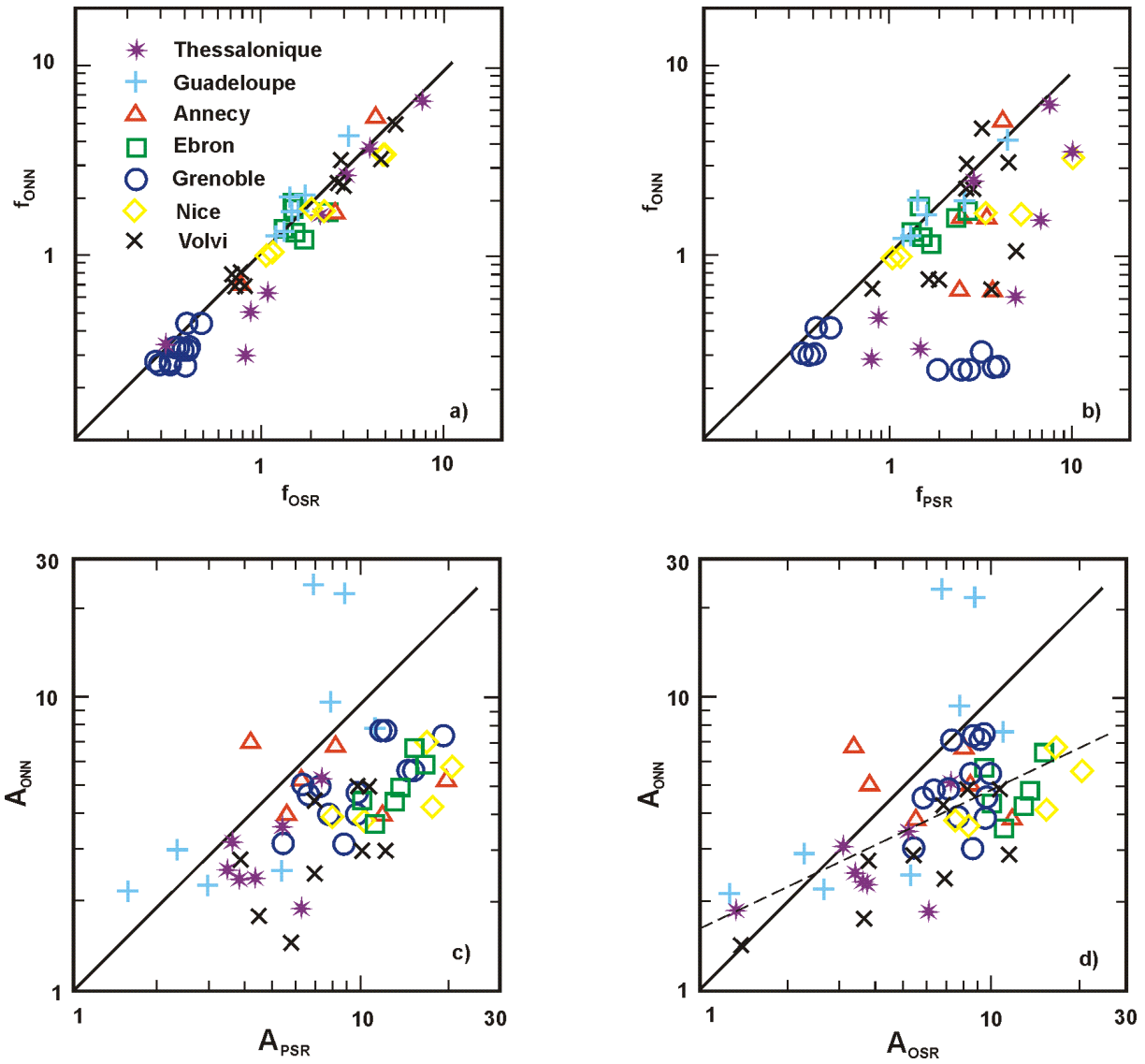

NHV provides a reliable estimate of the fund. freq.

The fund. freq. obtained by NHV is generally lower than the dominant one.

NHV provides a lower bound estimate of the amplification both at the fund. and at the dominant one.

After Duval et al. (2001)

Horizontal-to-vertical (H/V) spectral ratio or Nakamura method

Industrial noise can dominate spectra. In certain cases ist effect is removed in H/V spectral ratio.

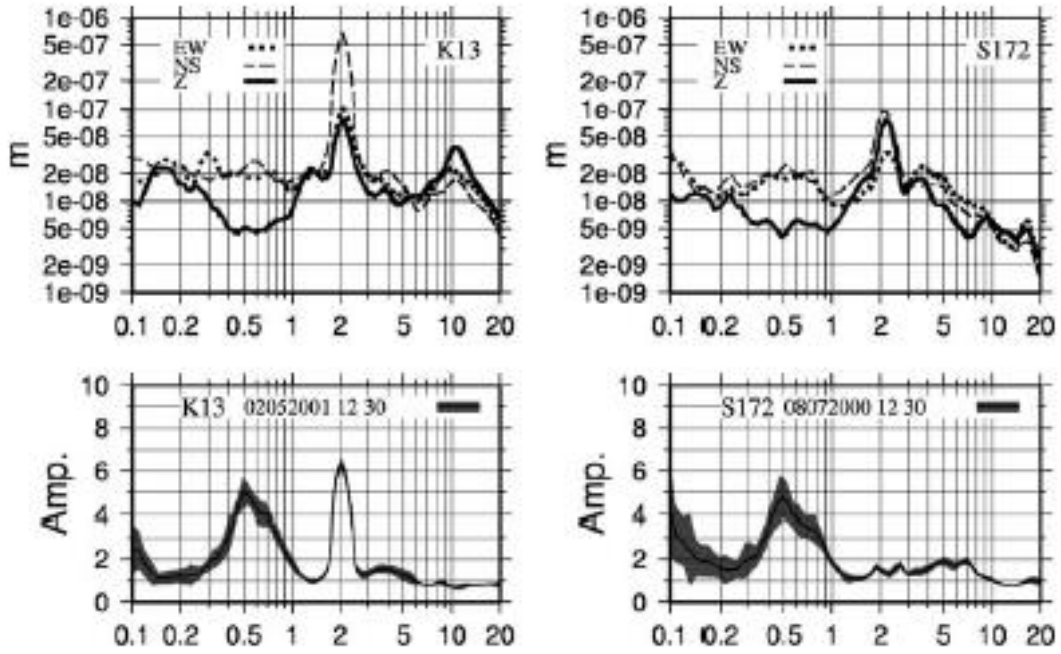

Fig. 3. Fourier spectra of all components (top) at stations K13 (left) and S172 (right) and averaged H/V spectral ratios± one standard deviation (bottom).

After Parolai et al. (2004)

How to measure seismic noise (e.g. Picozzi et al., 2005):

For the frequency range of 0.1-10 Hz the lenght of each time series should be 20-60 seconds

The recording duration should be enough to guarantee the statistical stabilization of the signal. As a general rule at least 20 minutes should be recorded and analysed.

Smoothing the spectra using a relative band width around the central frequency stabilizes the H/V curves and tends to minimize the dispersion

$$q = S(\rho) \Big/ M(\rho)$$

$$\varepsilon = q / \sqrt{n}$$

$S(\rho)$=sampling standard deviation of n realisations

$M(\rho)$=sample average

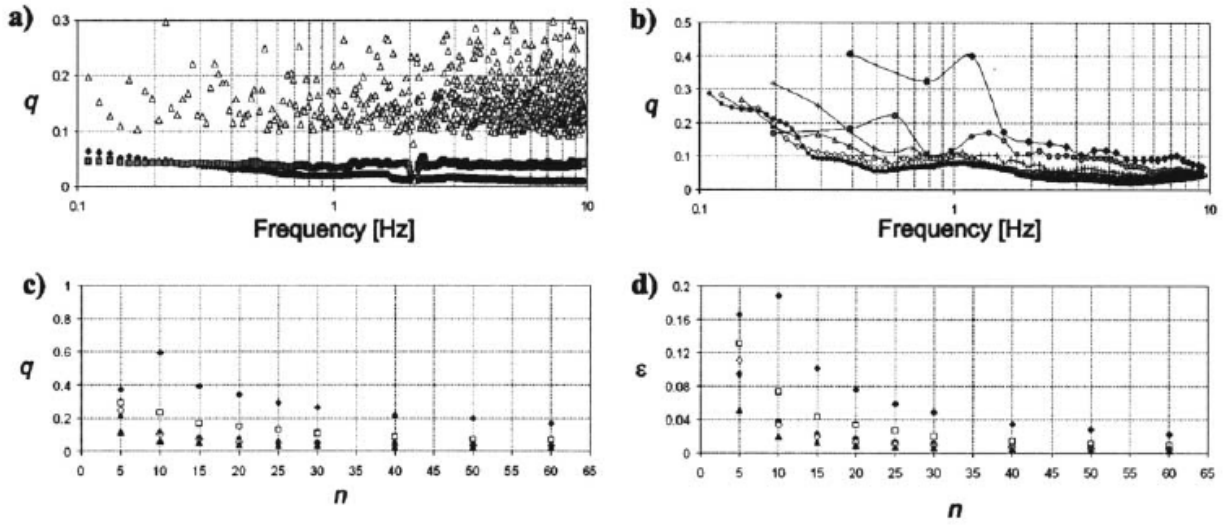

Figure 1. Statistical stability of spectral estimates for ESN recorded at the station K25, in the Cologne area (Parolai *et al.*, 2004), as a function of various analysis parameters: (a) Dispersion index q versus smoothing procedures for the raw spectra computation: no smoothing (white triangles), smoothing with fixed rectangular windows (gray squares), smoothing with relative bandwidth of ± 25% around the central frequency (black diamonds). (b) Dispersion index q versus time series lengths: 2 sec. (black diamonds), 5 sec. (gray dots), 10 sec. (black cross), 20 sec. (gray triangles), 30 sec. (white diamonds), 60 sec. (black dots). (c) Dispersion index q versus number of signal windows n for some significant sample frequencies: 0.1 Hz (black diamonds), 0.5 Hz (white squares), 1 Hz (black dots), 5 Hz (white diamonds), 10 Hz (black triangles). (d) Relative error ε versus different numbers of signal windows n for some significant sample frequencies, same symbols as in (c).

How to measure seismic noise (e.g. Strollo et al., 2008):

Different instruments have different self-noise. Furthermore different sensors act as different filter! If the seismic noise is lower than the self noise it cannot be recovered!

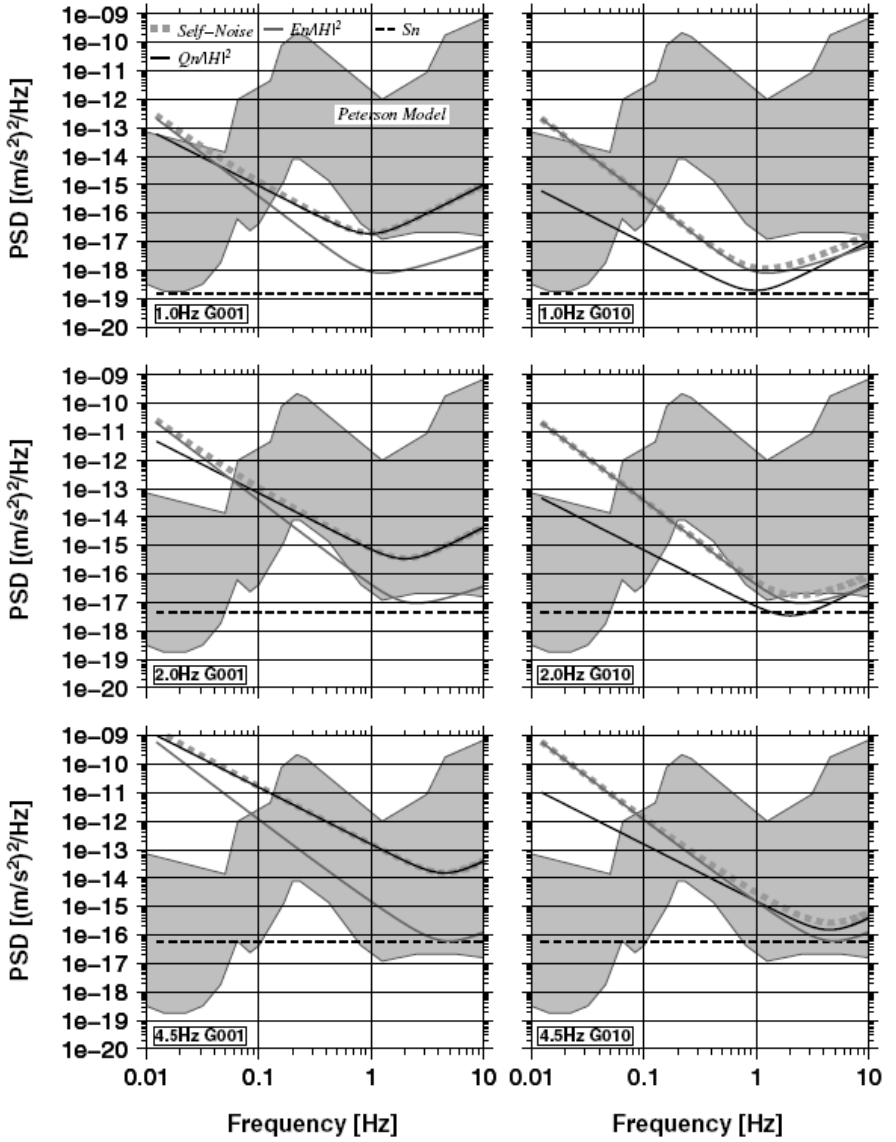

Figure 1. Comparison of different components of self-noise for the EDL. Electronic noise, E_n (gray); quantization noise, Q_n (suspension noise, S_n (dashed black); total self-noise, thick dashed gray. The gray shading indicates the area delimited by the NLN NHNM of Peterson (1993). Left: Results obtained for a gain equal to 1 and different SPESs (1,2, and 4.5 Hz). Right: Results obtained for equal to 10 and different SPESs.

UNIVERSITÀ DEGLI STUDI DI TRIESTE

Due to the combination of gain, self-noise an sensor the fundamental frequency peak might even disappear!

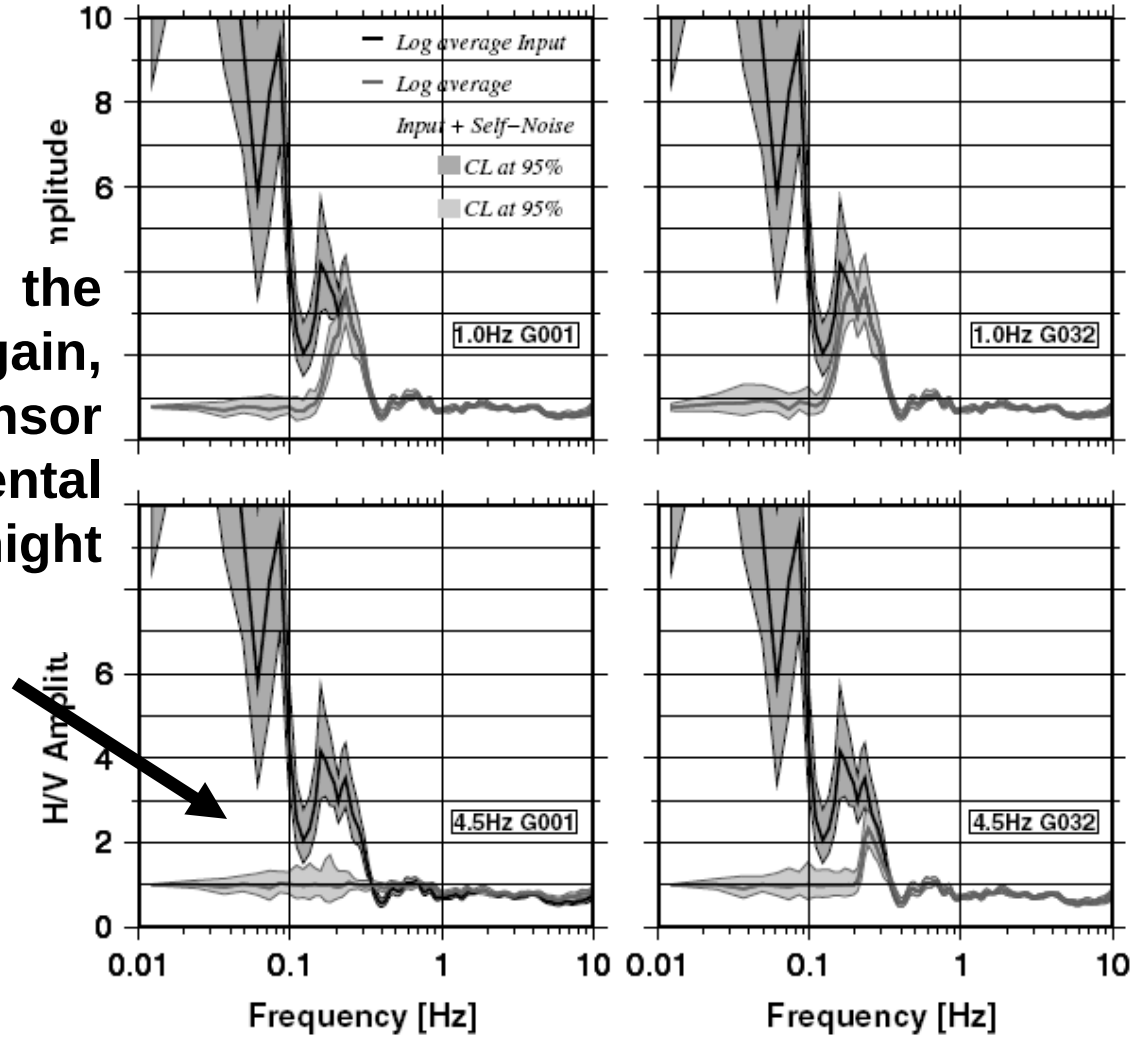

Figure 5. H/V spectral ratio results for the REFTEK 72 A and different SPESs. Left: Results for gain = 1. Right: Results for gain = 32. Top: Results for 1-Hz SPESs. Bottom: Results for 4.5-Hz SPESs.

Short period sensors (1Hz) represent a good compromise for noise measurements!

Broad band

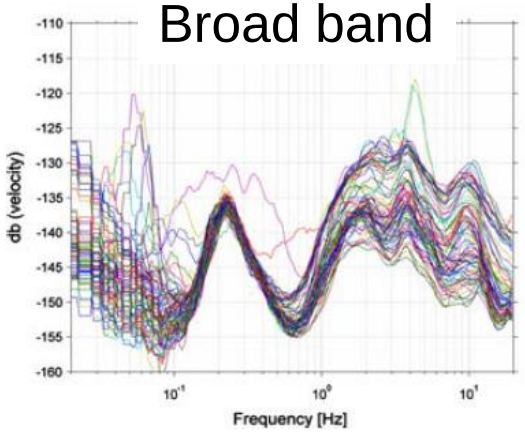

Short period

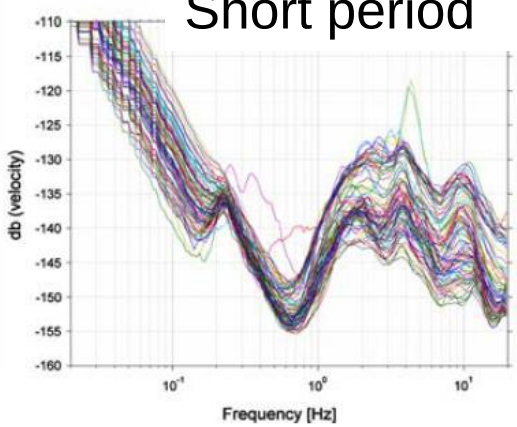

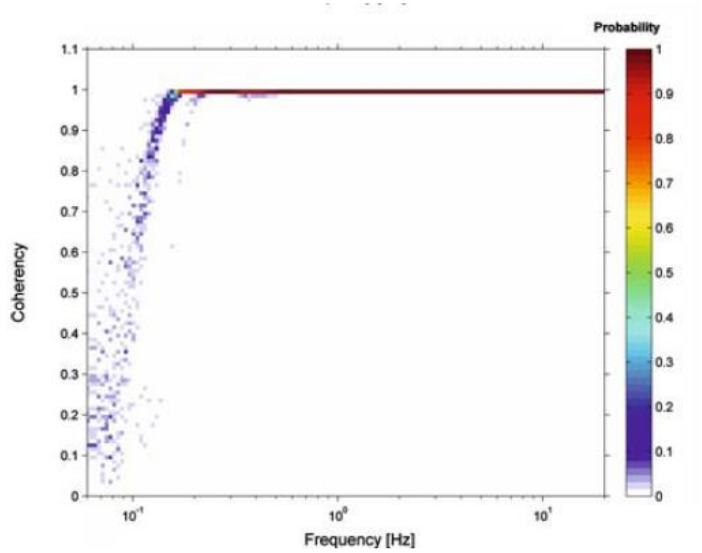

H/V

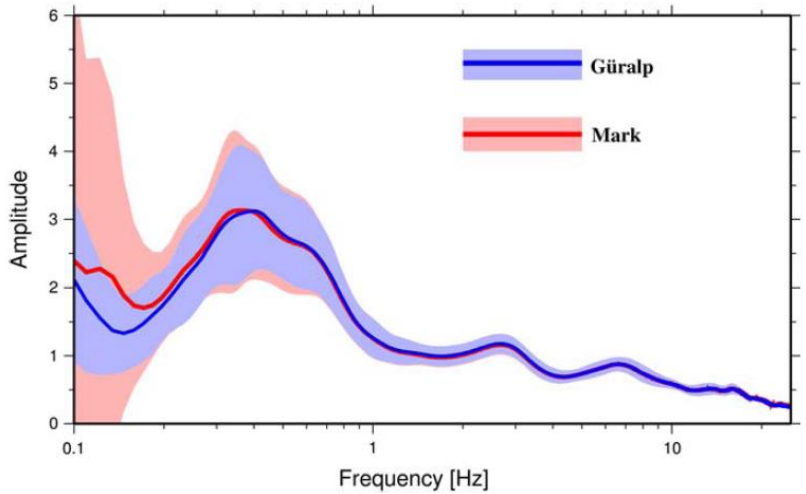

H/V spectral ratios

Ambient Seismic Noise

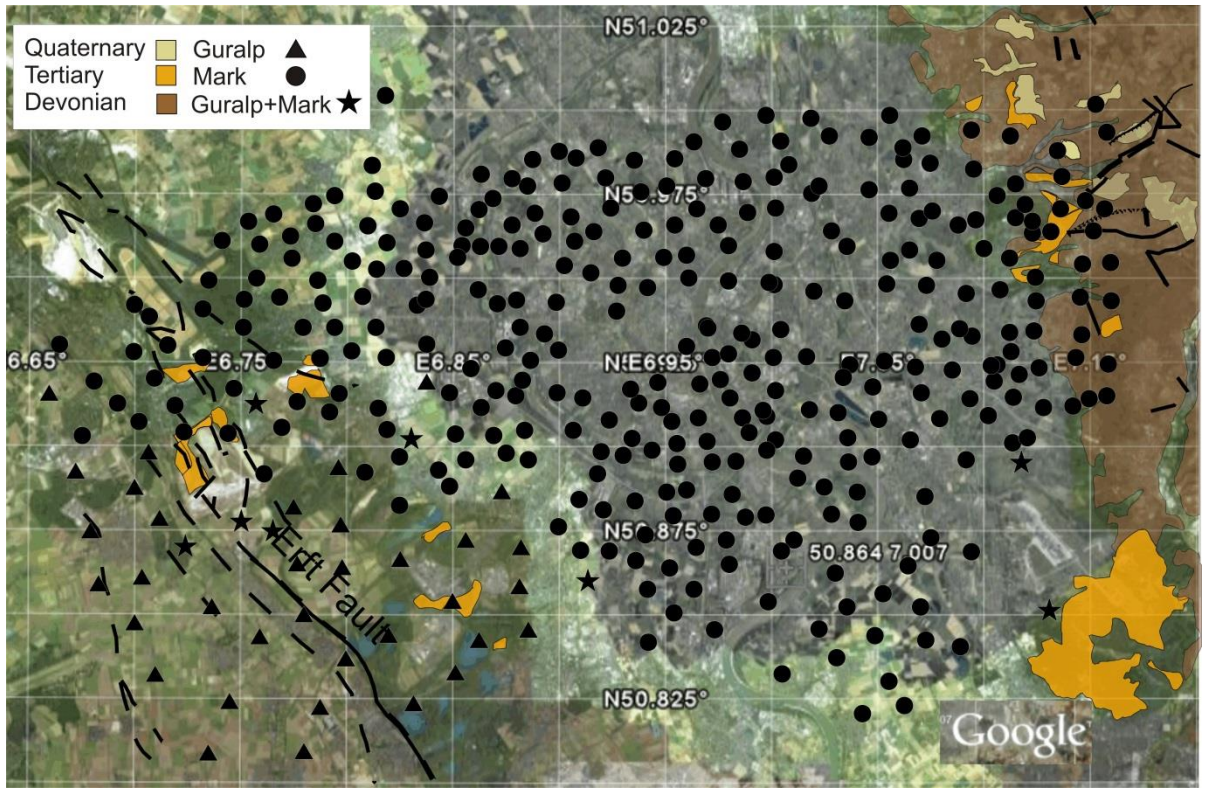

fundamental resonance frequency

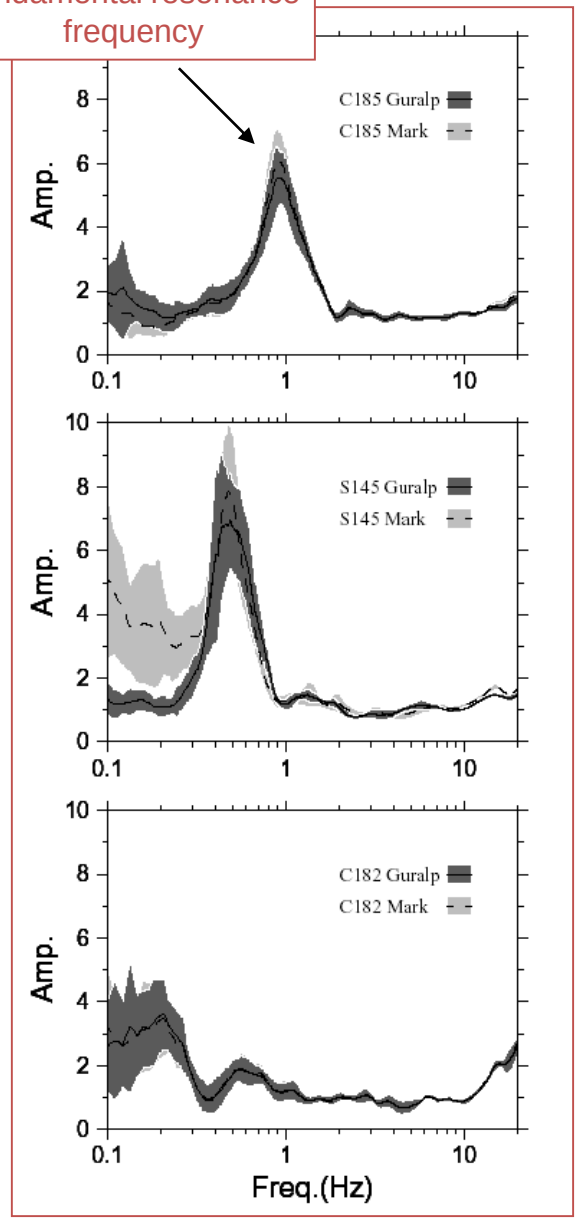

Parolai et al. (2001)

Seismological network: April-June 2001; November 2001

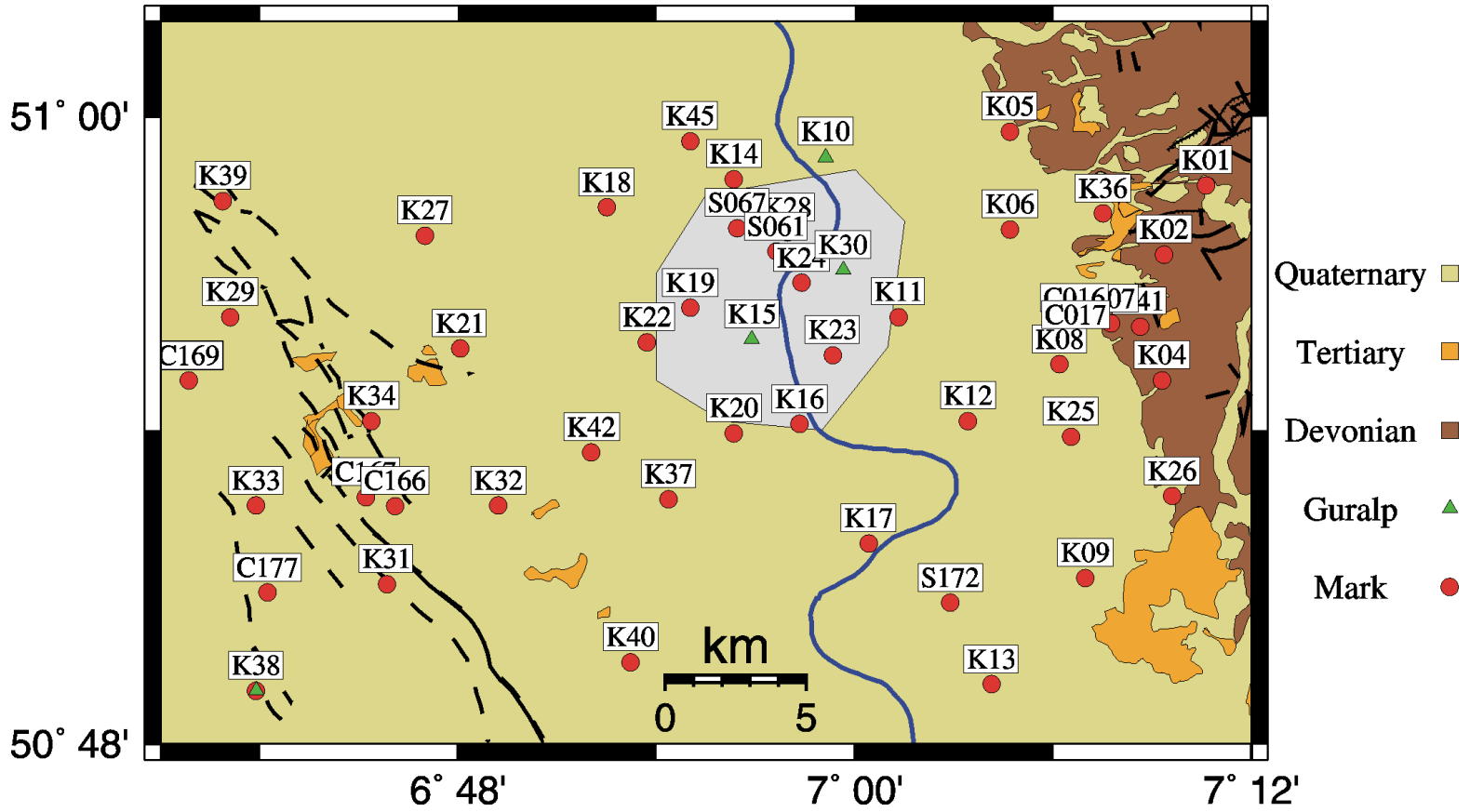

Fundamental resonance frequency map for Cologne

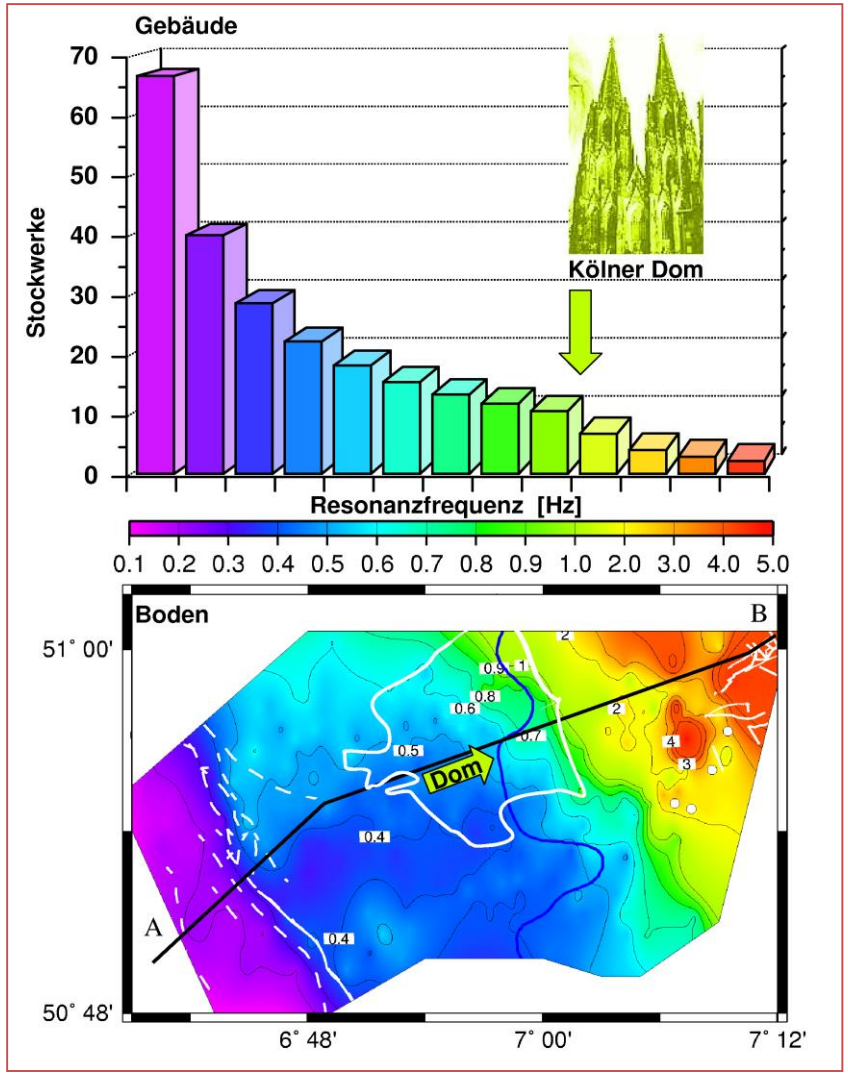

From T = $\frac{\text{number of storeys}}{10}$

the fundamental resonance frequency of the soil in Cologne matches the frequency only of buildings with more than 10 storeys.

Parolai et al. (2001)

H/V spectral ratios versus sedimentary cover thickness

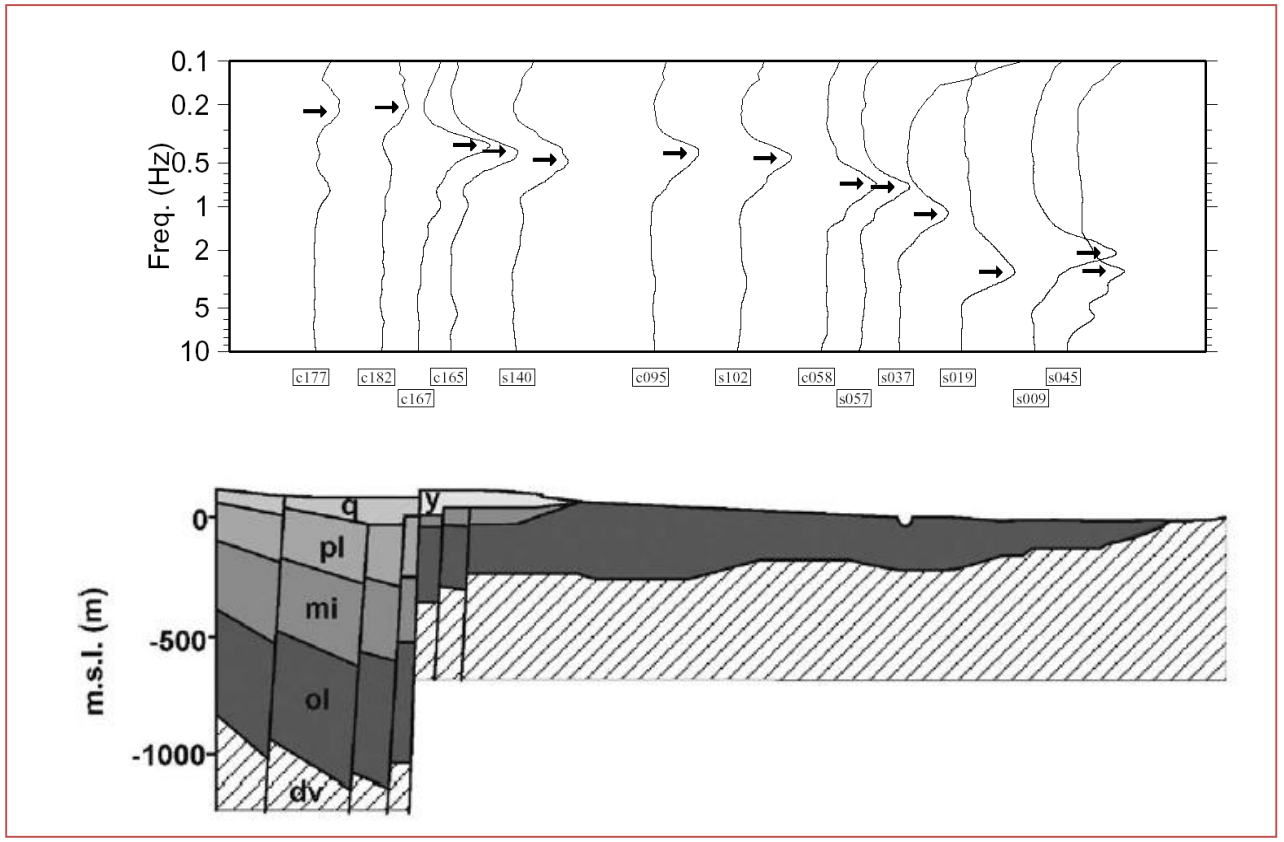

Parolai et al. (2001)

Horizontal-to-vertical (H/V) spectral ratio : Cologne

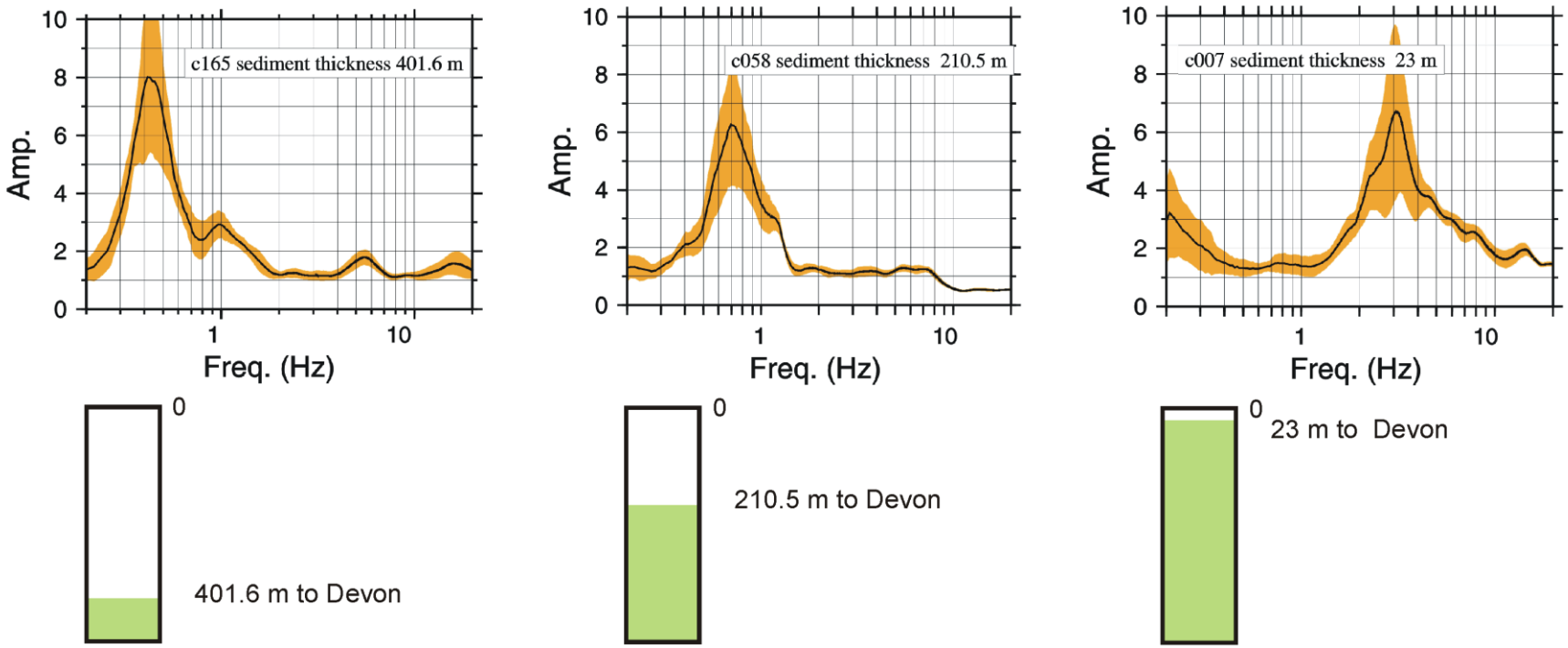

The resonance frequency is clearly shifted towards lower frequencies with increasing sediment thickness

H/V spectral ratios versus sedimentary cover thickness

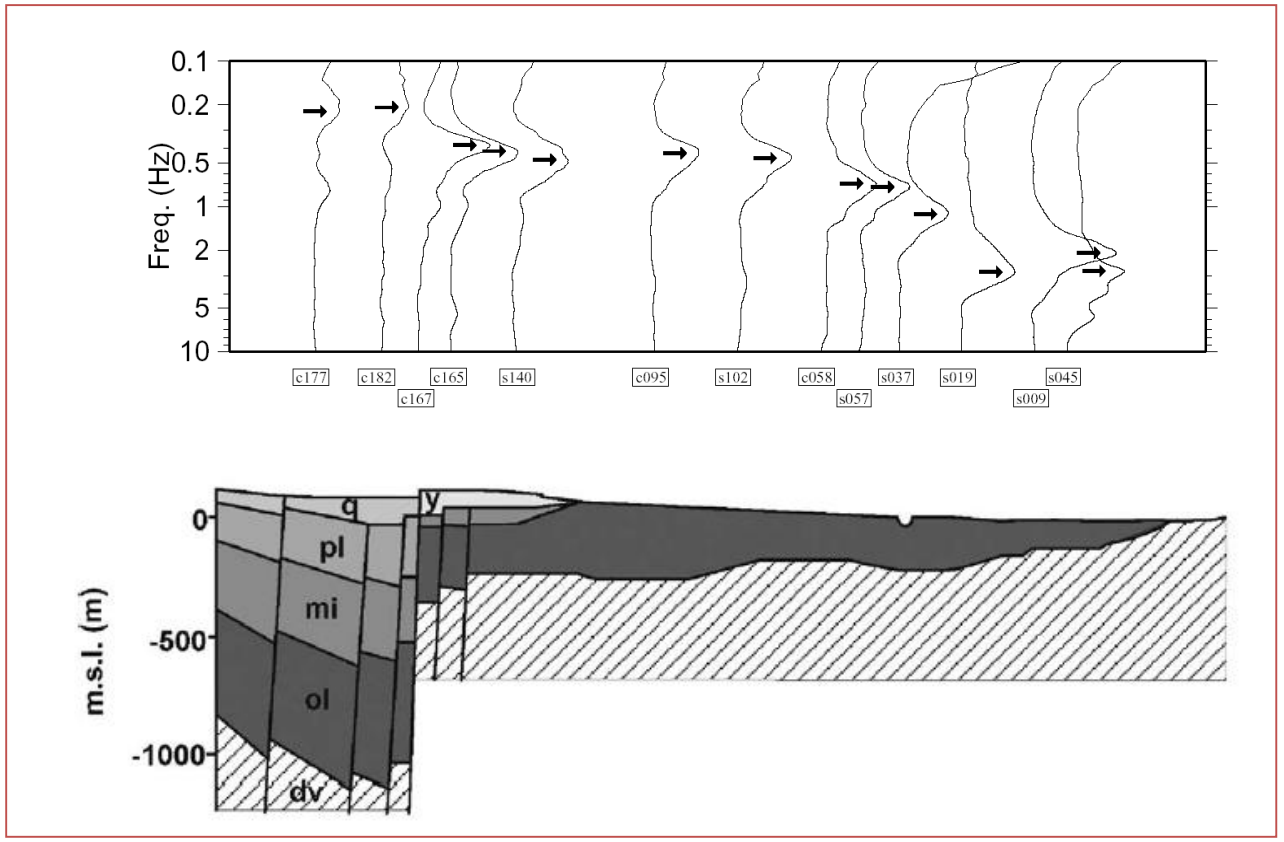

Parolai et al. (2001)

H/V as geophysical investigation tool:
H/V versus sedimentary cover thickness

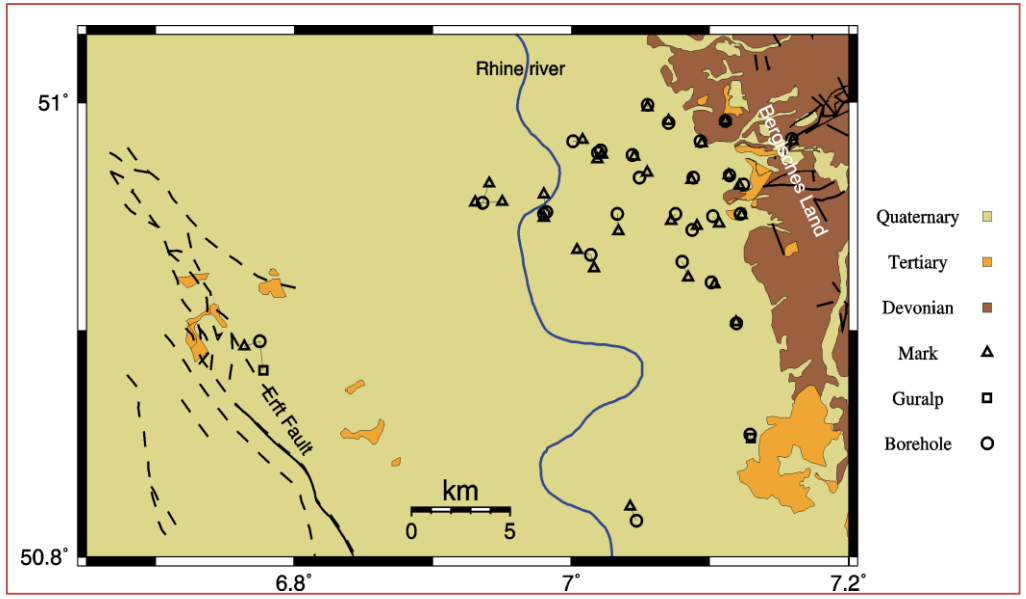

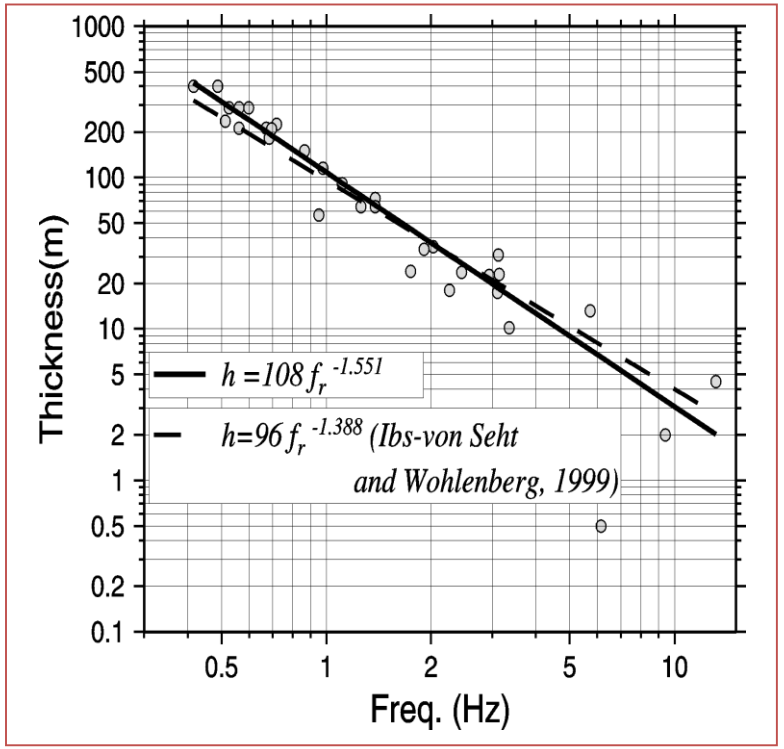

Parolai et al. (2002)

Fundamental resonance frequency map

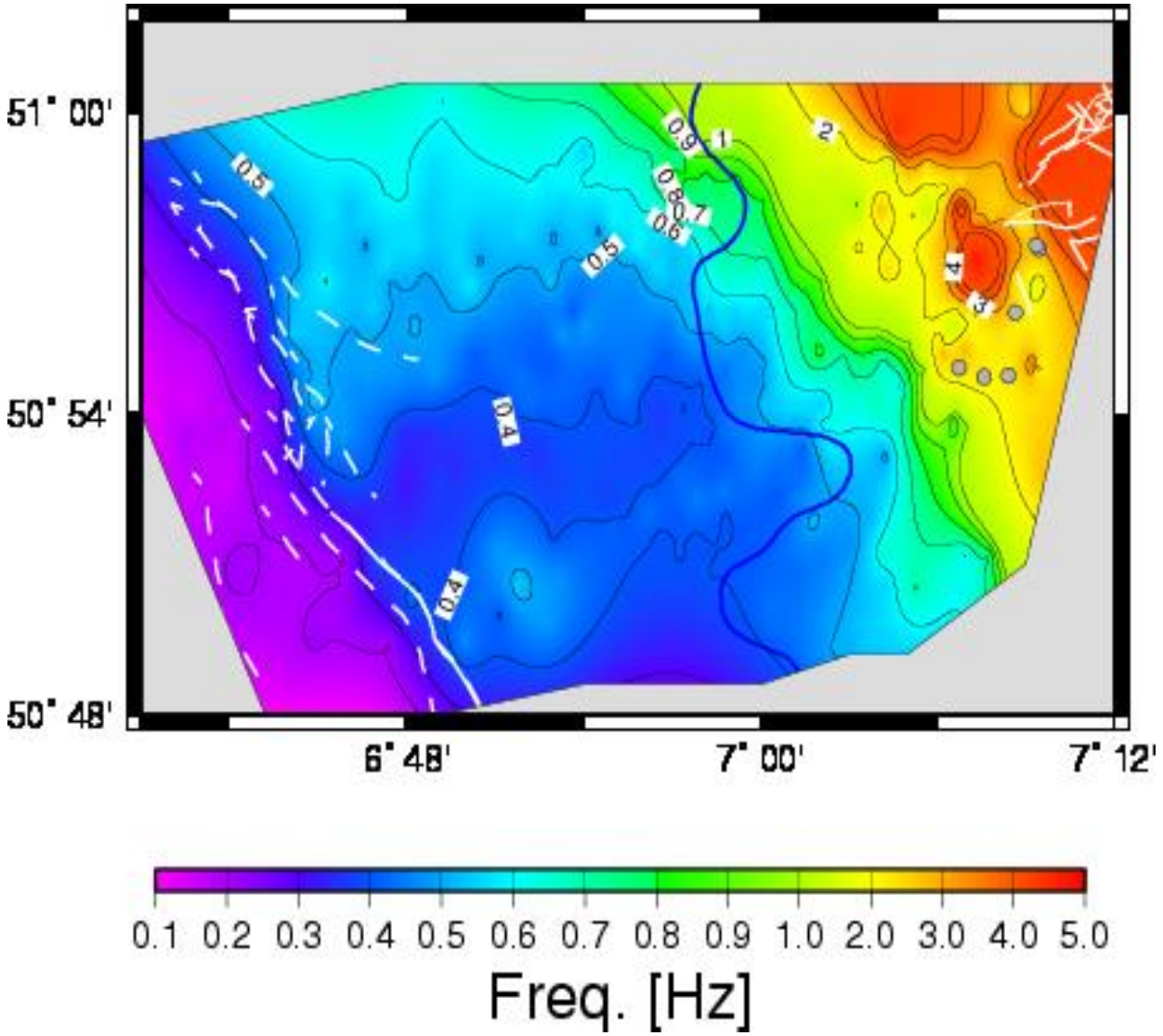

Sedimentary cover thickness

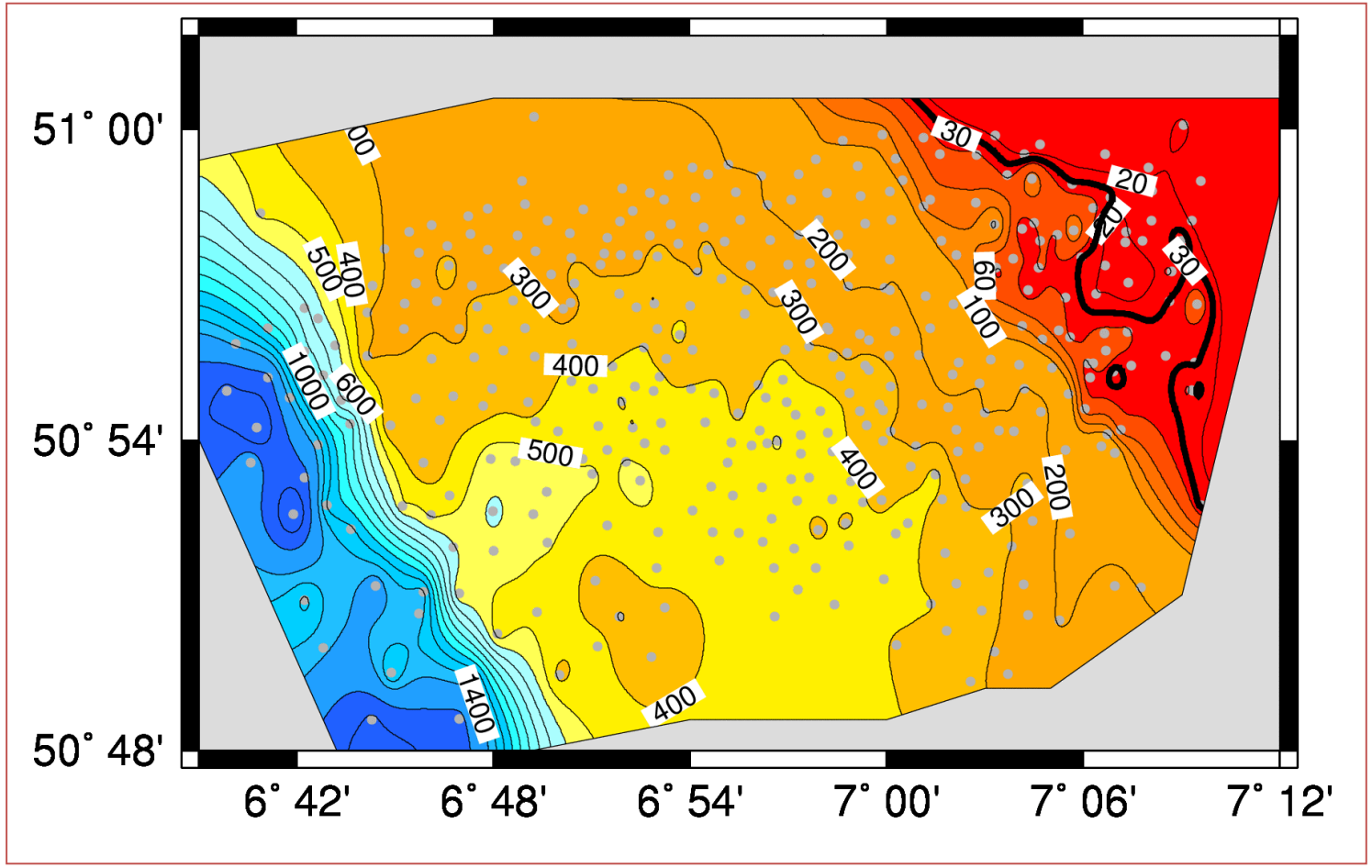

Parolai et al. (2002)

H/V as geophysical investigation tool: H/V inversion

Arai and Tokimatsu, (2000) and Parolai et al. (2005) considered also the contribution of Love waves and higher modes to the H/V spectral ratio shape.

1	H1, ρ1,Vp1,Vs1
2	H2, ρ2,Vp2,Vs2
3	H3, ρ3,Vp3,Vs3
N	∞, ρN,VpN,VsN

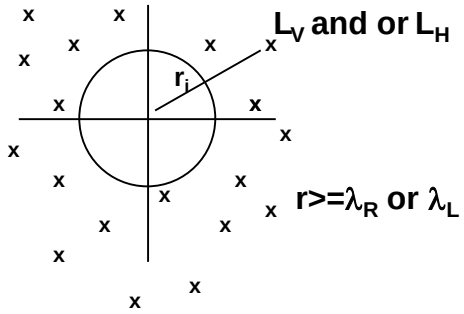

The Fourier transformed vertical and horizontal point forces $L_V(f)$ and $L_H(f)$ are randomly distributed on the free surface.
Each distance between the origin and the source is longer than a wavelength of Rayleigh or Love wave

A is the medium response

K is the wavenumber

ulw is the H/V ratio of Rayleigh mode at the free surface

J is the mode index

A is the H/V ratio of the loading forces L_H/L_V

$$(H/V)_s=(P_{HS}/P_{VS})^{1/2}$$

$$P_{VS}=P_{VR}=\sum_j \left(A_{Rj}/k_{Rj}\right)^2 \left\{1+\left(\alpha^2/2\right)\left(u/w\right)_j^2\right\}$$

$$P_{HS}=P_{HR}+P_{HL}$$

$$P_{HR}=\sum_j \left(A_{Rj}/k_{Rj}\right)^2 \left(u/w\right)_j^2 \left\{1+\left(\alpha^2/2\right)\left(u/w\right)_j^2\right\}$$

$$P_{HL}=\sum_j \left(A_{Lj}/k_{Lj}\right)^2 \left(\alpha^2/2\right)$$

However, the main limitation of the method consists in the strong trade-off between S-wave velocity and thickness of the sedimentary cover!

Sensitivity $D = \left| \left(p / (H/V)_s \right) \left(\partial (H/V)_s / \partial p \right) \right|$

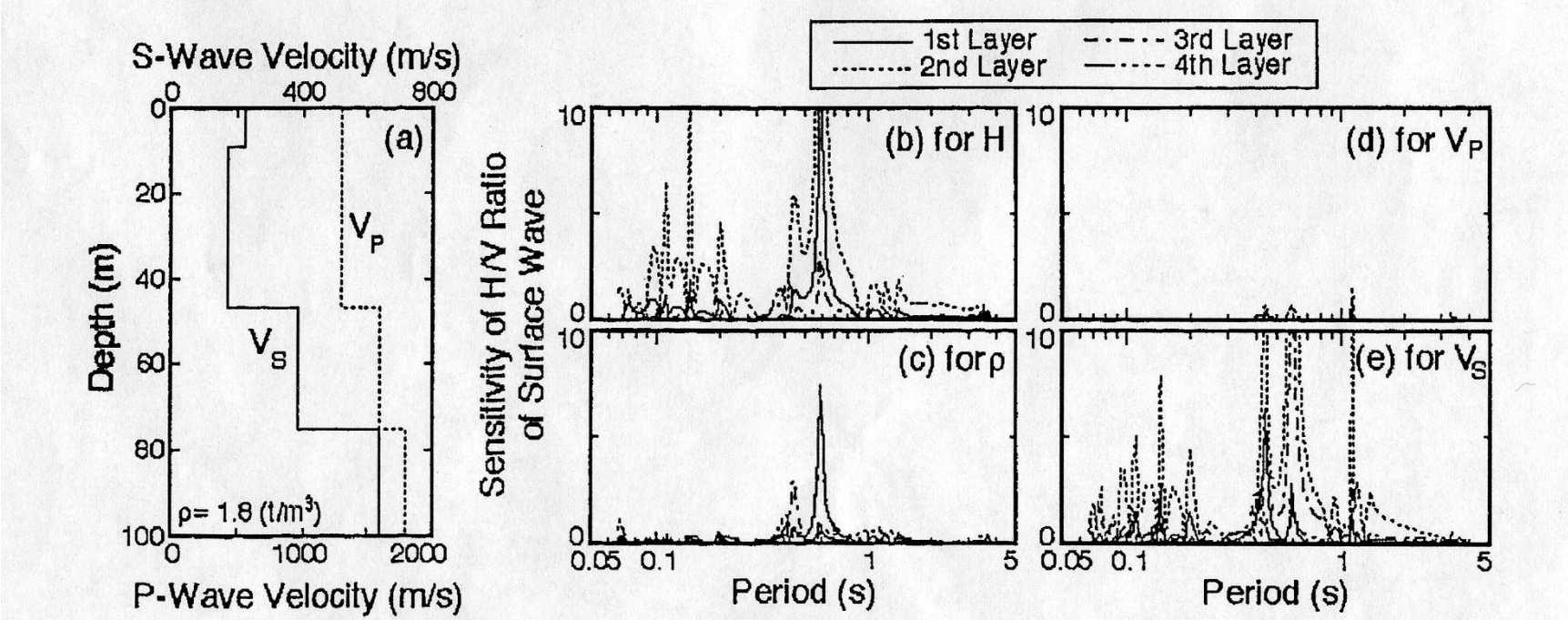

Figure 10: An example of sensitivity analyses of surface wave H/V ratio for soil model

After Arai and Tokimatsu (2000)

H/V inversion

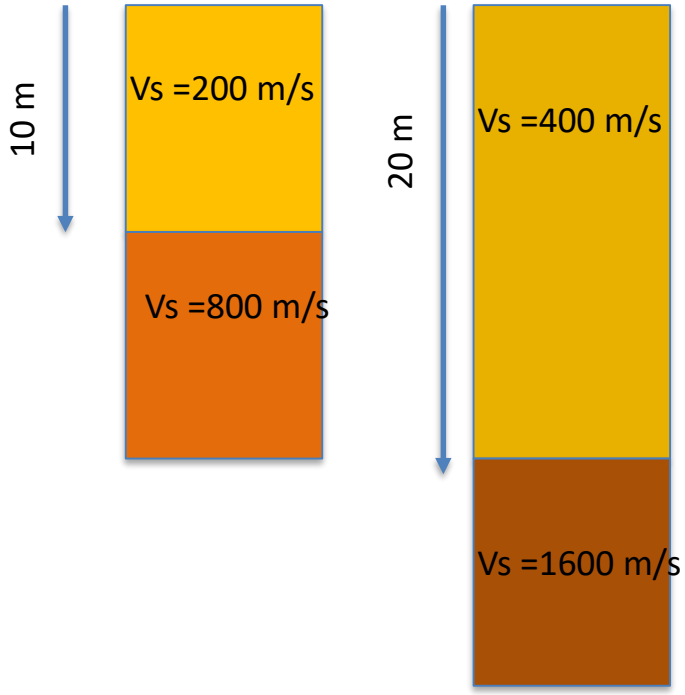

Different models…same H/V!!

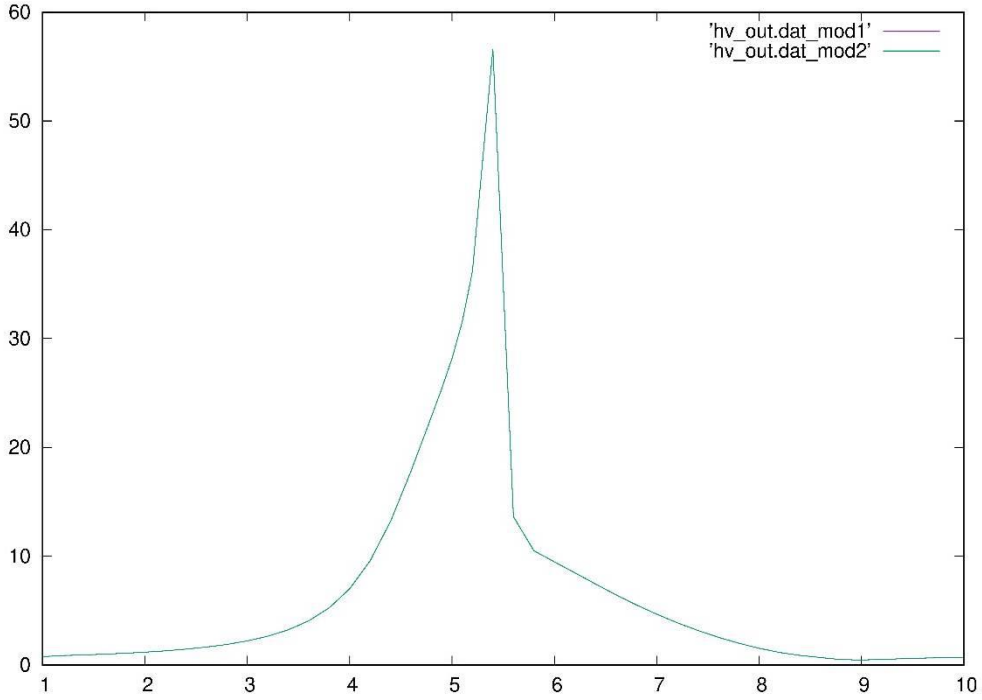

Horizontal-to-vertical (H/V) spectral ratio: Investigating the subsoil structure

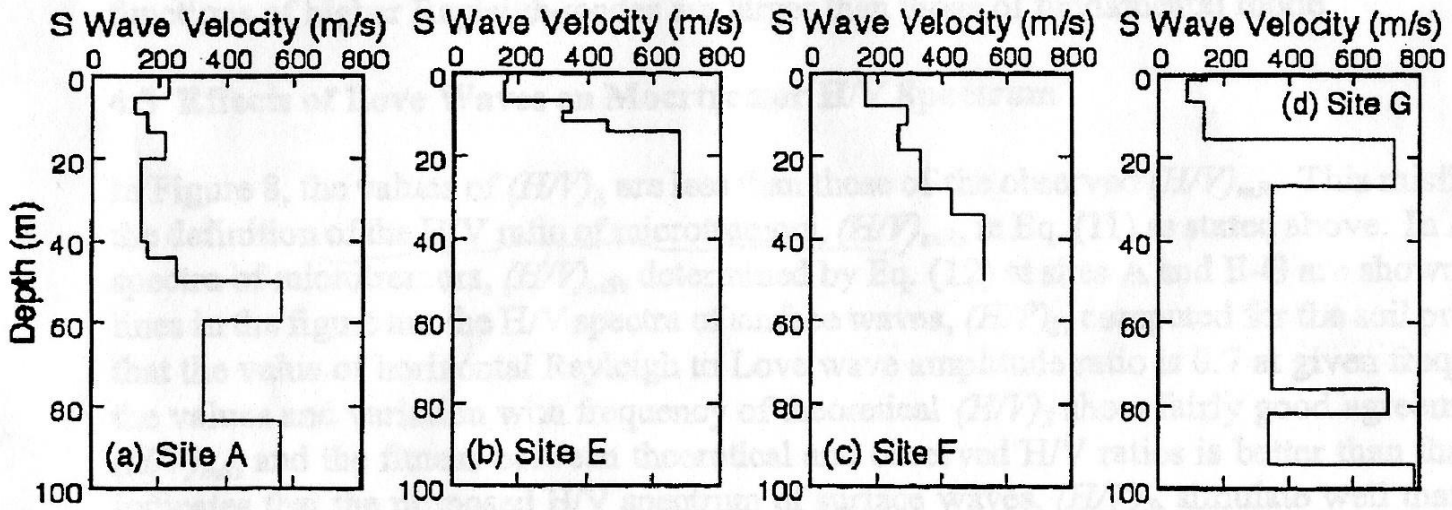

Figure 7: Shallow V_S profiles at sites A and E-G [(a)Ishihara *et al.*, 1989; (b)-(d)Tokimatsu, 1995]

Table 1: Deep soil profiles at sites A, E, and F [Shima *et al.*, 1976]

Depth(km)	ρ (t/m^3)	Vp(km/s)	Vs(km/s)
0.0 - 1.5	1.9	1.8	0.7
1.5 - 2.3	2.2	2.8	1.5
2.3 -	2.5	5.6	3.0

Table 2: Deep soil profile at site G [Higashi and Kudo, 1992]

Depth(km)	ρ (t/m^3)	Vp(km/s)	Vs(km/s)
0.0 - 0.3	2.0	2.3	0.8
0.3 - 2.0	2.3	3.0	1.5
2.0 - 3.2	2.5	4.2	2.4
3.2 -	2.8	5.5	2.8

After Arai and Tokimatsu (2000)

Horizontal-to-vertical (H/V) spectral ratio: Investigating the subsoil structure

Importance of considering also the effect of higher modes

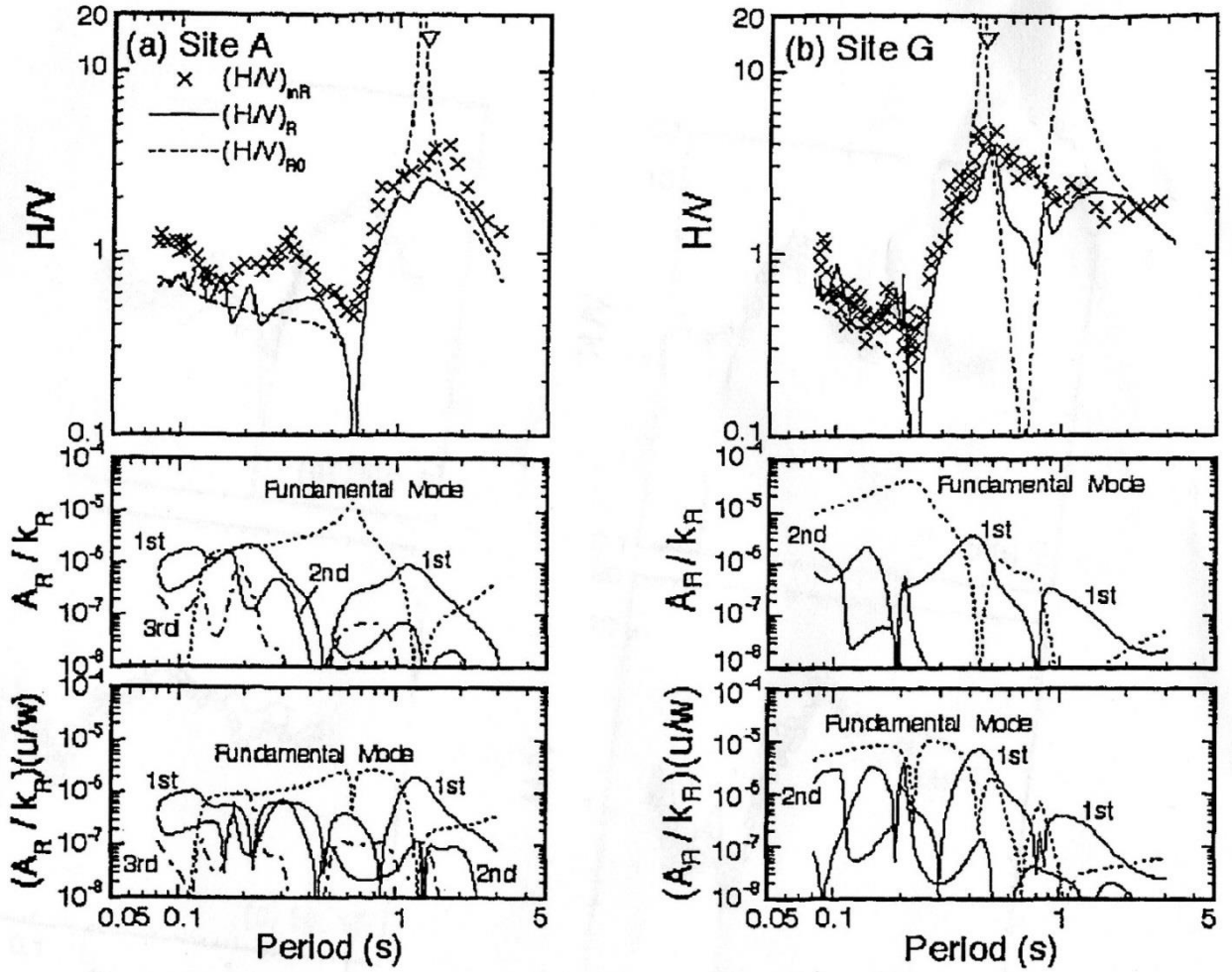

Figure 8: The H/V ratios of microtremors compared with those of Rayleigh waves at sites A and G

After Arai and Tokimatsu (2000)

Importance of considering also the effect of Love waves

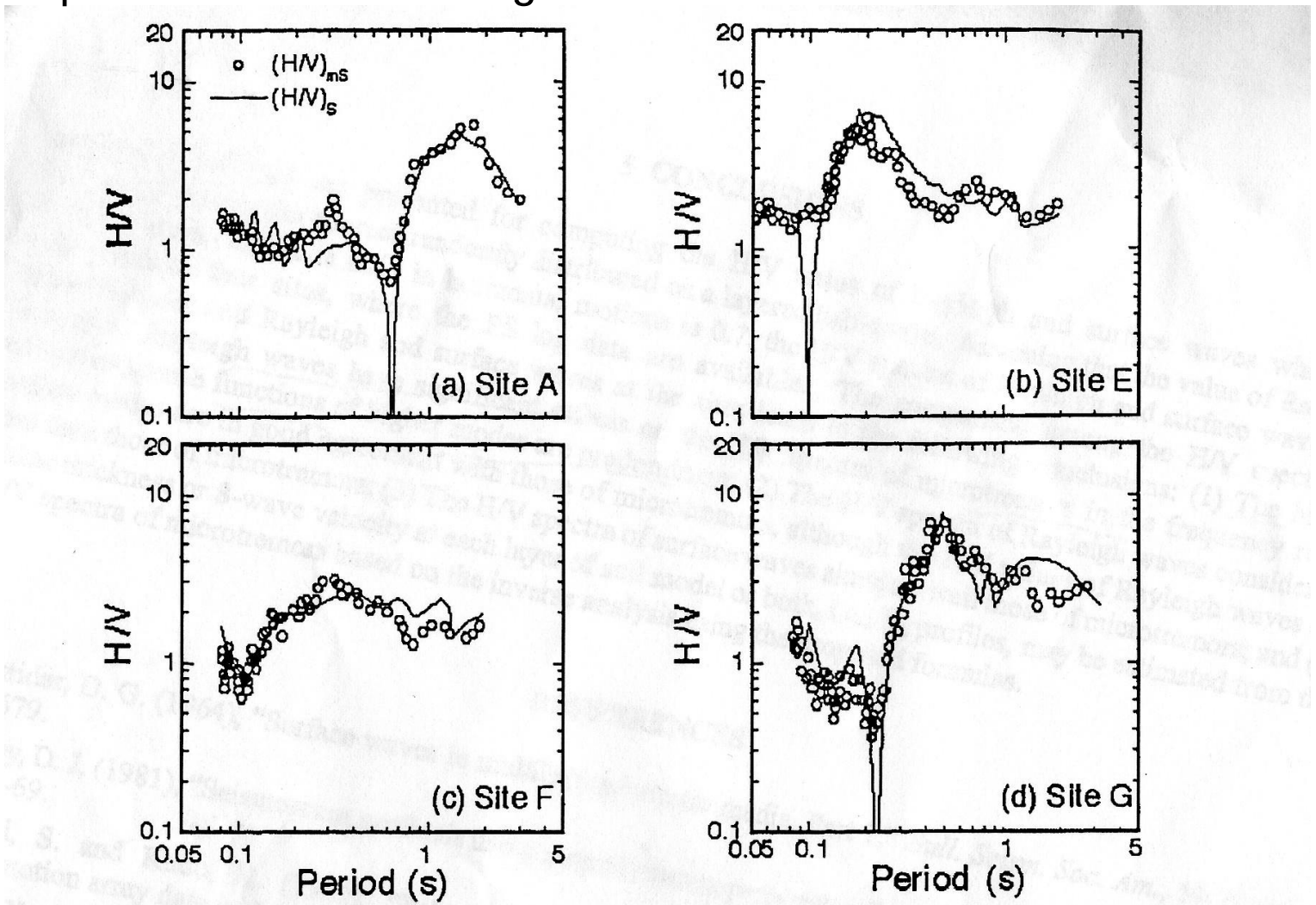

Figure 9: The H/V ratios of microtremors compared with those of surface waves at sites A and E-G

After Arai and Tokimatsu (2000)

H/V as geophysical investigation tool: H/V inversion

The inversion is perfomed using a Genetic Algorithm: see lecture on arrays.The algorithm minimizes the difference between observed and calculated H/V

H/V as geophysical investigation tool: H/V inversion

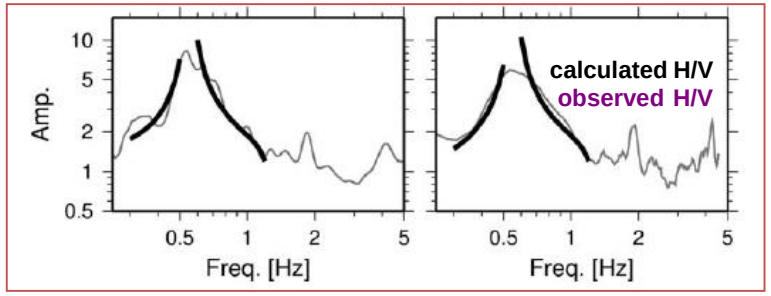

S-wave velocity profile

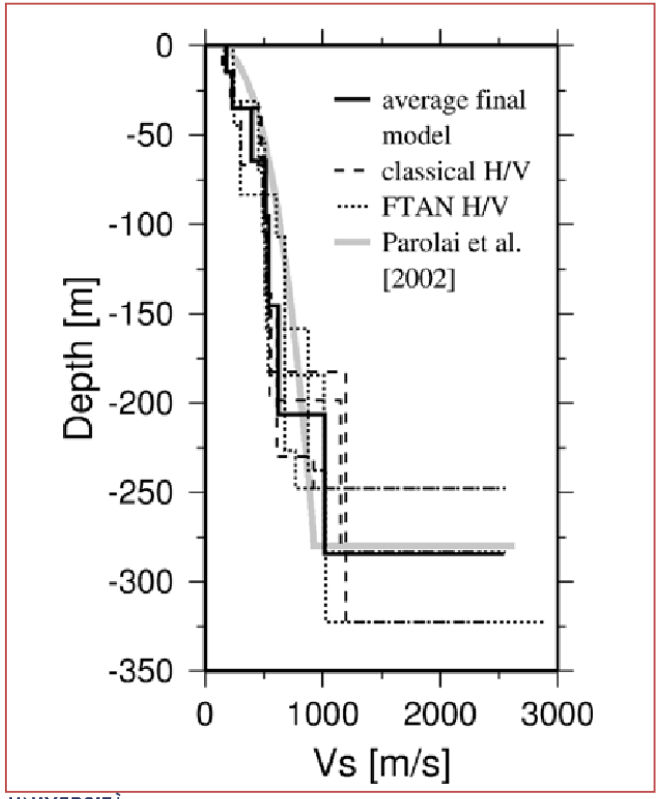

2D S-wave velocity section

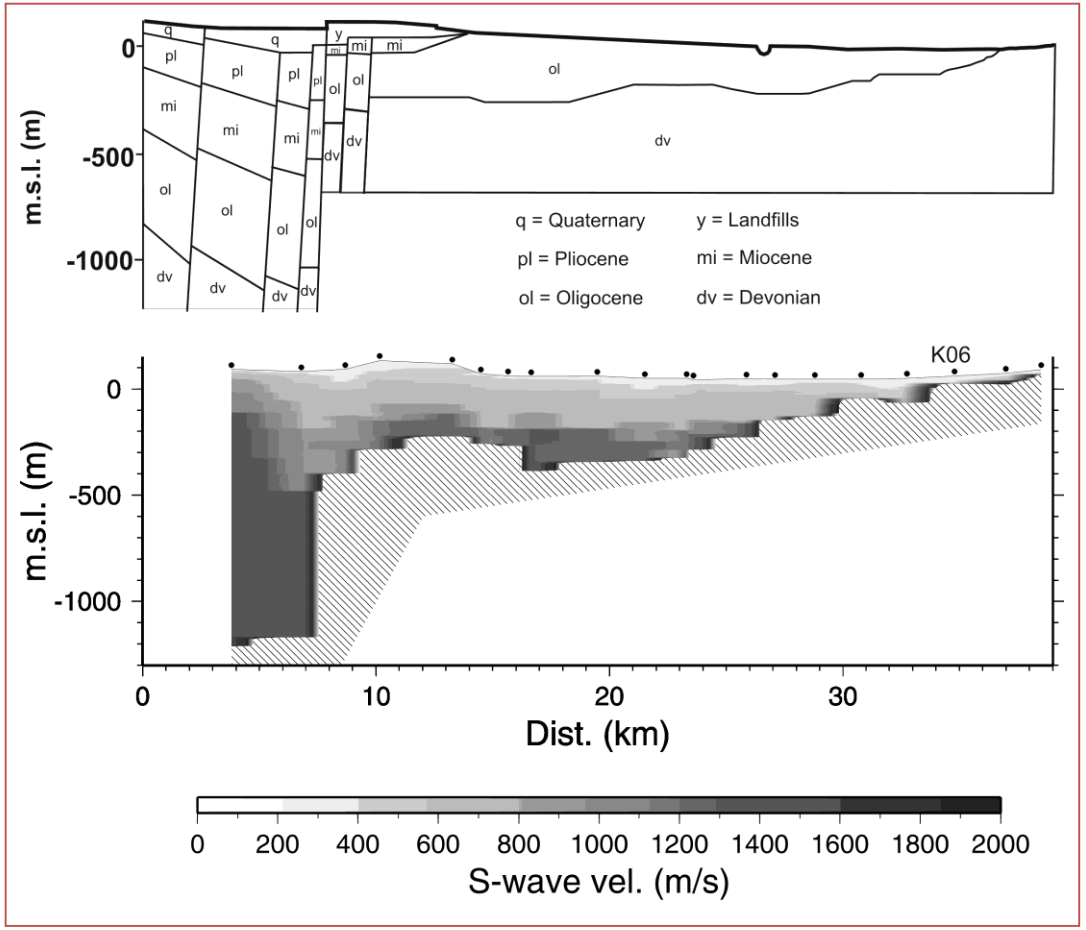

Parolai et al. (2006)

H/V as geophysical investigation tool: H/V inversion

2D-3D models can be sue for numerical simulations of ground motion!

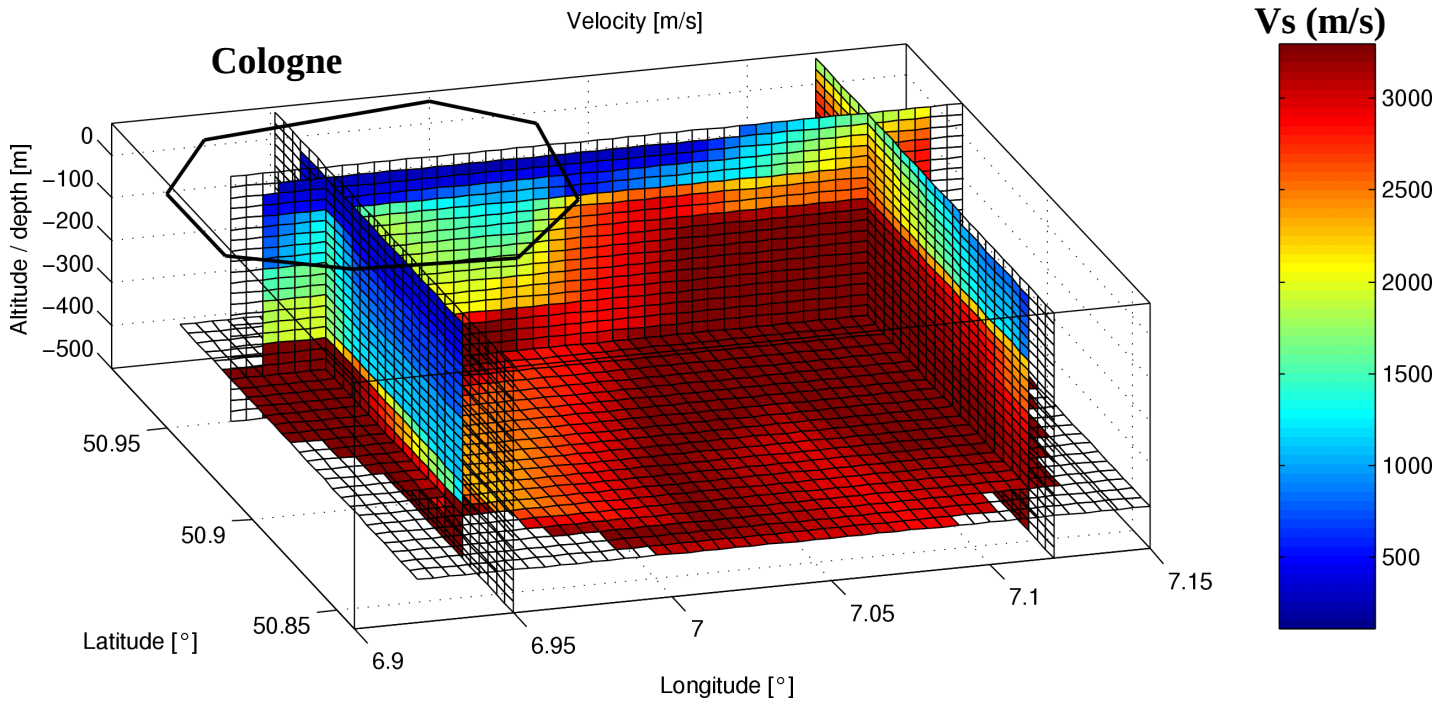

Investigating the frequency of vibration of buildings with seismic noise

Hospital Holweide

Inside

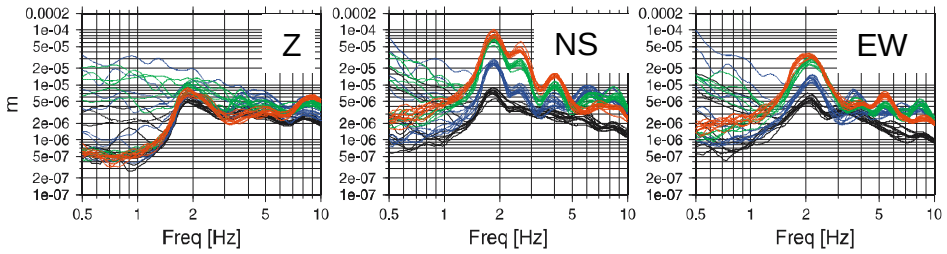

outside

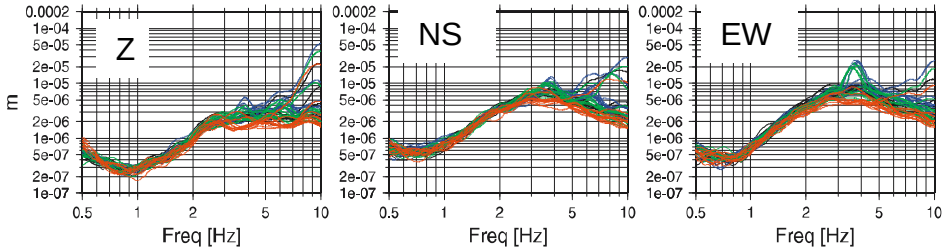

Investigating the frequency of vibration of buildings with seismic noise

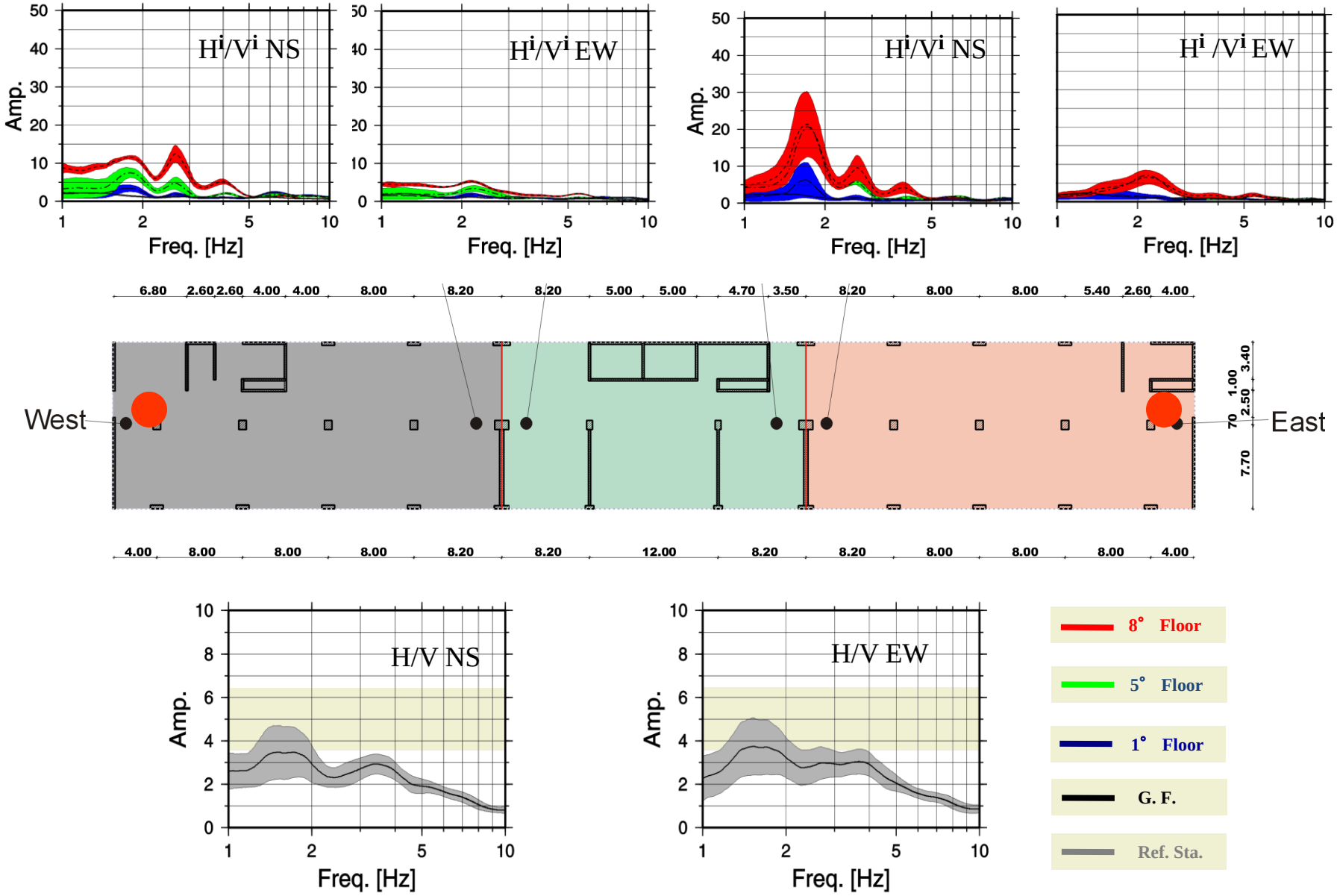

Investigating the frequency of vibration of buildings with seismic noise

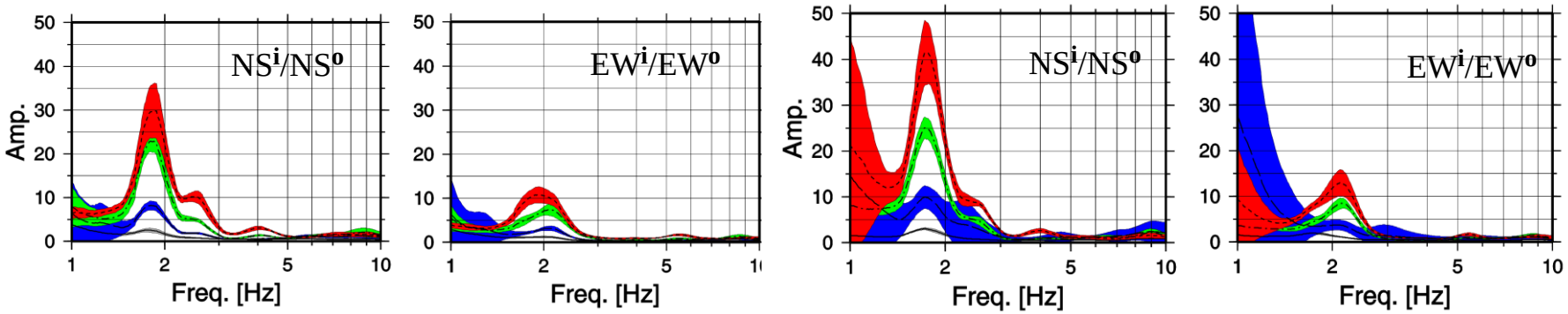

The estimated frequencies of vibration were compared with those obtained by fe-modeling of the building

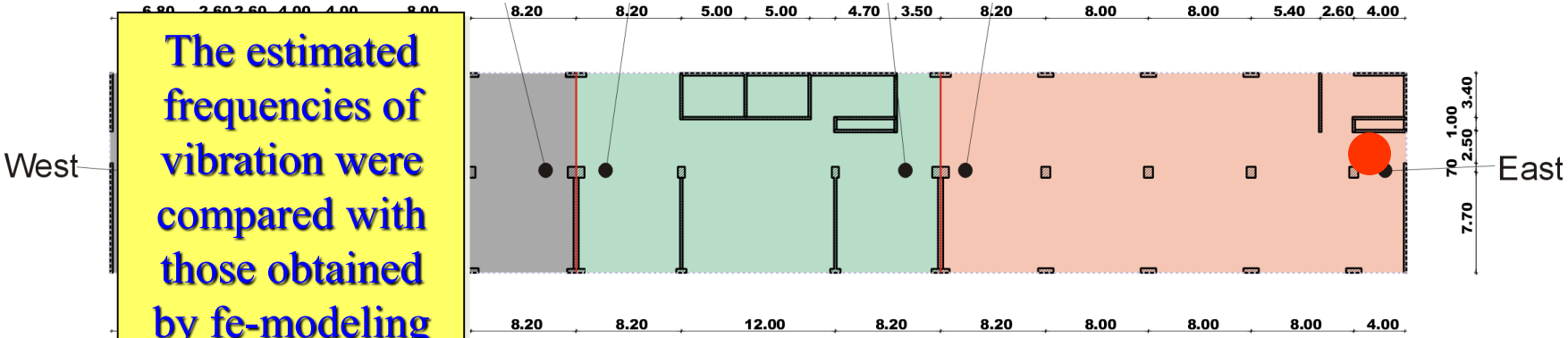

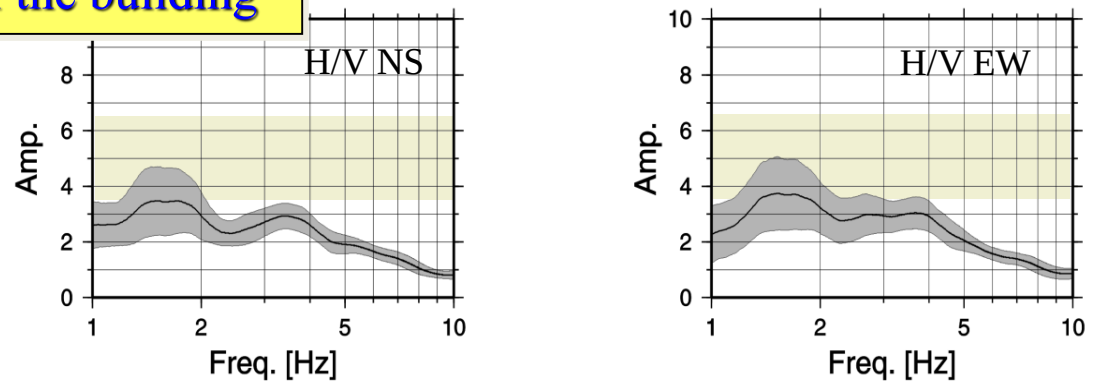

8° Floor

5° Floor

1° Floor

G. F.

Ref. Sta.

Seismic noise measurements : investigating the resonance frequencies of buildings

Table 1. Comparison of resonance frequencies at Holweide Hospital from FE modelling and ambient seismic noise measurements using the H/V ratio and spectral ratio (RSM) technique.

Mode	1	2	3	4	5	6
FE frequency (Hz)	1.78	1.94	2.34	2.78	4.15	5.83
NS modal mass (%)	59	10	1	1	0	3
EW modal mass (%)	1	16	59	0	1	0
H/V frequency (Hz)	1.75 NS	–	2.2 EW	2.65 NS	3.95 NS	5.45 EW
RSM frequency (Hz)	1.8 NS	–	2.0 EW	2.5 NS	4.0 NS	5.45 EW

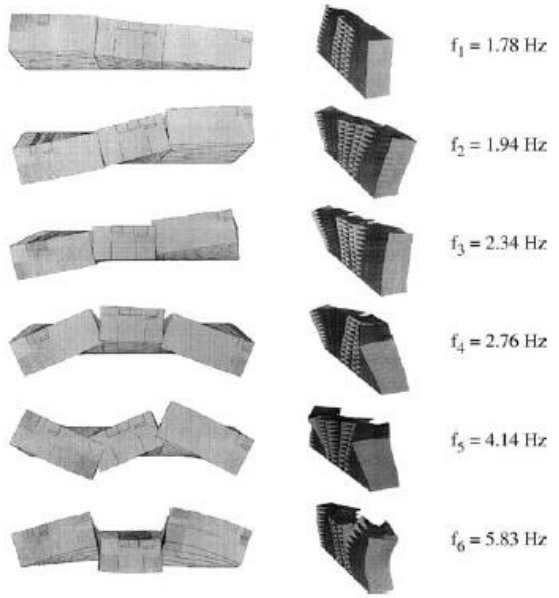

Figure 7. Top view (left) and perspective view (middle) with eigenfrequencies for the first six eigenmodes using the second model with springs in separation joints leading to coupled building sections.

Parolai et al. (2005)

Stefano Parolai

Using seismic noise to estimate the characteristics of a site: SASW

Spectral Analysis of Surface Waves (SASW) requires that:

Two vertical receivers are placed on the ground at equal distance from a fixed centerline

Tests are performed progressively moving the receivers away from the fixed centerline

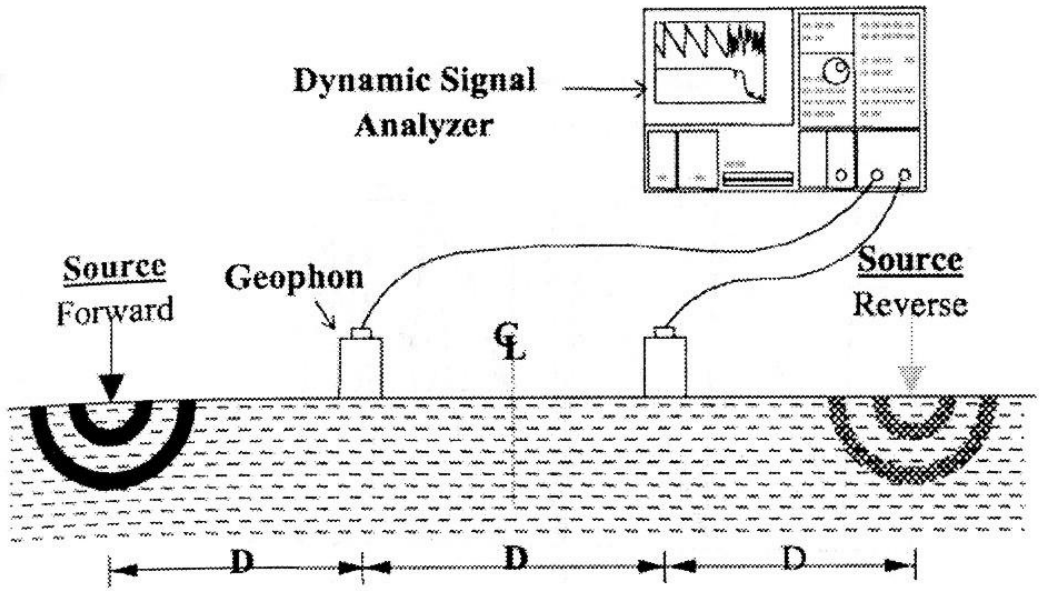

Fig. 1. General configuration of the SASW testing setup.

after Kim and Park (2002)

Stefano Parolai

Using seismic noise to estimate the characteristics of a site: SASW

Signal are transformed in the frequency domain via FFT

The cross-power spectrum between the two signal is calculated

The phase of the cross-power spectrum, which represents the phase difference between the two receiver signals as a function of frequency, is calculated

The time delay $t(f)$ between the receiver fro each frequency is calculated by:

$$t(f) = \frac{\theta_{xy}(f)}{2\pi f} \qquad (1)$$

θ_{xy} is the phase shift of the cross-power spectrum in radian

f is the frequency

$$\Delta\emptyset(\omega) = \emptyset1(\omega) - \emptyset2(\omega) = \tan^{-1}\theta1 - \tan^{-1}\theta2 = \tan^{-1}\frac{\theta1-\theta2}{1+\theta1\theta2}$$

$$= \tan^{-1}\frac{\frac{b}{a}-\frac{d}{c}}{1+\frac{bd}{ac}} = \tan^{-1}\frac{\frac{bc-da}{ac}}{1+\frac{bd}{ac}} = \tan^{-1}\frac{\frac{bc-da}{ac}}{\frac{ac+bd}{ac}} = \tan^{-1}\frac{bc-da}{ac+bd}$$

$F(\omega) = FFT(f(t))$

$G(\omega) = FFT(g(t))$

$a = real\ F(\omega)$
$b = imag\ F(\omega)$

$$\theta1 = \frac{b}{a}$$

$c = real\ G(\omega)$
$d = imag\ G(\omega)$

$$\theta2 = \frac{d}{c}$$

$$\boldsymbol{Cross-spectrum} = F(\omega)^*G(\omega)$$

$$(a+ib)(c-id) = ac - iad + ibc - i^2bd = ac + bd + i(bc-ad)$$

$$\Delta\emptyset(\omega) = \tan^{-1}\frac{bc-ad}{ac+bd}$$

Stefano Parolai

Using seismic noise to estimate the characteristics of a site: SASW

The phase velocity V_R is then calculated by:

$$V_R = D/t(f) \qquad (2)$$

D is the distance between the two receivers

The corresponding wavelength λ_R of the surface wave that determined the depth of investigation (of about $\lambda_R/3$, $\lambda_R/2$) is:

$$\lambda_R = V_R/f \qquad (3)$$

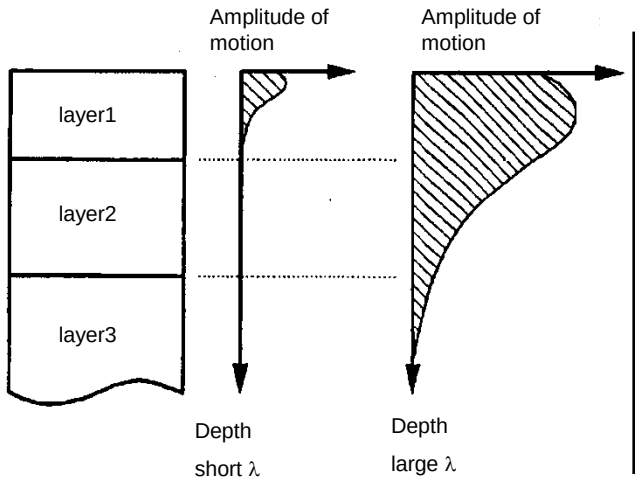

Stefano Parolai

Using seismic noise to estimate the characteristics of a site: SASW

The dispersion curve may be disturbed in the low frequency range because of the near field effect which occurs due to the presence of body waves.

Many criteria for data acquisition have been proposed (however the price to pay is to loose information at low frequency and therefore to limit the depth of investigation)

Heisey et al. criteria $d1=d2$ $0.33\lambda<d2<2\lambda$

Tokimatsu et al. Criteria $0.25\lambda<d1+0.5d2$ $0.0625\lambda<d2<\lambda$

d1 is the near receiver distance from the source

d2 is the receiver spacing

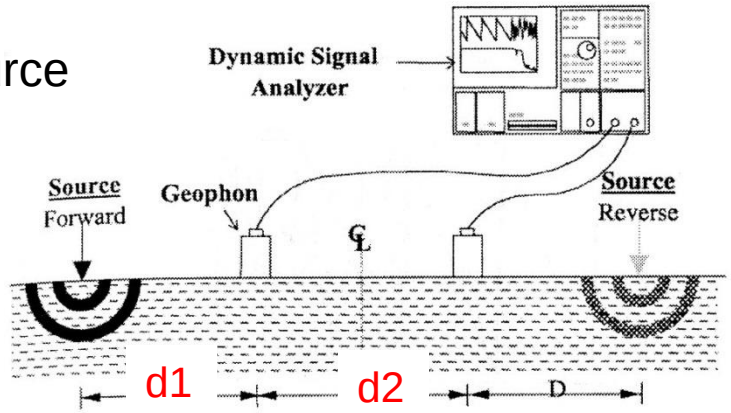

Fig. 1. General configuration of the SASW testing setup.

after Kim and Park (2002)

Stefano Parolai

Using seismic noise to estimate the characteristics of a site: SASW

The procedure described before is based on Fourier Transform

At each frequency the phase difference between the two sinusoidal component with constant frequency and amplitude over the whole record length must be in the range +/- 180°

Therefore in the conventional SASW the unwrapping process of relative phase angle is required (adding or subtracting the correct number of 360° cicles) before evaluating the phase velocity

$$\theta_{unwrap}(f)=2\pi n+ \theta_{unwrap}(f) \qquad (4)$$

At each frequency the phase difference between the two sinusoidal component with constant frequency and amplitude over the whole record length must be in the range +/- 180°

Stefano Parolai

Using seismic noise to estimate the characteristics of a site: MASW

Multichannel Analysis of Surface Wave was found to be more efficient for unraveling the dispersive properties (Park et al., 1996).

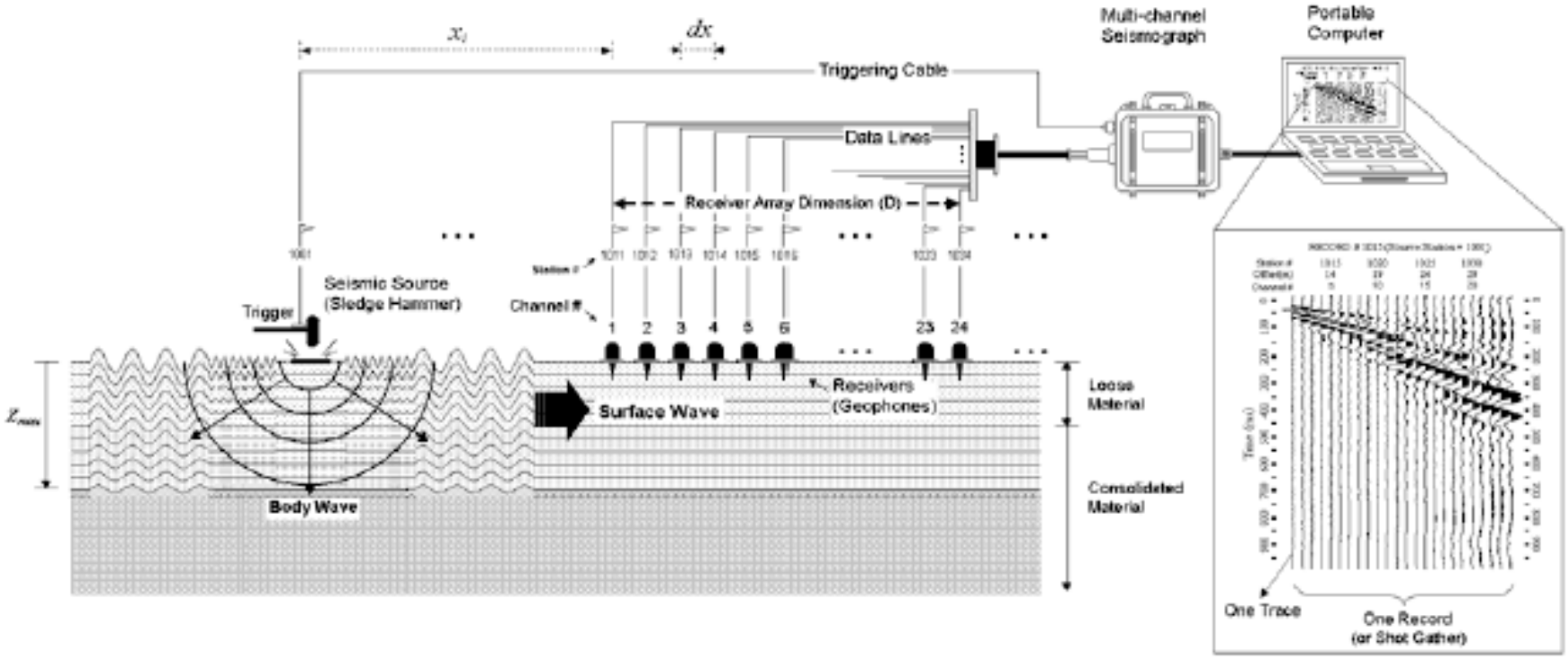

Stefano Parolai

Using seismic noise to estimate the characteristics of a site: MASW

The dispersion spectrum S(ω,*v*)from multichannel surface wave data is determined by the equation

$$S(\omega, v) = \int e^{-i(k-\omega/v)x} A(x,\omega)dx = \int e^{-i(\omega/V-\omega/v)x} A(x,\omega)dx \qquad (5)$$

A(ω) is the normalized energy spectrum fro each receiver, *k* the wavenumber, ω the circular frequency, *v* the assumed phase velocity and *V* the phase velocity for a given frequency

When *v* is equal to *V* , S(ω,*v*) is maximized

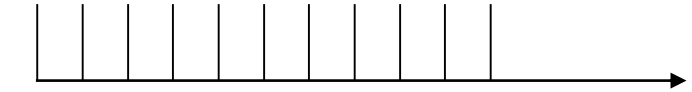

sampling

0 dt 2dt …… Ndt=T

Timet [s]

N intervals with spacing dt
Duration T of the whole signal
T=N*dt

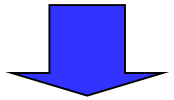

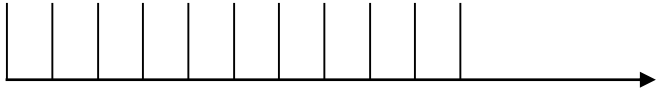

Sampling

N intervals of width df

Nyquist frequency: $f_N=1/(2*dt)$

$N*df=2f_N$ →

$df=2f_N/N=1/Ndt=1/T$

$-f_N$ $-f_N$ +df……. f_N

Frequency [Hz]

df=1/T df depends on the window length

df dt=1/N

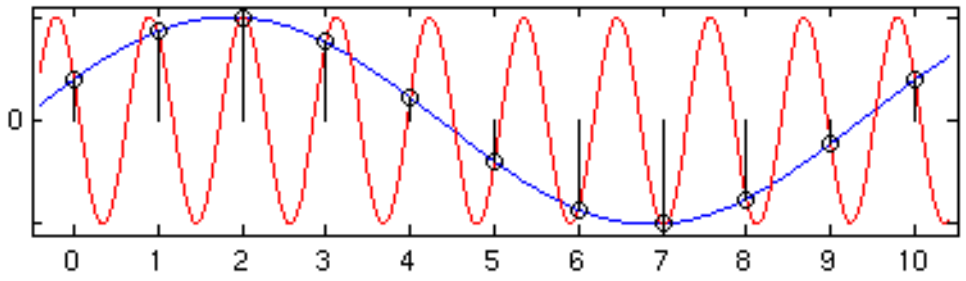

dt=1s;
→f_N=0.5Hz
f>0.5Hz cannot be retrieved en
(Periods T< 2 s)

The red curve has a period of T=1.1s
red: freq>Nyquist
Look at the blue curve!!!

Due to Aliasing the data must be low-pass filtered before the analog to digital conversion (anti-alias filter). The corner frequency of the filter $0.8f_{N.}$

Input: Time signal

signal $y(t_n)$

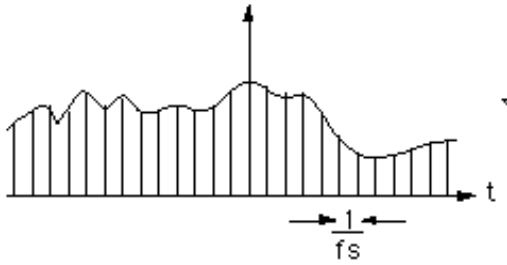

Fourierspectrum $Y(\omega)$

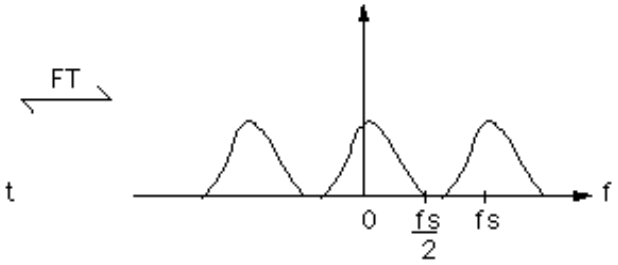

Sinus form **Period T**

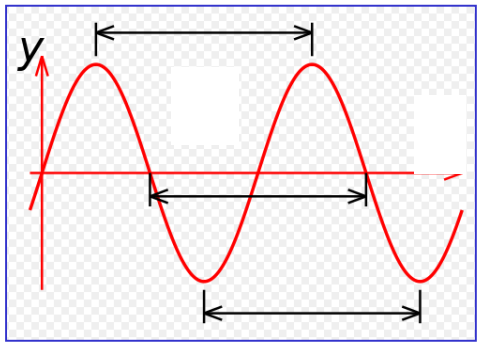

$fs=1/dt$ $f_{Nyquist}=fs/2$ $\omega=2\pi f=2\pi/T$ (angular frequency [rad/s])

(time) Aliasing

Signal $y(x_n)$

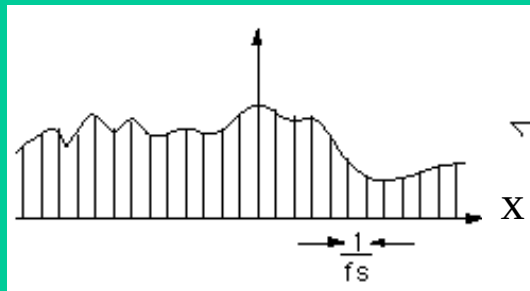

Fourierspectrum $Y(\kappa)$

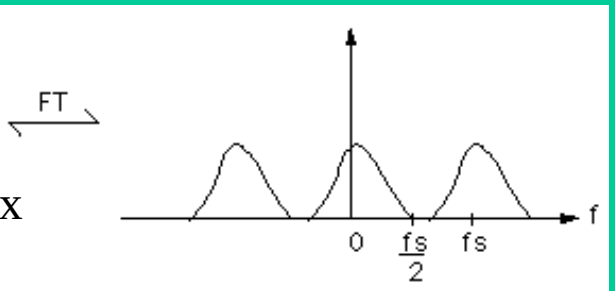

Sinus form **wavelength λ**

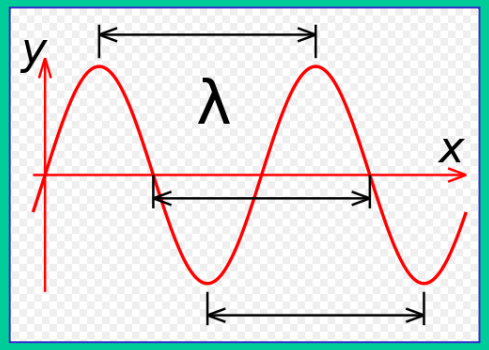

$fs=1/dx$ $f_{Nyquist}=fs/2$ $\kappa=2\pi f=2\pi/\lambda$

(Wavenumberl [rad/m])

(spatial) Aliasing

Using seismic noise to estimate the characteristics of a site

Aki in 1957 proposed the analysis of ambient seismic noise as a tool for investigating the S-wave velocity structure below a site. This S-wave velocity structure can be used to calculate the site response by numerical simulations. He derived dispersion curves by analyzing the correlation between noise recordings made at sites close to each other.

Using seismic noise to estimate the characteristics of a site : SPAC

Aki assumed that noise represents the sum of waves propagating in a horizontal plane in different directions with different powers, but with the same phase velocity for a given frequency. He also assumed that waves with different propagation directions and different frequencies are statistically independent. A spatial correlation function can therefore be defined as:

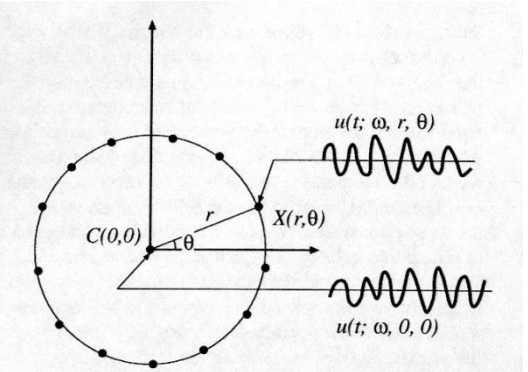

Figure 1. A schematic description of the symbols for the observation sites and the vertical component of the microseisms. $u(t; \omega, 0, 0)$ and $u(t; \omega, r, \theta)$ denote the harmonic waves at frequency ω, which are obtained at the center $C(0, 0)$ of the array and site $X(r, \theta)$ on the circle shown by "●".

after Morikawa et al. (2004)

$$\phi(r,\lambda) = < u(x,y,t)(x + r\cos(\lambda), y + r\sin(\lambda), t) > \qquad (1)$$

$u(x, y, t)$ is the velocity observed at point (x,y) at time t; r is the inter-station distance; λ is the azimuth and < > denotes the ensemble average

Using seismic noise to estimate the characteristics of a site : SPAC

An azimutal average of this function is given by:

$$\phi(r) = \frac{1}{\pi}\int_0^{\pi} \phi(r,\lambda)d\lambda \qquad (2)$$

The autocorrelation function is related to the power spectrum $\phi(\omega)$ by

$$\phi(r) = \frac{1}{\pi}\int_0^{\infty} \phi(\omega)J_0\left(\frac{\omega r}{c(\omega)}\right)d\omega \qquad (3)$$

Where J_0 ($\omega r/c(\omega)$) is the zeroth order Bessel function and $c(\omega)$is the frequency dependent phase velocity.

Using seismic noise to estimate the characteristics of a site : SPAC

The space-correlation function for one angular frequency ω_0, normalized to the power spectrum, will be of the form

$$\phi(r,\omega_o) = J_0\left(\frac{\omega_0}{c(\omega_0)}r\right) \qquad (4)$$

J_0 is the zero order Bessel function.
$c(\omega)$ is the frequency-dependent phase velocity

Using seismic noise to estimate the characteristics of a site : SPAC

For every couple of stations (fixed the distance r) the function $\phi(\omega)$ can be calculated in the frequency domain by means of (Malagnini et al., 1993; Ohori et al., 2002; Okada, 2003):

$$\phi(\omega) = \frac{\frac{1}{M}\sum_{m=1}^{M} \mathrm{Re}\left({}_m S_{jn}(\omega)\right)}{\sqrt{\frac{1}{M}\sum_{m=1}^{M} {}_m S_{jj}(\omega) \sum_{m=1}^{M} {}_m S_{nn}(\omega)}} \qquad (5)$$

where ${}_mS_{jn}$ is the cross-spectrum for the *m*th segment of data, between the *j*th and the *n*th station, and *M* is the total number of used segments. The power spectra of the *m*th segment at station *j* and station *n* are ${}_mS_{jj}$ and ${}_mS_{nn}$, respectively.

After azimuthal integration and Fourier transformation, the spatial correlation function can be calculated for a given angular frequency ω_0 (normalized to the power spectrum)

$$\phi(r,\omega_o) = J_0\left(\frac{\omega_0}{c(\omega_0)}r\right)$$

J_0 Bessel function of 0th order
$c(\omega)$ frequency-dependent phase velocity

For each pair of stations (with distance r) can $\phi(\omega)$ be calculated using the spectra (Malagnini et al., 1993; Ohori et al., 2002; Okada, 2003):

$$\phi(\omega) = \frac{\frac{1}{M}\sum_{m=1}^{M}\mathrm{Re}\left({}_mS_{jn}(\omega)\right)}{\sqrt{\frac{1}{M}\sum_{m=1}^{M}{}_mS_{jj}(\omega)\sum_{m=1}^{M}{}_mS_{nn}(\omega)}}$$

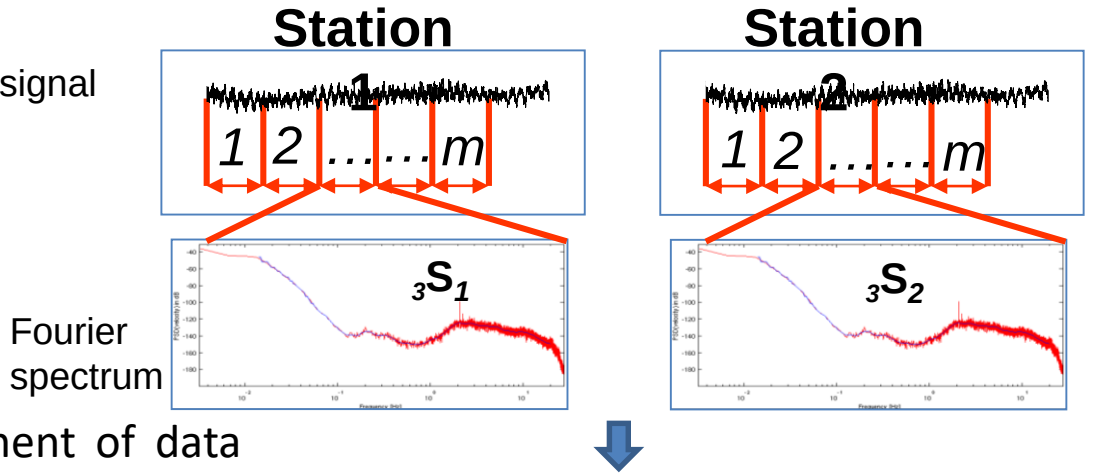

${}_mS_{jn}$ Cross-spectrum of the m-ten segment of data (between the j-th and the n-th station)
M is the number of segment of data
For ${}_mS_{jj}$ and ${}_mS_{nn}$ the same is valid.

Using seismic noise to estimate the characteristics of a site : SPAC

Spatial correlation values $\phi(\omega)$ are plotted as function of distance. A grid search procedure is applied to find the $c(\omega)$ that gives the best fit to the data

$$RMS = \sqrt{\frac{\sum_{n=1}^{N}\left[\bar{\rho}(r_n, f_o) - J_o\left(\frac{2\pi f_o r_n}{c(f_o)}\right)\right]^2}{N}}$$

High frequencies lose coherency at shorter distances

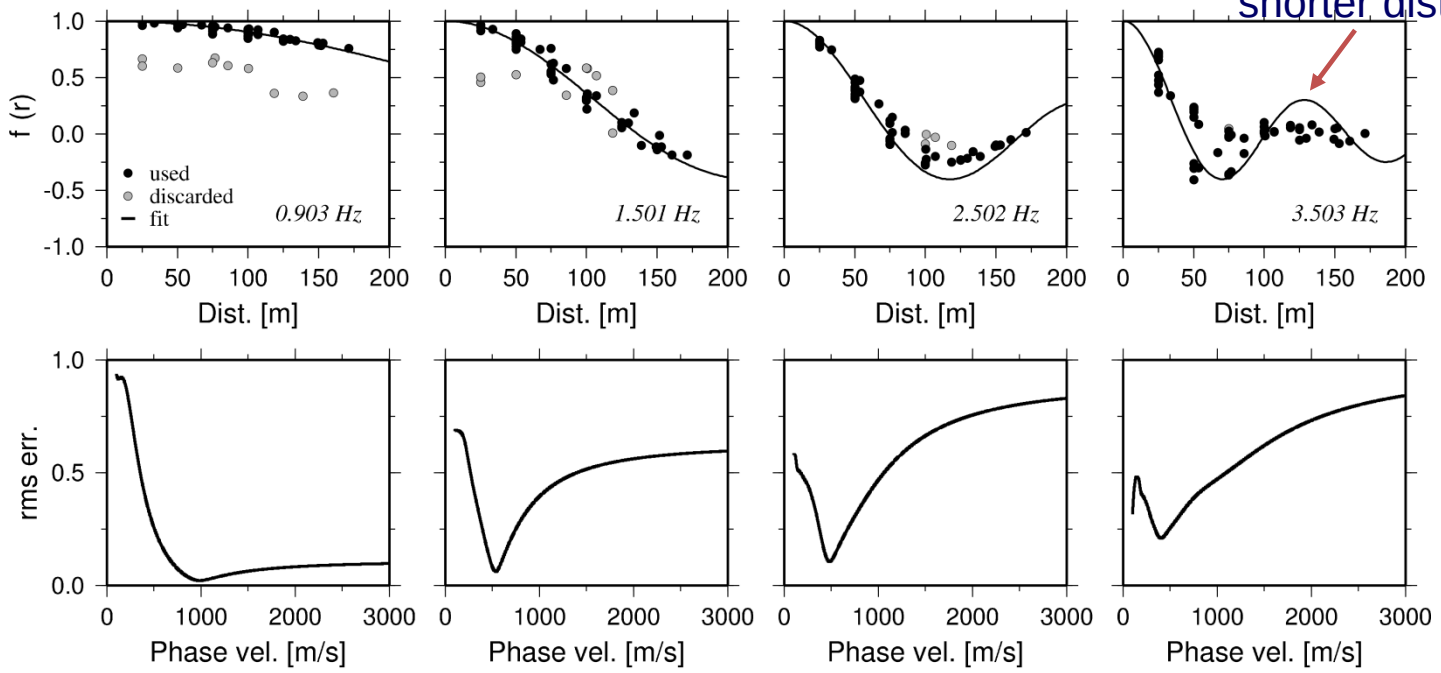

Using seismic noise to estimate the characteristics of a site : SPAC

Observed and calculated spatial correlation values $\phi(\omega)$ for all the considered frequencies

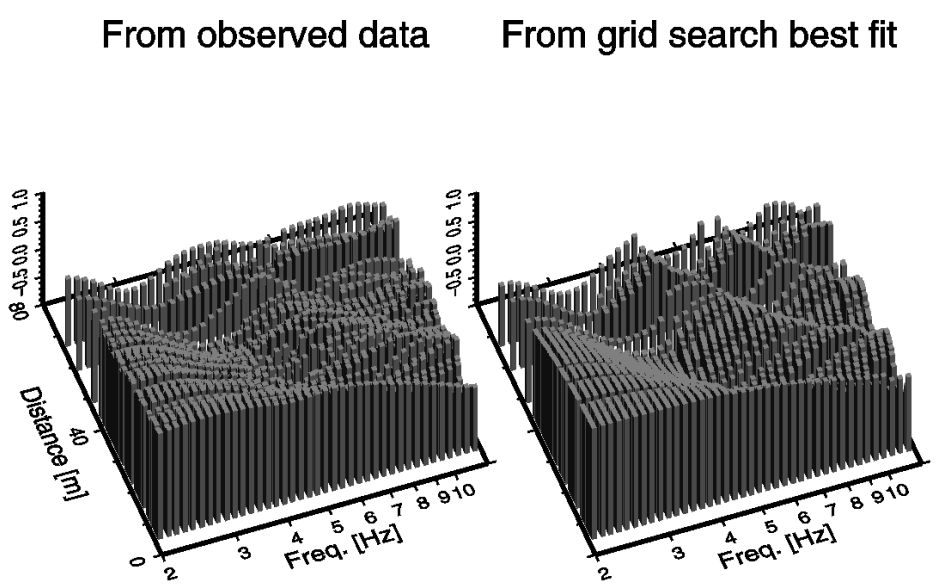

Using seismic noise to estimate the characteristics of a site : SPAC

The $c(\omega)$ values plotted versus the frequency provide the dispersion curve. Since the phase velocity is related to the S-wave velocity structure of the site, the dispersion curve can be inverted to obtain the model that allows to better justify the observed data.

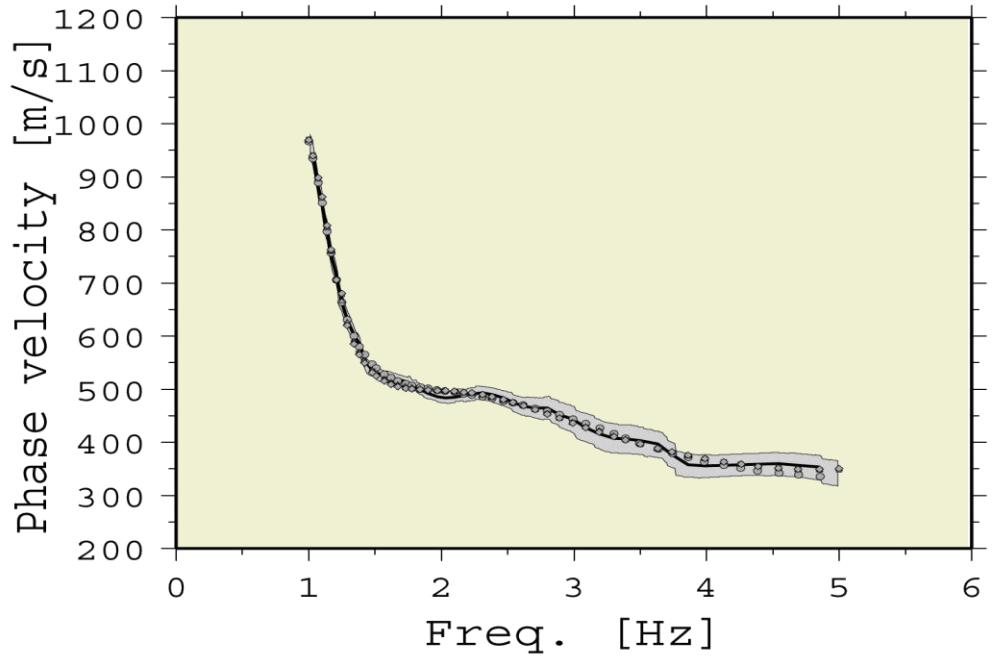

Using seismic noise to estimate the characteristics of a site : BFM

The estimate of the frequency-wavenumber (F-K) spectra *Pb(f,k)* by the Beam Forming Method is given by:

$$P_b(f,k) = \sum_{l,m=1}^{n} \phi_{lm} \exp\{ik(X_l - X_m\} \qquad (4)$$

Where *f* is the frequency, *k* the two-dimensional horizontal wavenumber vector, *n* the number of sensors. ϕ_{lm} is the estimate of the cross-power spectra between the *l*-th and the *m*-th data, X_i and X_m, are the coordinated of the *l*-th and the *m*-th sensors, respectively.

Using seismic noise to estimate the characteristics of a site : MLM

The Maximum Likelihood Method gives the estimate of the F-K spectra *Pm*(*f*,*k*) as:

$$P_m(f,k) = \left(\sum_{l,m=1}^{n} \phi_{lm}^{-1} \exp\{ik(X_l - X_m\} \right)^{-1} \qquad (5)$$

Where *f* is the frequency, *k* the two-dimensional horizontal wavenumber vector, *n* the number of sensors. Φ_{lm}^{-1} is the element of the corresponding inverse of the matrix Φ_{lm} , X_i and X_m, are the coordinated of the *l*-th and the *m*-th sensors, respectively.

Using seismic noise to estimate the characteristics of a site : MLM and BFM

The main difference between the two methods is the window function:

$$W_b(k,k_0) = \frac{1}{n^2}\sum_{l,m=1}^{n}\exp\{i(k-k_o)(X_l - X_m\} \quad (6)$$

BFM: determined only by sensor location

$$W_m(k,k_0) = \left|\sum_{j=1}^{n} A_j(f,k_0)\right| W_b(k,k_0) \quad (7)$$

$$A_j(f,k_0) = \left(\sum_{l=1}^{n}\left(\phi_{jl}\exp\{ik_0(X_j - X_l)\}\right)^{-1}\right) \Big/ \sum_{j,l=1}^{n}\left(\phi_{jl}\exp\{ik_0(X_j - X_l)\}\right)^{-1} \quad (8)$$

MLM: depends also on the quality of the data

Capon (1969) showed that the resolving power of the MLM is higher than the BFM, however the MLM is more sensitive to measurements errors.

Using seismic noise to estimate the characteristics of a site : BFM and MLM

From the peak in the F-K spectrum occurring a coordinates k_{xo} and k_{yo} for a certain frequency f_0 the phase velocity c_0 can be calculated by:

$$c_0 = \frac{2\pi f_0}{\sqrt{k_{xo}{}^2 + k_{y0}{}^2}} \qquad (9)$$

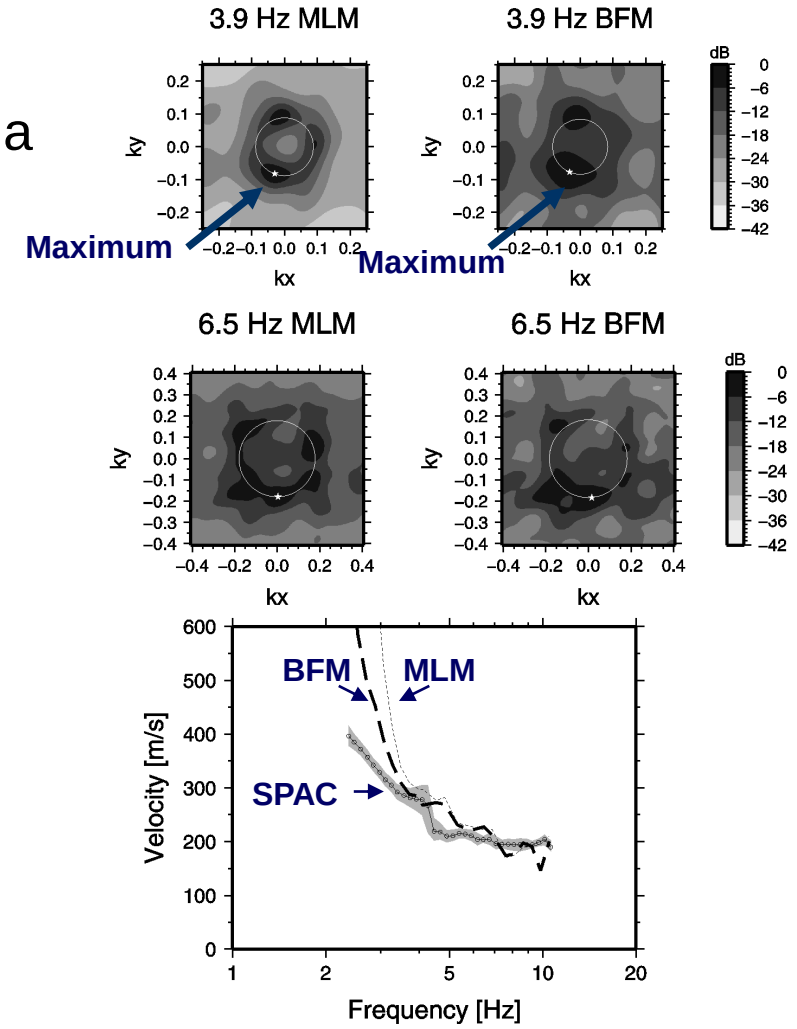

Using seismic noise to estimate the characteristics of a site : MLM and BFM

The array transfer function depends on the array geometry and varies depending on the frequency of the observed signal.

$$\left|C(k_0 - k)\right|^2 = \left|\frac{1}{n}\sum_{j=1}^{n} \exp\left\{i\ (k_o - k)(X_l - X_m\right\}\right|^2 \quad (10)$$

The array transfer function always exibits a central peak the value of which is 1 and lateral aliasing peaks with amplitude smaller than 1.

The position of the aliasing peaks define the maximum *k* that can be used for the chosen array geometry.

The thinner the central peak is, the more capable is the array to distinguish between waves travelling at close wave-numbers.

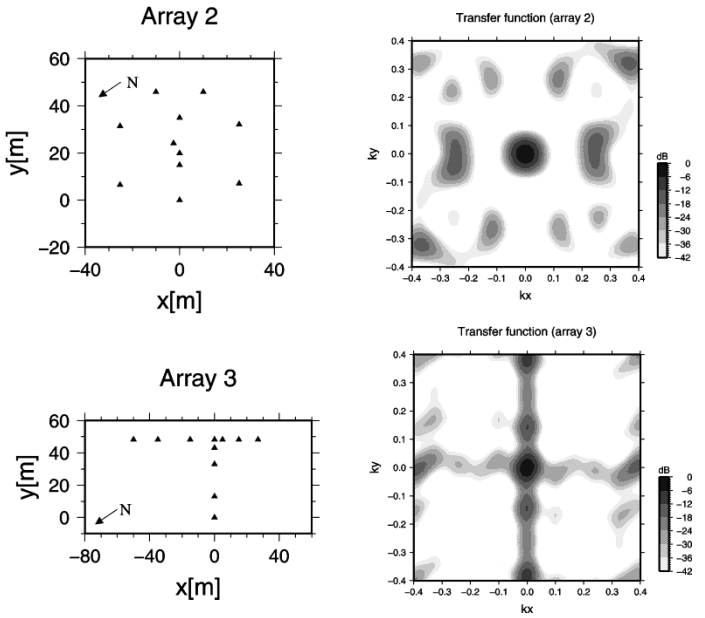

Using seismic noise to estimate the characteristics of a site : BFM and MLM

Deconvolution of the array transfer function

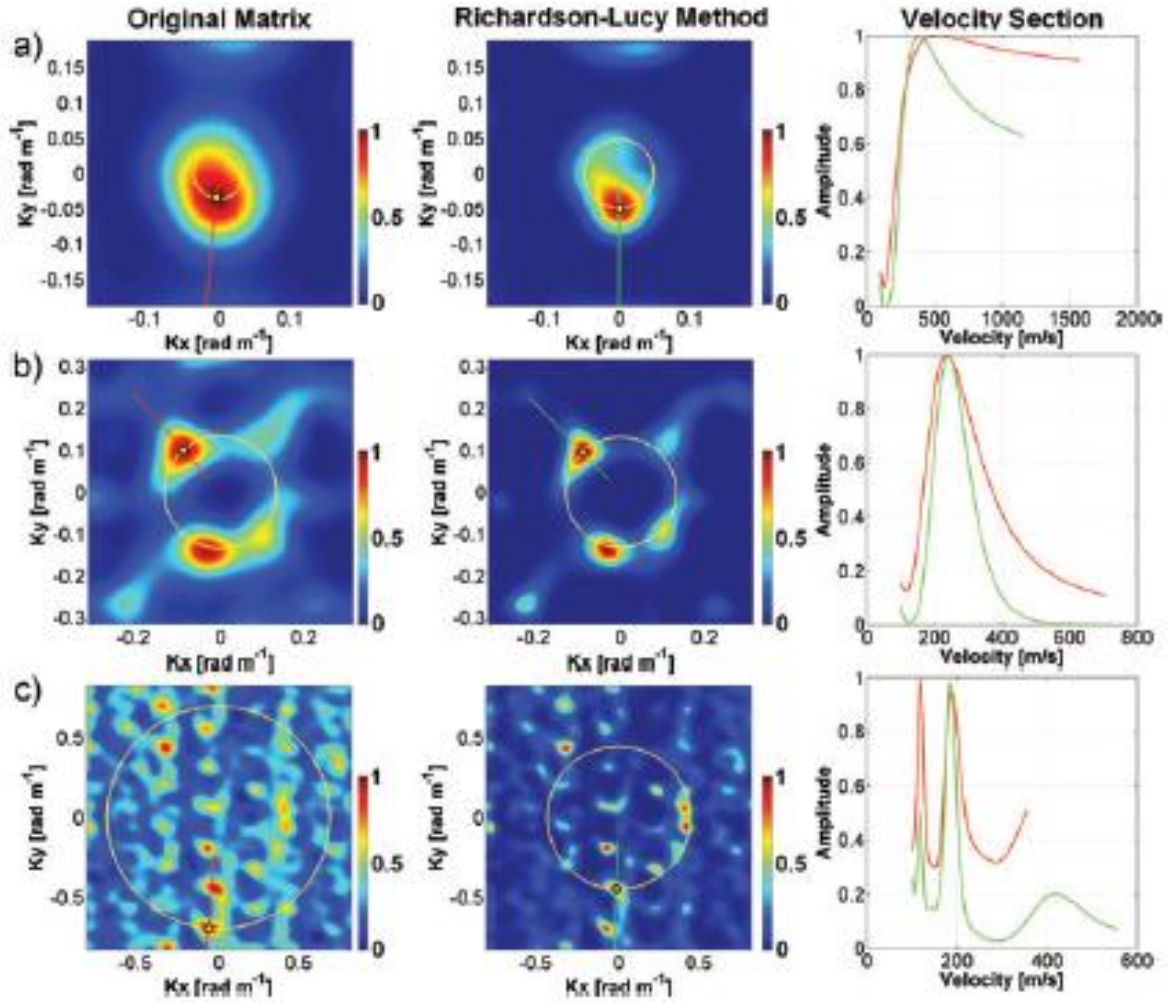

Figure 6. Results of the *f*–*k* analysis for Array 1 data set using the BFM. (a) Panels for the frequency 3Hz. Original matrix (panel *a* – left-hand panel), Richardson–Lucy method matrix (panel *a* – middle panel), Velocity sections for the input matrix (red) and for the deconvolved matrix (green) (panel *a* – right-hand panel). (b) Same as (a), but for frequency 5 Hz. (c) Same as (a), but for frequency 13 Hz. Yellow dots indicate the position of the maximum used to estimate the phase velocity. The yellow circle joins points with the same *k* value.

Picozzi et al . (2010)

The F-K spectra *Pm*(*f*,*k*) methods allow to check the azimuthal distribution of the noise sources at each frequency.

The ESAC method (under the condition that noise is stationary in space and time) appears to be more suitable than F-K analysis for providing reliable dispersion curves over a larger –extended toward lower frequency- frequency range (i.e. larger depth of investigation up to more than 2 times the array dimension)

Using seismic noise to estimate the characteristics of a site : Summary

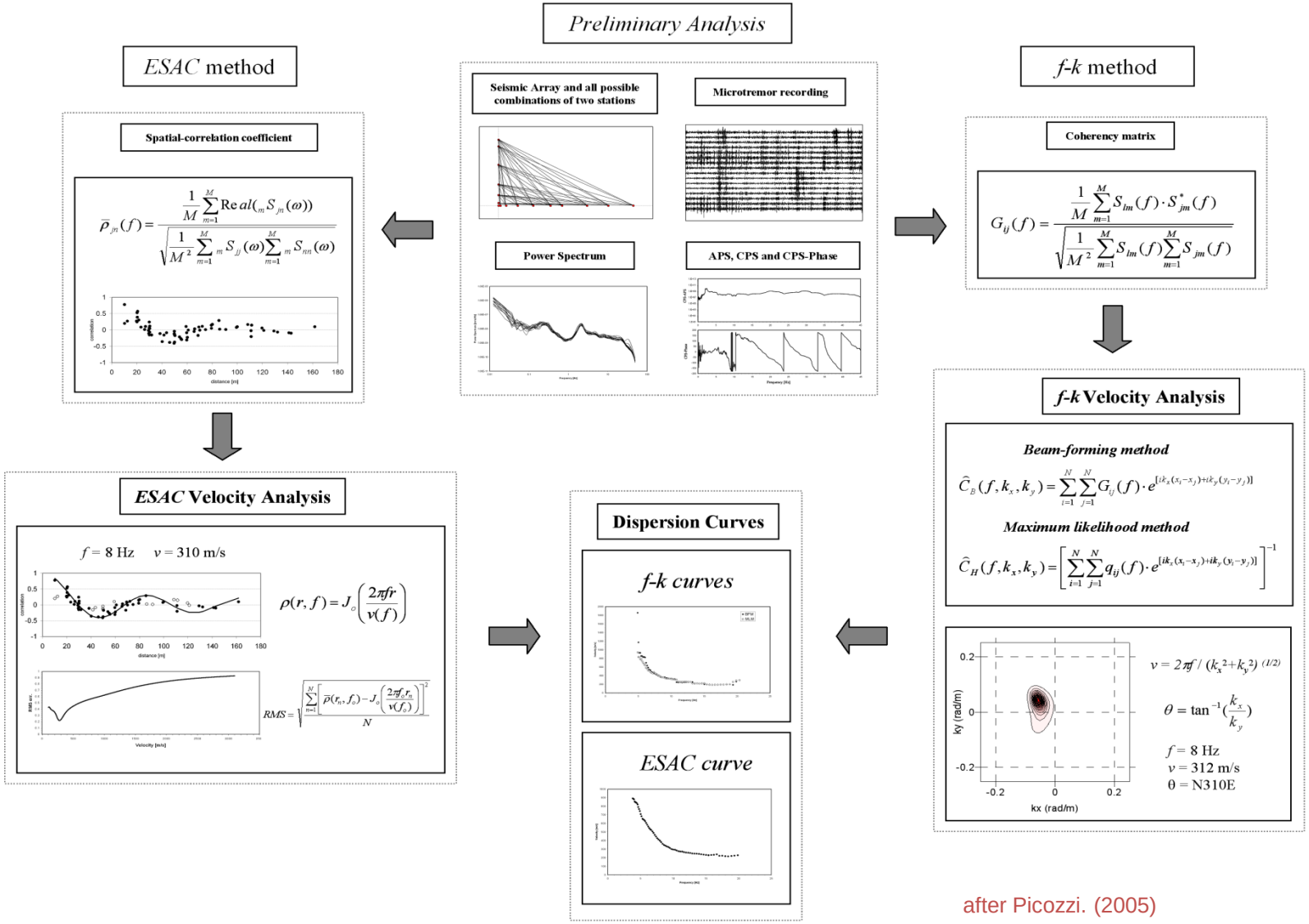

after Picozzi. (2005)

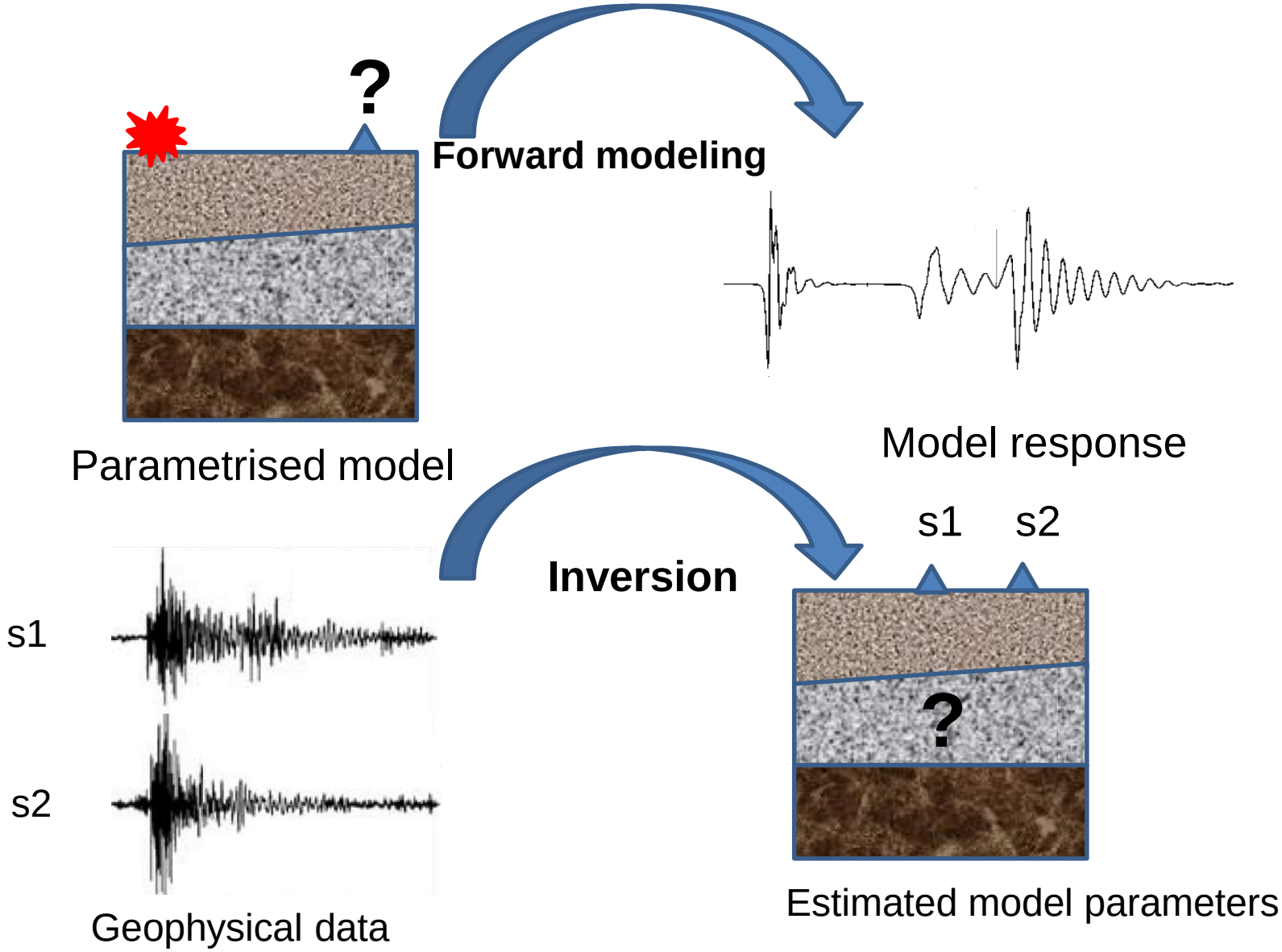
?
Forward modeling
Parametrised model
Model response
s1
s2
Inversion
s1
s2
?
Geophysical data
Estimated model parameters

Acoustic Tomography

Characterisation of the structure from travel times

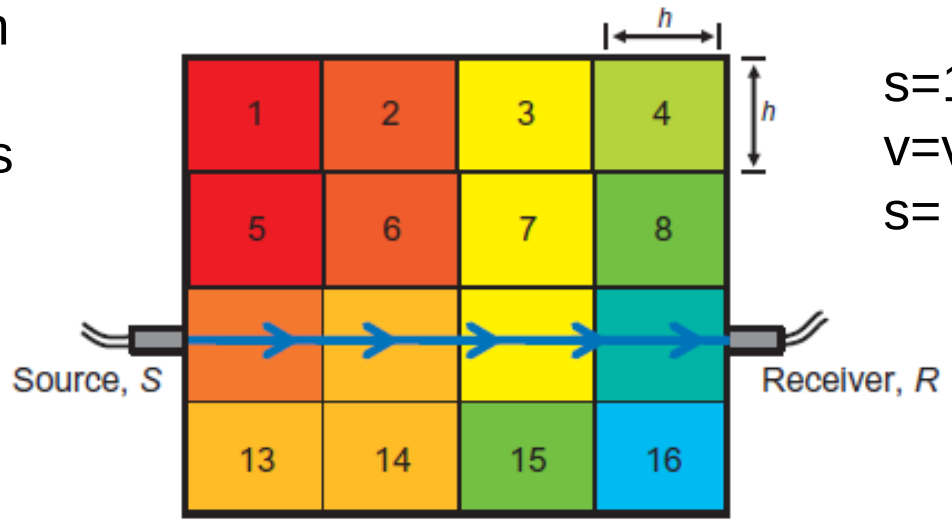

s=1/v
v=velocity
s= slowness

Reihe 1 $: T_1 = hs_1 + hs_2 + hs_3 + hs_4$
Reihe 2 $: T_2 = hs_5 + hs_6 + hs_7 + hs_8$
.
.
Reihe 8 $: T_8 = hs_4 + hs_8 + hs_{12} + hs_{16}$

$$\begin{bmatrix} T_1 \\ T_2 \\ \vdots \\ T_8 \end{bmatrix} = h \begin{bmatrix} 1 & 1 & 1 & 1 & 0 & 0 & 0 & 0 & 0 & 0 & 0 & 0 & 0 & 0 & 0 & 0 \\ 0 & 0 & 0 & 0 & 1 & 1 & 1 & 1 & 0 & 0 & 0 & 0 & 0 & 0 & 0 & 0 \\ \vdots & \vdots & \vdots & \vdots & \vdots & \vdots & \vdots & \vdots & \vdots & \vdots & \vdots & \vdots & \vdots & \vdots & \vdots & \vdots \\ 0 & 0 & 0 & 1 & 0 & 0 & 0 & 1 & 0 & 0 & 0 & 1 & 0 & 0 & 0 & 1 \end{bmatrix} \begin{bmatrix} s_1 \\ s_2 \\ \vdots \\ s_{16} \end{bmatrix}$$

after Menke (2012)

Acoustic Tomography

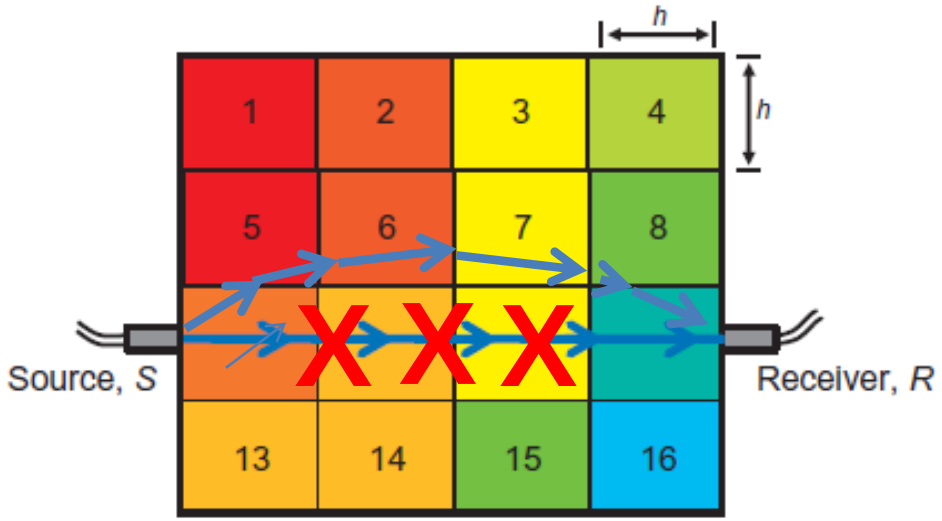

But the paths depend on the velocity!
Non linear

after Menke (2012)

Differences between linear and non linear problems

In a **linear problem** the misfit function *S(m)* has only **one global minima**

In a **non-linear problem** there are **more local minima** of the misfit function *S(m)*

linear Problem

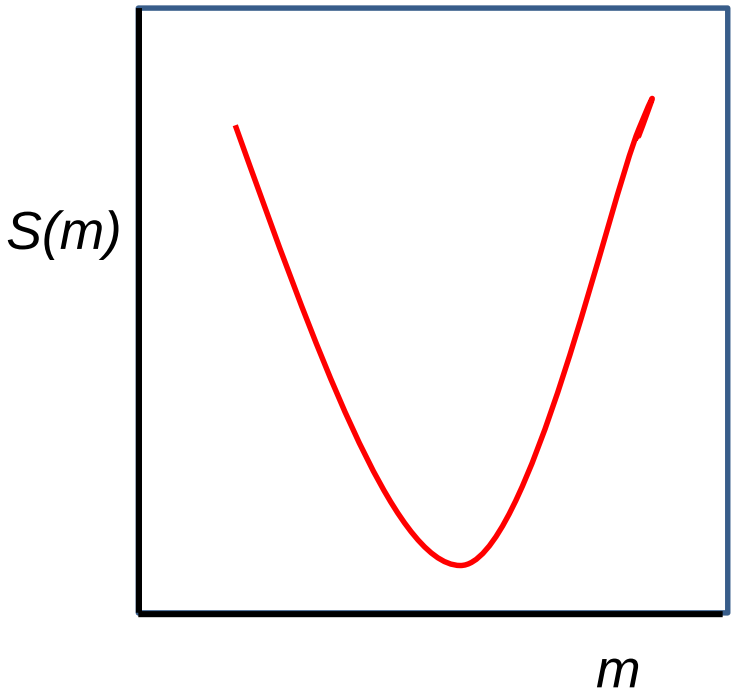

Non Linear Problem

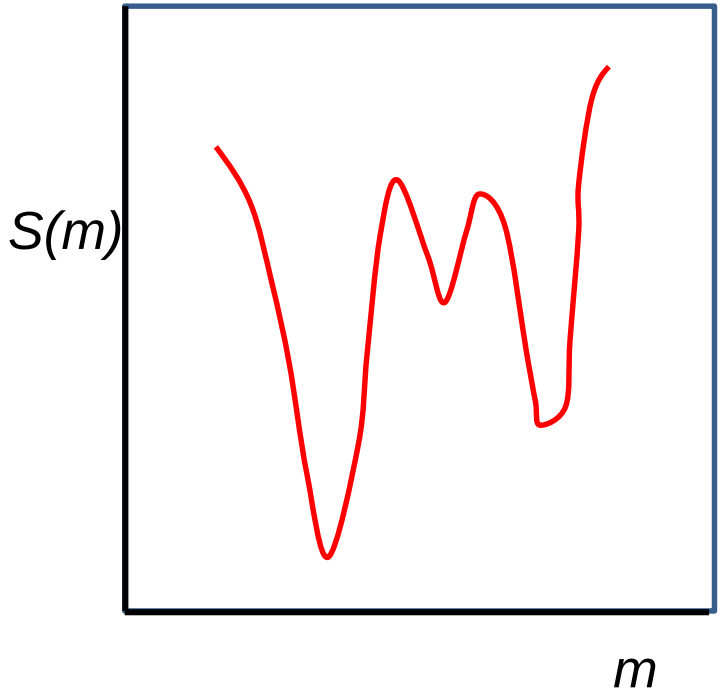

S(m) is the *misfit function* and can be calculated as the root mean square of the residuals between observed (T_r) and theoretical (z.B. T_o) data..

Exploration= minimizing the misfit by looking randomly in different region of parameter space without considering what was learned from previous samples

Exploitation: one decide where to sample by using the previous sample or the current best fit one only.

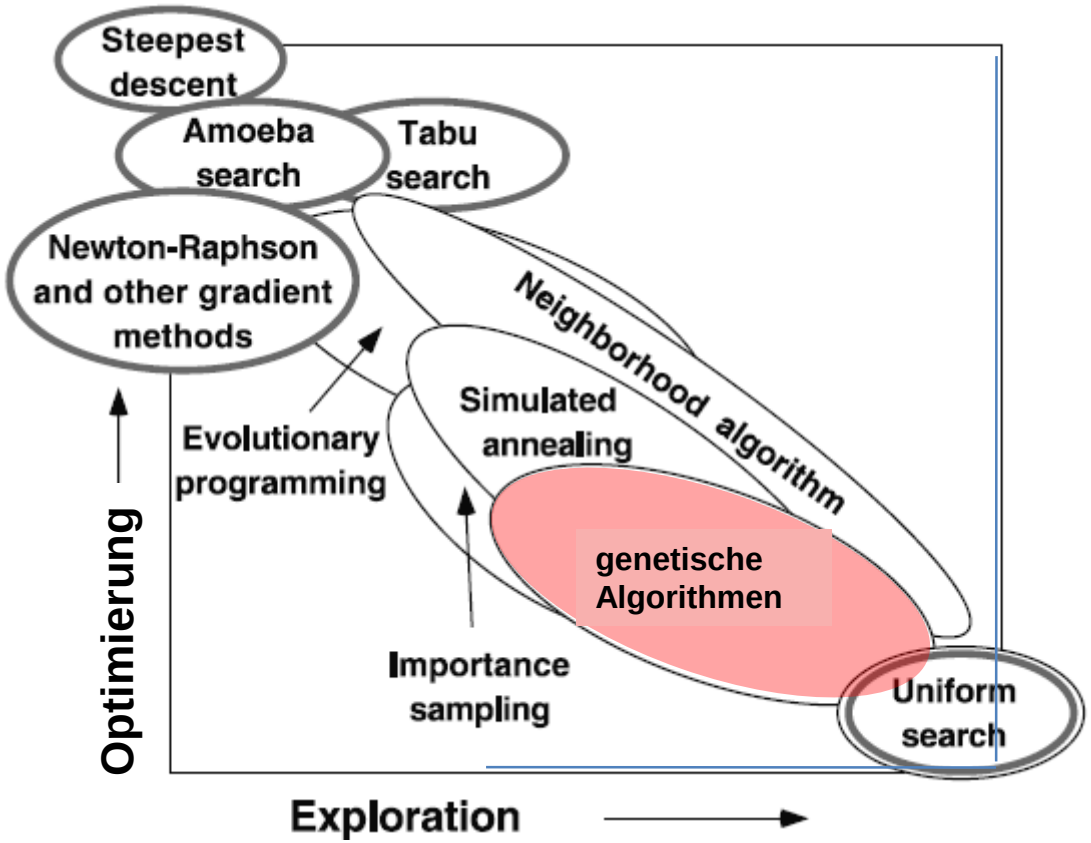

Inversion of surface waves
An example of non linear Problem

Analysis of Surface waves

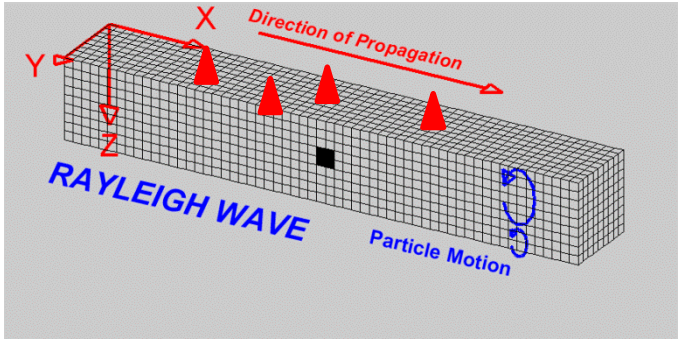

Seismic stations

Calculation of phase velocities

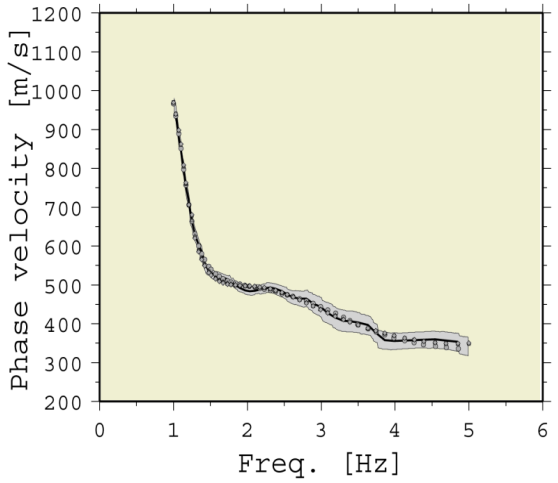

Inversion

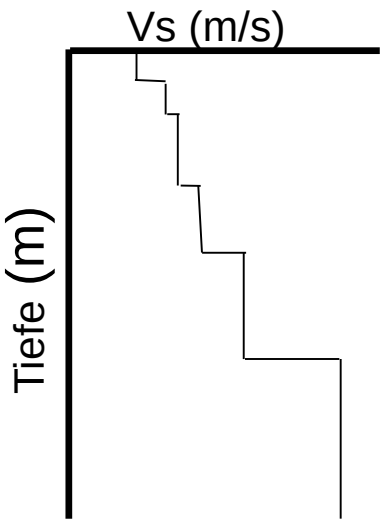

$$\begin{bmatrix} C(\omega 1) \\ \vdots \\ C(\omega i) \end{bmatrix} = \begin{bmatrix} \frac{\delta C(\omega 1)}{\delta Vs1} & \cdots\cdots & \frac{\delta C(\omega 1)}{\delta Vsj} \\ & \vdots & \\ \frac{\delta C(\omega i)}{\delta Vs1} & \cdots\cdots & \frac{\delta C(\omega i)}{\delta Vsj} \end{bmatrix} \begin{bmatrix} \Delta Vs1 \\ \vdots \\ \Delta Vsj \end{bmatrix}$$

QUI Using seismic noise to estimate the characteristics of a site : Inversion

The dispersion curves of the fundamental and higher mode Rayleigh waves mainly depend non-linearly on the S-wave velocity structure, but also the density and P-wave velocity structure.

The inversion can be carry out **linearizing** the problem, that is calculating the Jacobian matrix that links the model parameters to the phase velocity.

$$C = J\Delta V \qquad (11)$$

Where C= vector whose i elements are the $c_{obsi}(\omega)$-$c_{calci}(\omega)$

J=matrix with i rows and j (number of unknown, e.g. S-wave velocity in each layer) whose elements are $\delta\, c_{calci}(\omega)/\, \delta Vs_j$
ΔV is an array whose j elements are the correction values of the starting j layer velocities

The inverse problem can be solved using Singular Value Decomposition (SDV, Press et al., 1986) and the RMS of differences between observed and theoretical phase velocities is generally minimized.
However the final results strongly depends on the starting model!

C=JΔV

In the vector **C**, each *i* Element represents, **$C = c_{obs}(\omega) - c_{cal}(\omega)$**

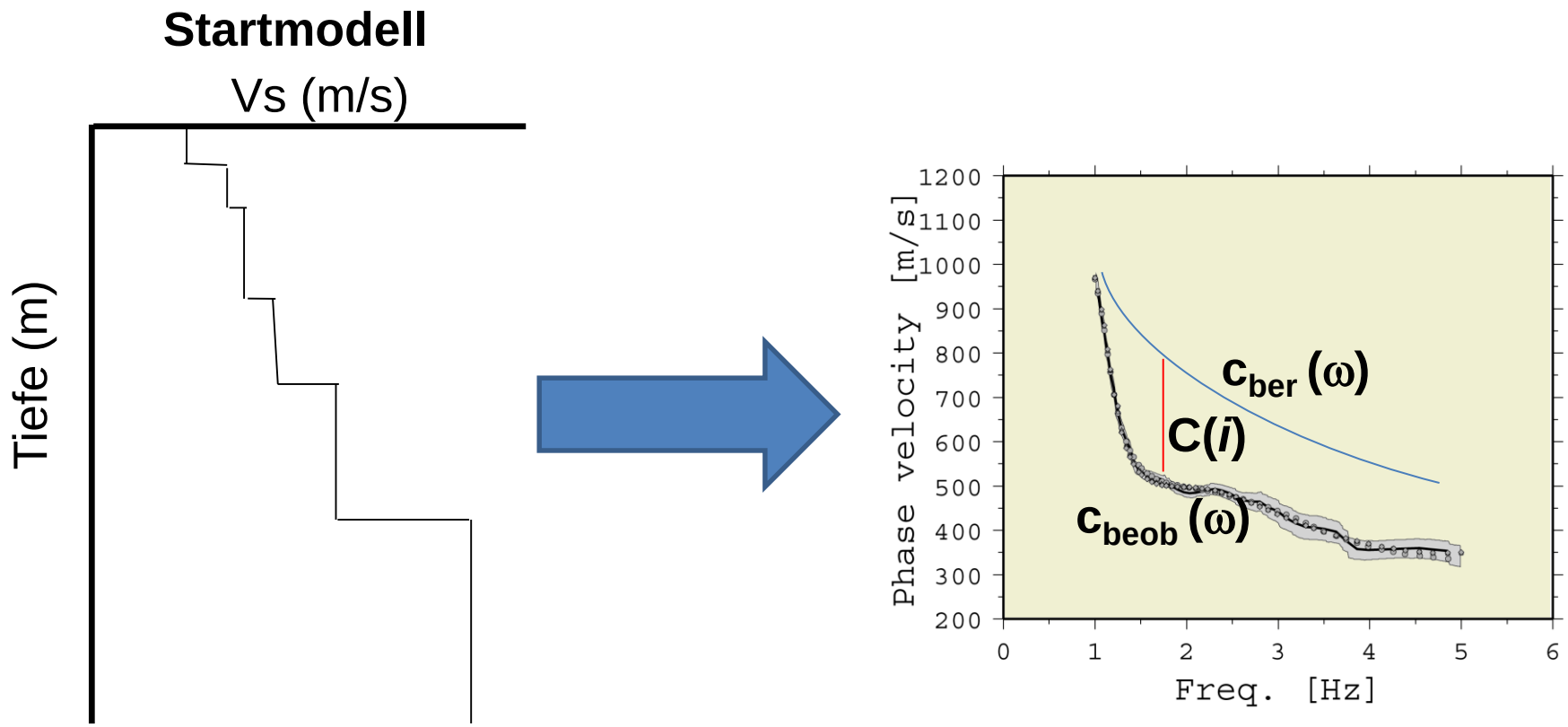

The Jacobian Matrix J=matrix with i rows and j (number of unknown, e.g. S-wave velocity in each layer) whose elements are $\delta c_{calci}(\omega)/ \delta Vs_j$
ΔV is an array whose j elements are the correction values of the starting j layer velocities

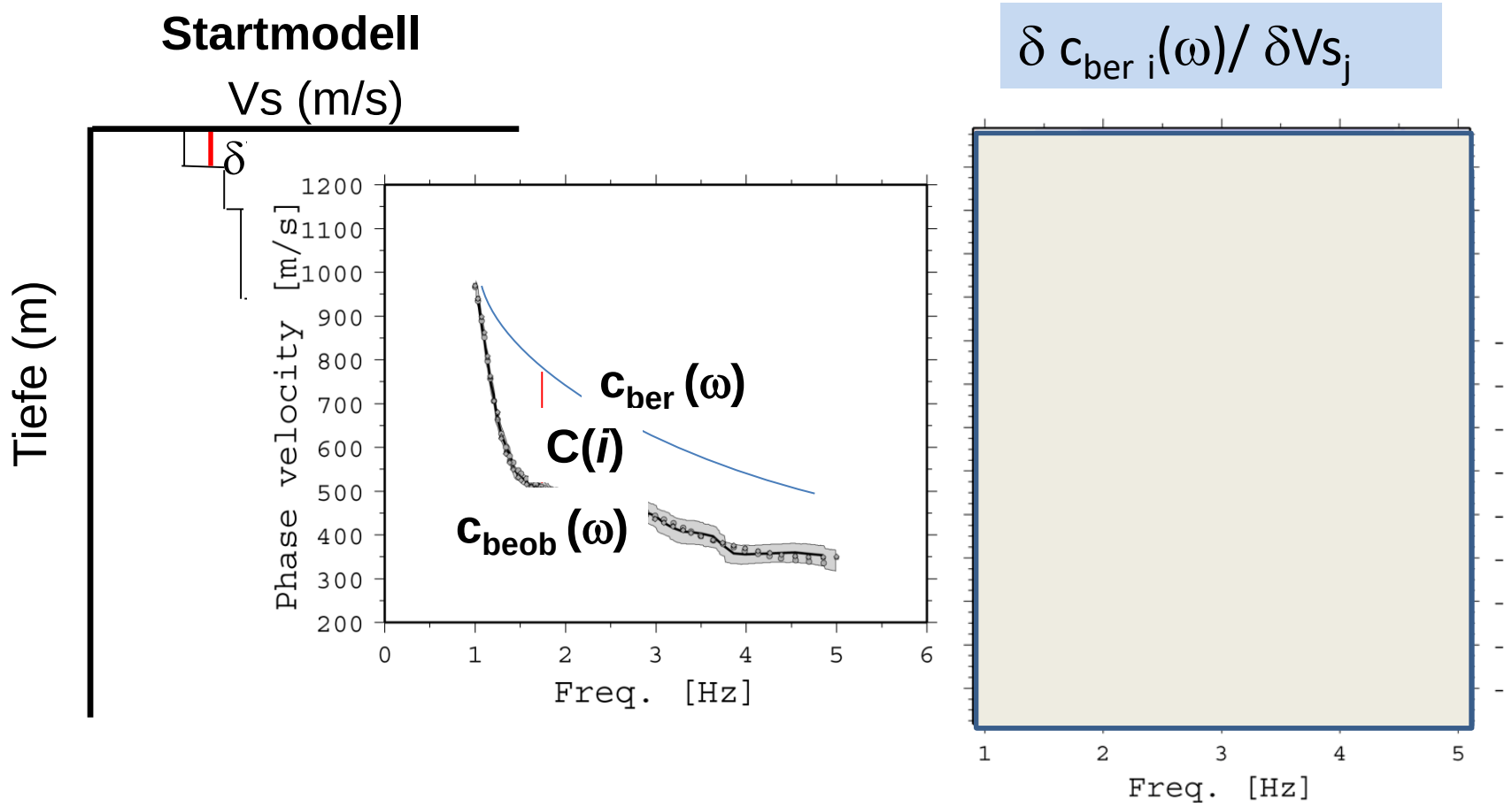

The inverse problem can be solved using Singular Value Decomposition (SDV, Press et al., 1986) and the RMS of differences between observed and theoretical phase velocities is generally minimized.

However the final results strongly depends on the starting model!

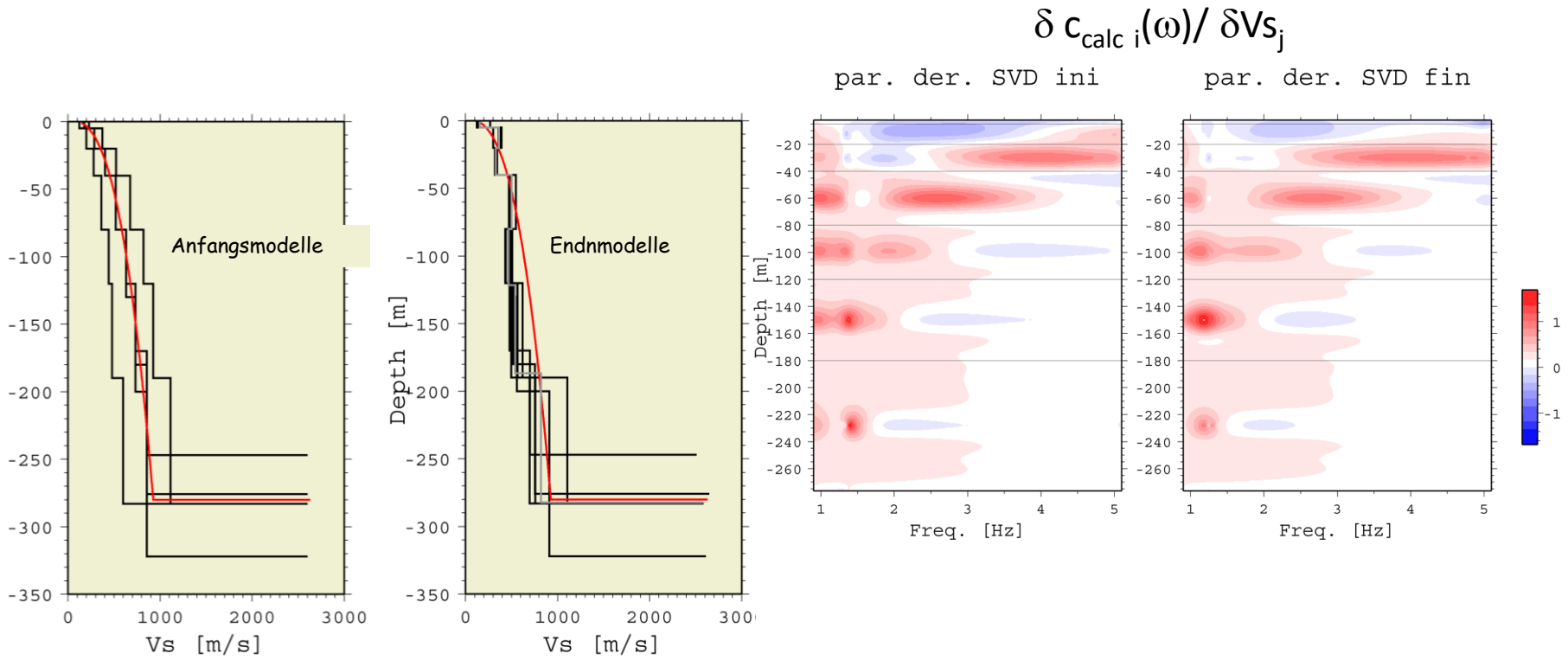

The elements of the Jacobian matrix shows that high frequency only sample the shallowest model layers. Lower frequencies allow to investigate deeper.

Other methods can be used to solve the non-linear problem.

Parolai et al. (2005), following Yamanaka and Ishida (1996) adopted the non-linear optimization method that uses a genetic algorithm (e.g. Goldberg, 1989). In contrast to linearized inversion schemes, this method requires only an evaluation of the functions, not their derivatives.

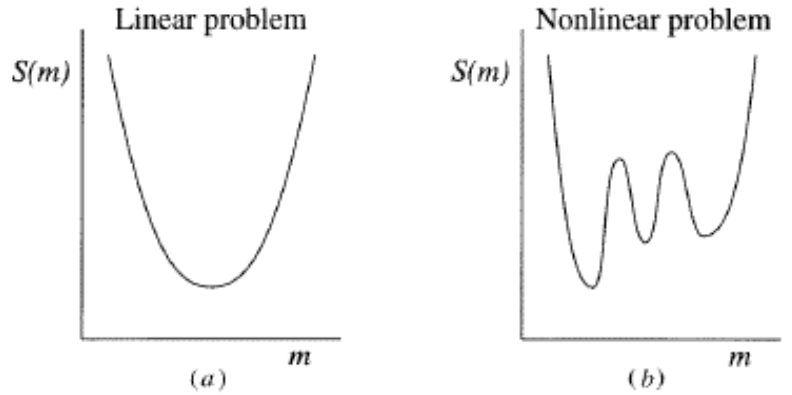

Modified Genetic Algorithm *(GA; Yamanaka and Ishida, 1996)*

With this algorithm, a search area is defined both for the S-wave velocity and thickness of the layers. An initial population of 30 individuals is generated. *Yamanaka and Ishida* [1996] adopted the binary representation (*bin*) for each model. For the *bin*, each parameter (e.g. Vs or thickness) in the search area is digitized with a *n*-bit binary string of 2^n. In other words, parameters at the lower and upper limits became (00…0) and (11…1), respectively. genetic operations (cross-over and mutation) are applied in order to generate a new population with the same size. This new population is reproduced based on a fitness function f_j for each individual

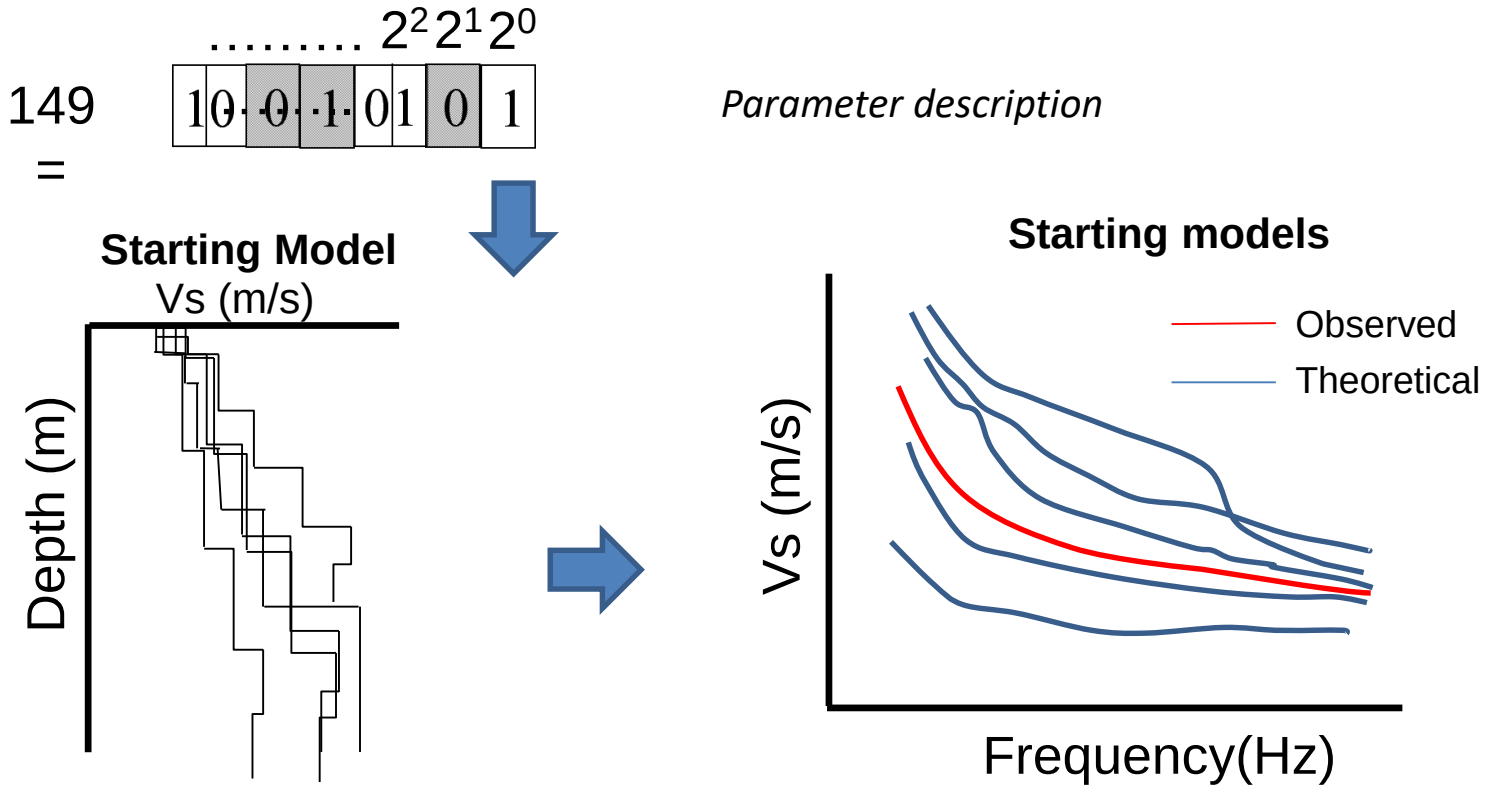

$$\phi_j = \frac{1}{N}\sum_{i=1}^{N}\left[\frac{(d_o)_i - (d_t)_i}{\sigma(d_o)_i}\right]^2$$

ϕ *misfit function* can be calculated as the average root-means-squares (*RMS*) of the differences between observed (d_o) and theoretical (d_t) data for each generated model *j*.

N is the number of data and $\sigma(d_o)_i$ is the standard deviation as regard the observed data *i*. If no uncertainty is provided, $\sigma(d_o)_i$ can be replaced by $(d_o)_i$

$$f_j = \frac{1}{\phi_j}$$

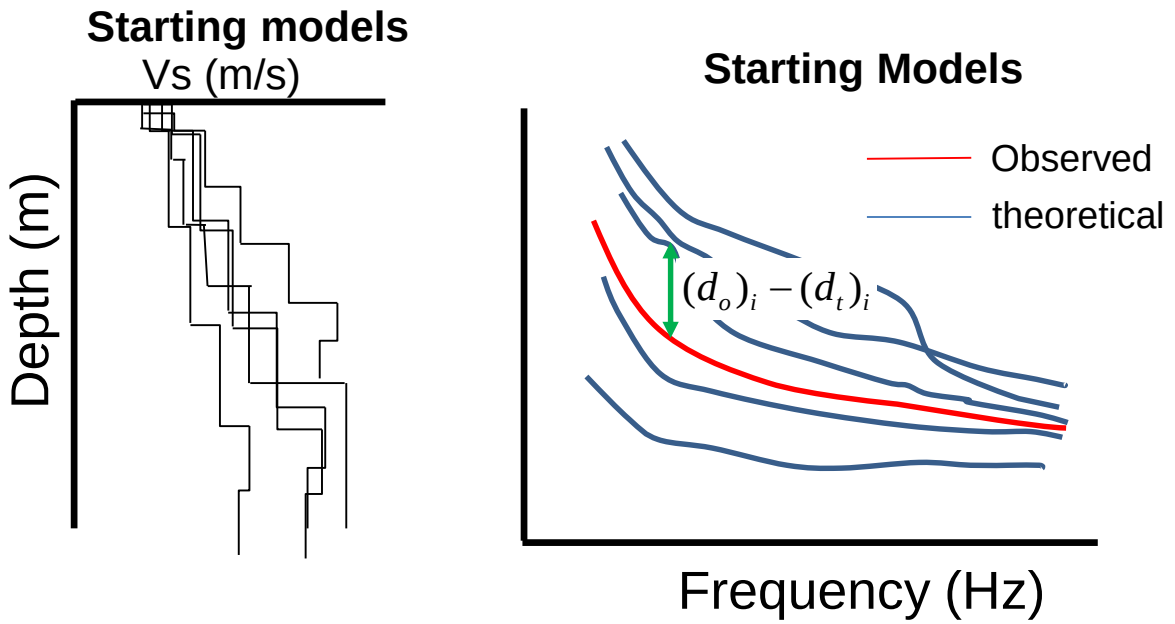

A probability of being reproduced for each model is calculated. In fact, it is realistic that models with higher values of f_i (or equivalently lower ϕ_i) should have higher probability of proceeding to the next model generation [*Gallagher and Sambridge*, 1994]. The probability, *pr*, for the *j*th individual of being reproduced is expressed in the form

$$p_r^j = \frac{f_j}{\sum_{k=1}^{Q} f_k}$$

Q is the number of generated models

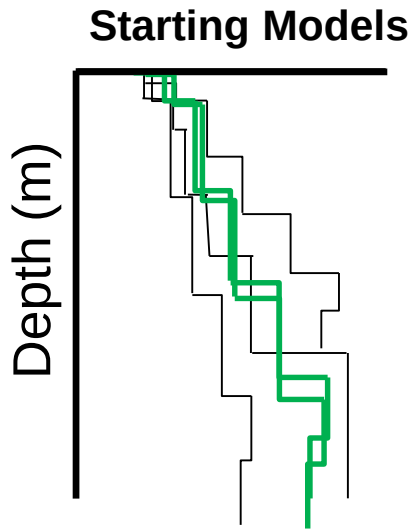

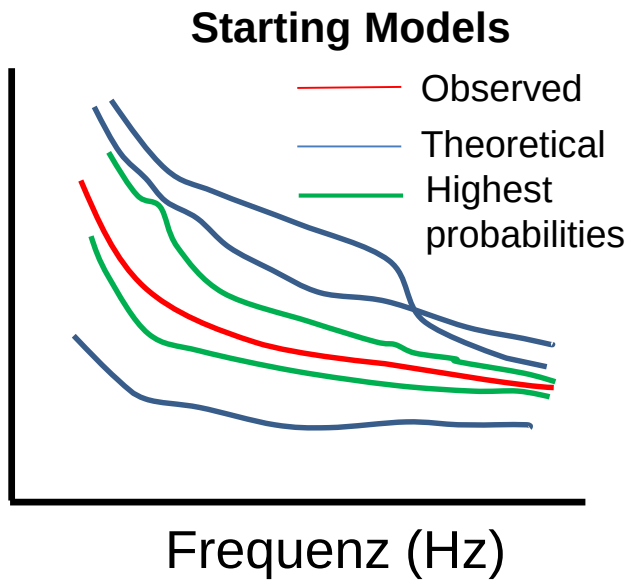

Genetic operations (**Crossover and Mutation**) are applied and a new population is generated. The new population will be than reproduced on the basis of a new misfit function.

The **crossover** operator is used to combine randomly desirable features contained within two (or more) "parent" selected models.

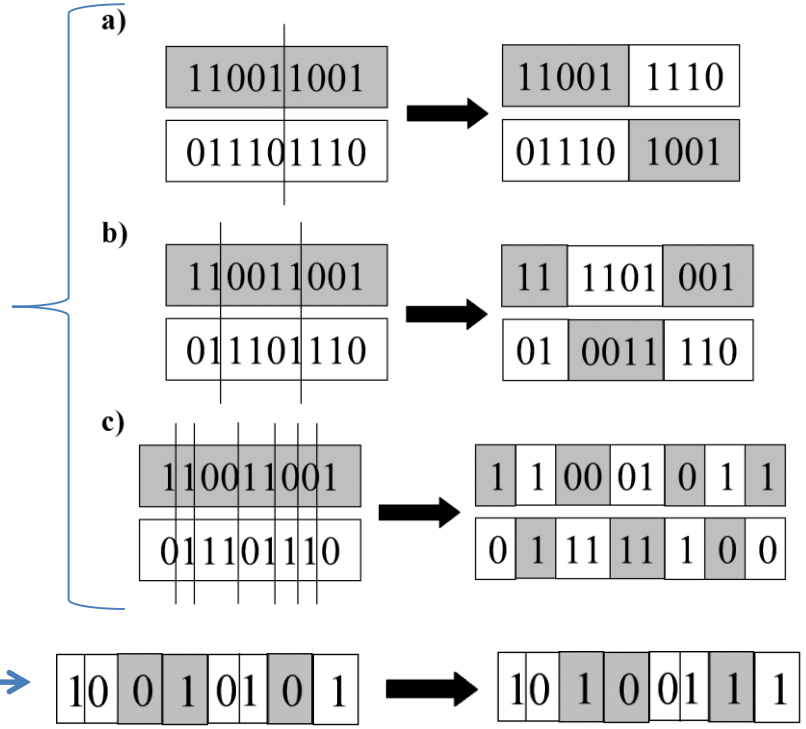

Mutation is a particular operator that considers each gene separately and has been introduced in *GA* with the aim of maintain a degree of diversity in the population (while on the contrary, crossover acts to remove diversity). Random variation of a bit

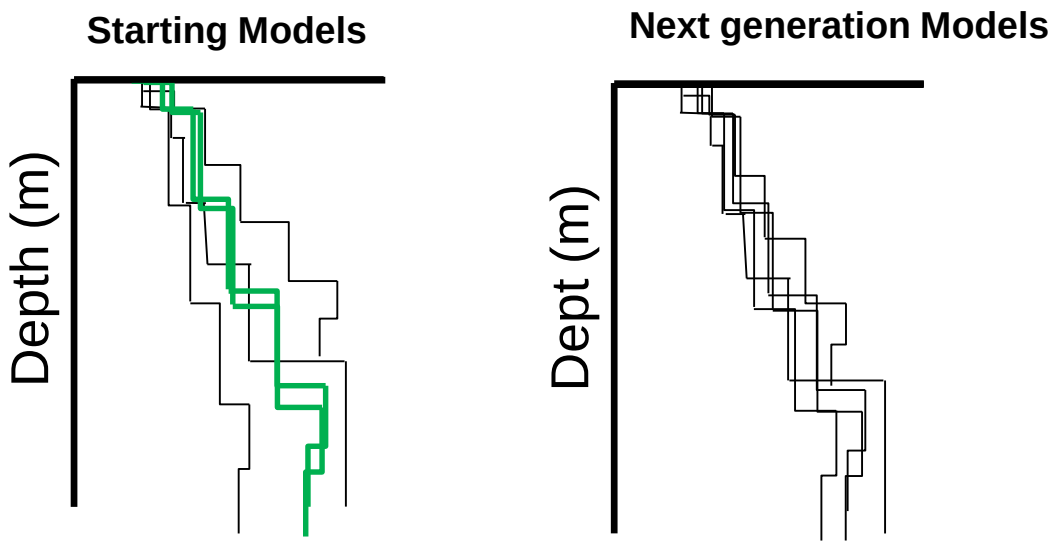

The **misfit function** is again calculated considering the differences between obserd and theoretical phase velocities

The fitness function can be defined considering the average of the differences between the observed and the theoretical phase velocities.

Two more genetic operations can be used to increase convergence, namely elite selection and dynamic mutation. Elite selection assures that the best model appears in the next generation, replacing the worst model in the current one. The dynamic mutation operation is used to increase the variety in the population, avoiding a premature convergence of the solution into a local minimum.

GA is a non-linear optimization method that simultaneously searches locally and globally for optimal solutions by using several models.

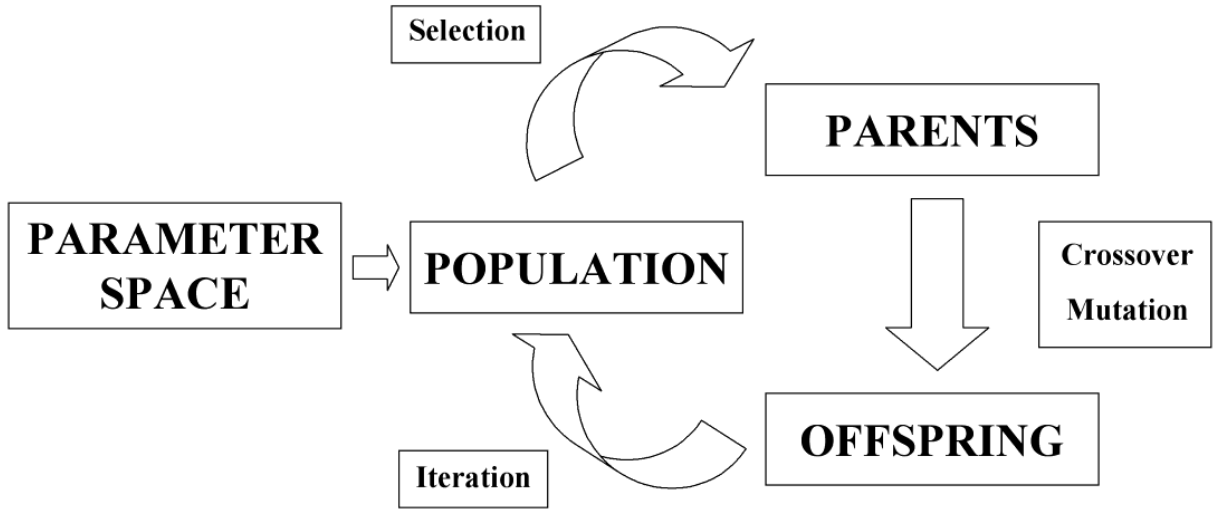

http://joinv.crs.ogs.it/test/

Joint inversion of Rayleigh, Love and H/V curves

$$\overline{\rho}_r(r,\omega_0) = \alpha\left[J_o\left(\frac{\omega_0}{c_R(\omega_0)}r\right) - J_2\left(\frac{\omega_0}{c_R(\omega_0)}r\right)\right] + (1-\alpha)\left[J_o\left(\frac{\omega_0}{c_L(\omega_0)}r\right) + J_2\left(\frac{\omega_0}{c_L(\omega_0)}r\right)\right],$$

$$\overline{\rho}_t(r,\omega_0) = \alpha\left[J_o\left(\frac{\omega_0}{c_R(\omega_0)}r\right) + J_2\left(\frac{\omega_0}{c_R(\omega_0)}r\right)\right] + (1-\alpha)\left[J_o\left(\frac{\omega_0}{c_L(\omega_0)}r\right) - J_2\left(\frac{\omega_0}{c_L(\omega_0)}r\right)\right],$$

$$\text{cost} = [(1-p-q)N + qM + pK]\left\{\frac{1-p-q}{N}\left[\sum_{j=1}^{N}\left(\frac{c_{R_o}(f)-c_R(f)}{c_{R_o}(f)}\right)^2\right] + \frac{q}{M}\left[\sum_{j=1}^{M}\left(\frac{c_{L_o}(f)-c_L(f)}{c_{L_o}(f)}\right)^2\right] + \frac{p}{K}\left[\sum_{j=1}^{K}\left(\frac{hv_o(f)-hv(f)}{hv_o(f)}\right)^2\right]\right\},$$

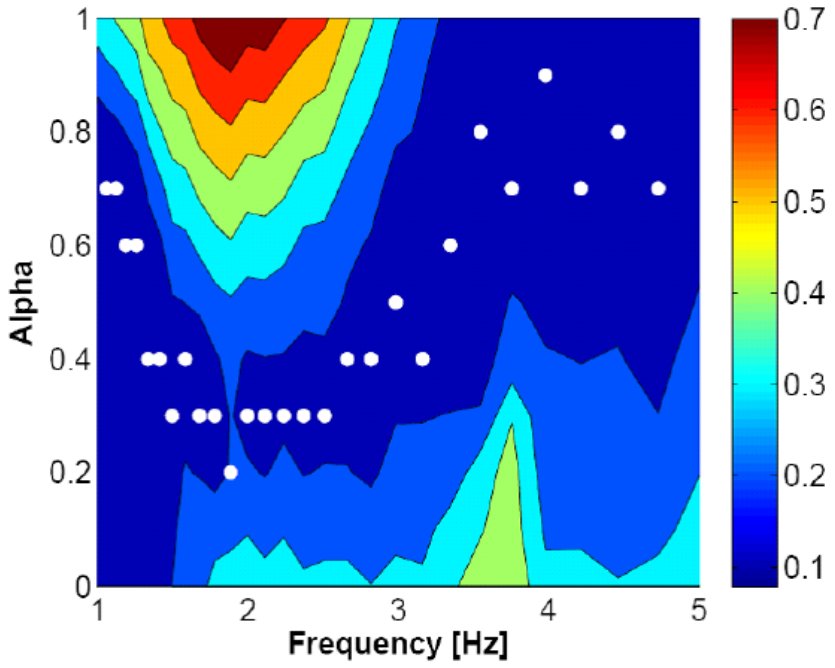

Figure 3: Distribution of α values (white dots) for different frequencies and the associated RMS error.

Joint inversion of Rayleigh, Love and H/V curves

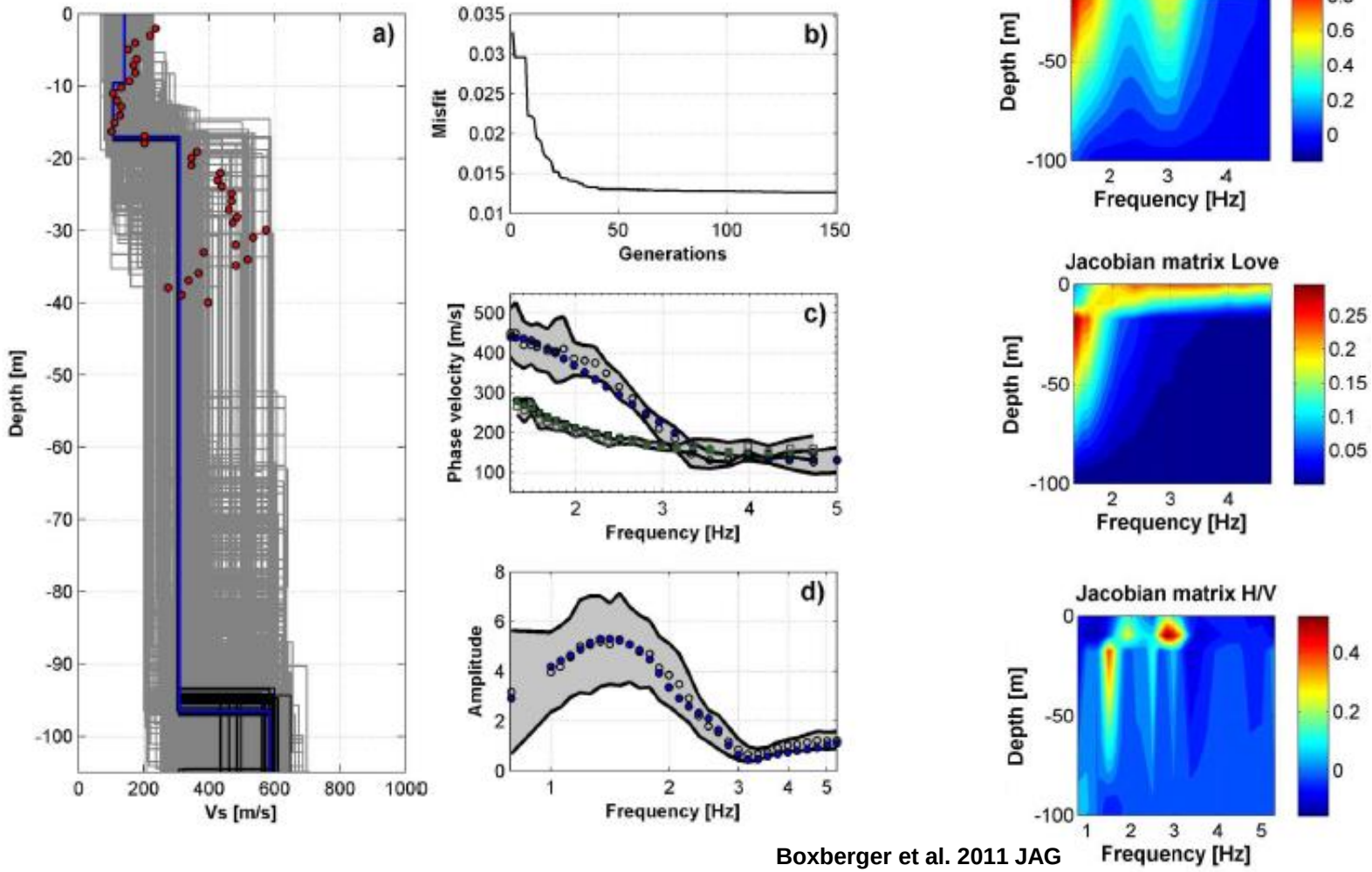

Boxberger et al. 2011 JAG

Joint inversion of reyleigh and H/V curve

Different models, same H/V but different dispersion curve

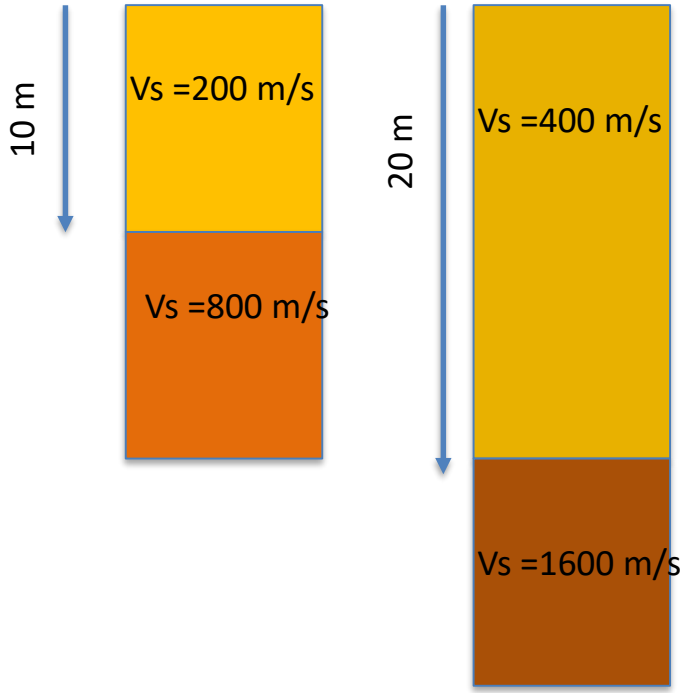

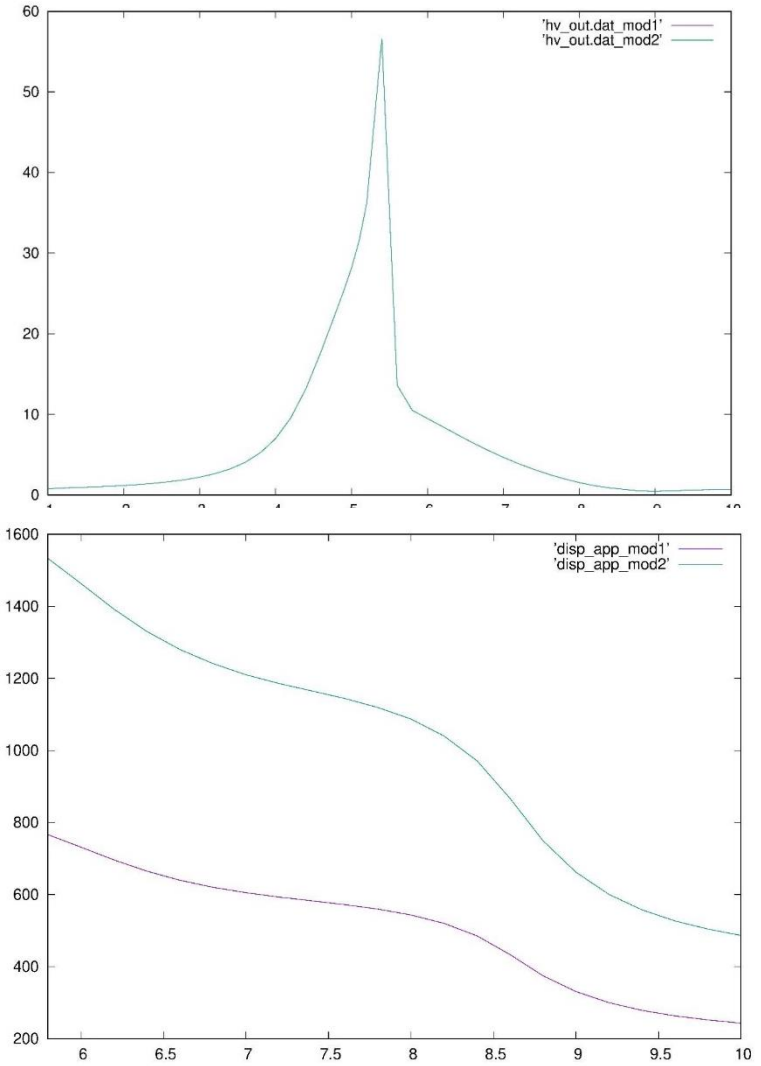

Estimation of the Quality factor

$$\varphi(r,\omega) = J_0\left(\frac{\omega}{c(\omega)}r\right)e^{-\alpha(\omega)r}$$

$$\alpha(\omega) = \frac{2\pi f}{2Q_r(\omega)c(\omega)}$$

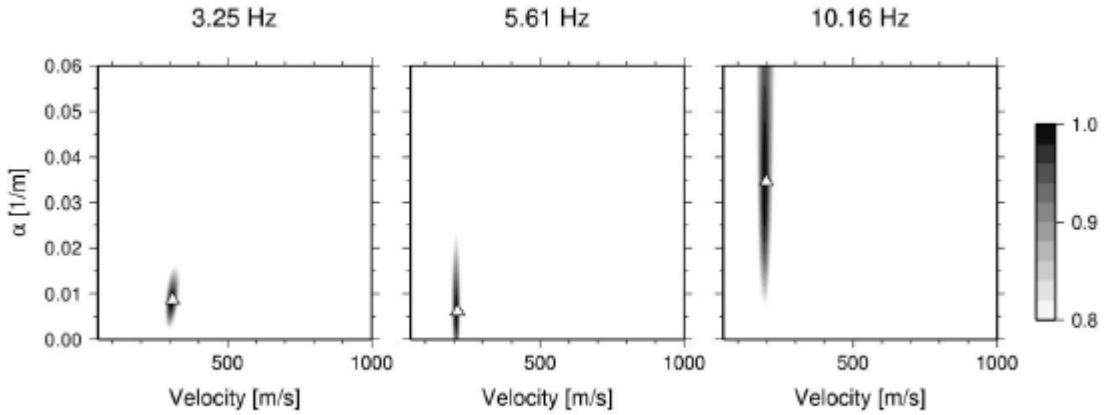

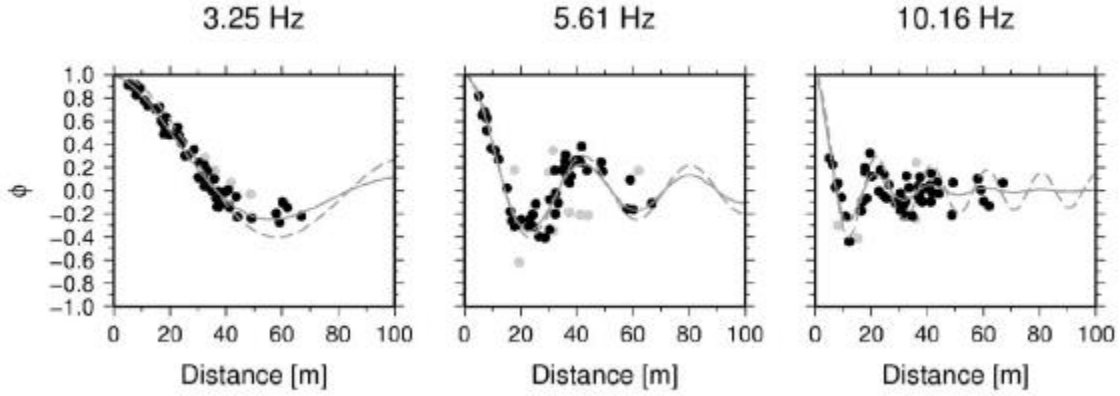

Parolai et al. 2014 JoSE

Estimation of the Quality factor

a)

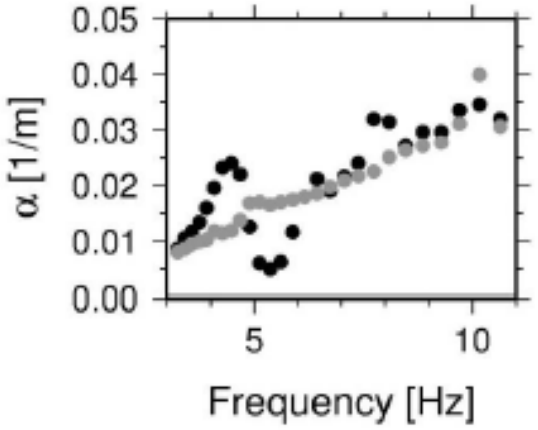

b)

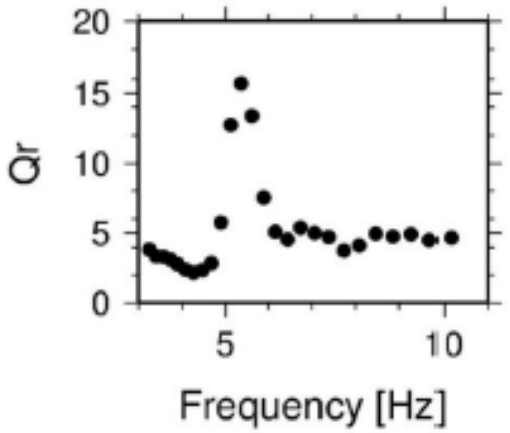

c)

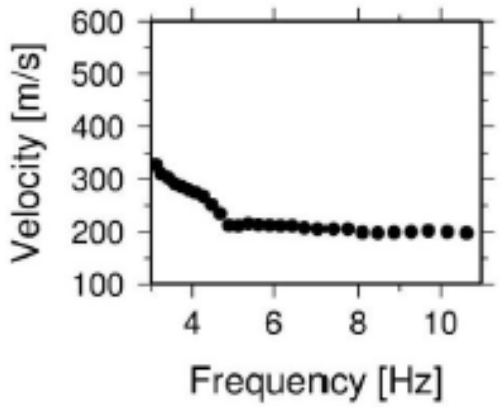

Estimation of the Quality factor

$$\alpha(\omega) = \frac{\omega}{2c(\omega)^2}\left[\sum_{i=1}^{m} Vpi \frac{\partial c(\omega)}{\partial Vpi} Qpi^{-1} + \sum_{i=1}^{m} Vsi \frac{\partial c(\omega)}{\partial Vsi} Qsi^{-1}\right]$$

$$\begin{bmatrix} \frac{\omega 1}{2c(\omega 1)^2} Vs1 \frac{\partial c(\omega 1)}{\partial Vs1} & \cdots & \frac{\omega 1}{2c(\omega 1)^2} Vsm \frac{\partial c(\omega 1)}{\partial Vsm} \\ \vdots & & \vdots \\ \frac{\omega n}{2c(\omega n)^2} Vs1 \frac{\partial c(\omega n)}{\partial Vs1} & \cdots & \frac{\omega n}{2c(\omega n)^2} Vsm \frac{\partial c(\omega n)}{\partial Vsm} \\ \lambda 1 & & \\ & \ddots & \\ & & \lambda m \end{bmatrix} \cdot \begin{bmatrix} Qs1^{-1} \\ \vdots \\ Qsm^{-1} \end{bmatrix} = \begin{bmatrix} \alpha(\omega 1) \\ \vdots \\ \alpha(\omega n) \\ 0_1 \\ \vdots \\ 0_m \end{bmatrix}$$

Estimation of the Quality factor

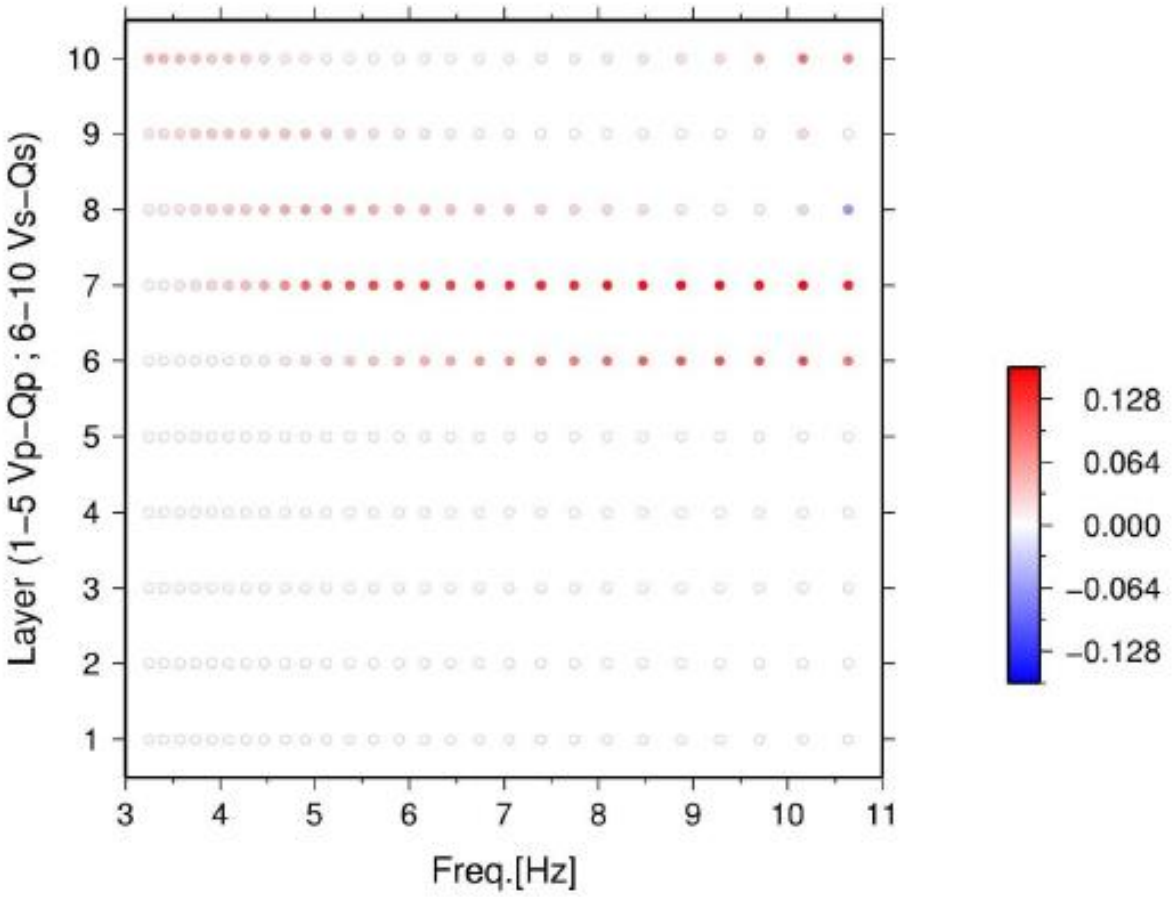

Seismic Interferometry
Claerbout's conjecture

"By cross correlating noise traces recorded at two locations on the surface, we can construct the wavefield that would be recorded at one of the locations if there was a source at the other."

$$C_{ij}(1,2,t) = \int_0^T v_i(\mathbf{r}_1,\tau)v_j(\mathbf{r}_2,\tau+t)\mathrm{d}\tau$$

C_{ij} is the cross correlation of the observed fields $v_i(\mathbf{r_1},t)$ and $v_j(\mathbf{r_2},t)$

The time derivative of the noise cross correlation *Cij*(1,2,*t*) between two seismic stations (located at $\mathbf{r_1}$recording component *i*) and 2 (recording component *j*) is related to the Time Domain Green's Function G_{ij} ($\mathbf{r_1}$; $\mathbf{r_2}$,*t*) by :

$$\frac{dC_{ij}}{dt} \approx -G_{ij}(\mathbf{r}_1;\mathbf{r}_2,t) + G_{ji}(\mathbf{r}_2;\mathbf{r}_1,-t)$$

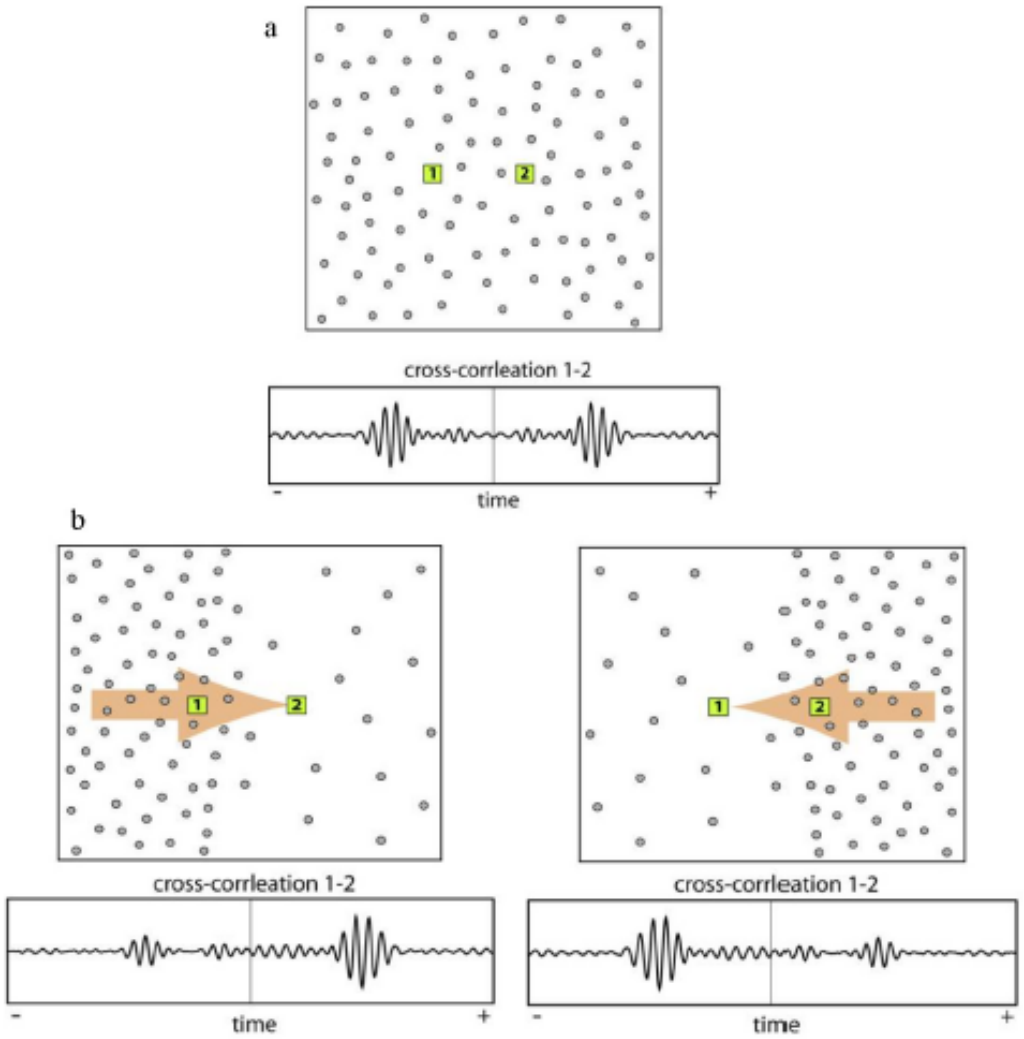

Figure 1. Schematic illustration of the effect of inhomogeneous noise sources distribution on the degree of symmetry of cross correlation. (a) Symmetric cross correlation between 1 and 2 obtained when the sources of noise are evenly distributed. (b) Asymmetric cross correlation (but symmetric travel times) associated with a nonisotropic distribution of sources.

Stefano Parolai

Data analysis

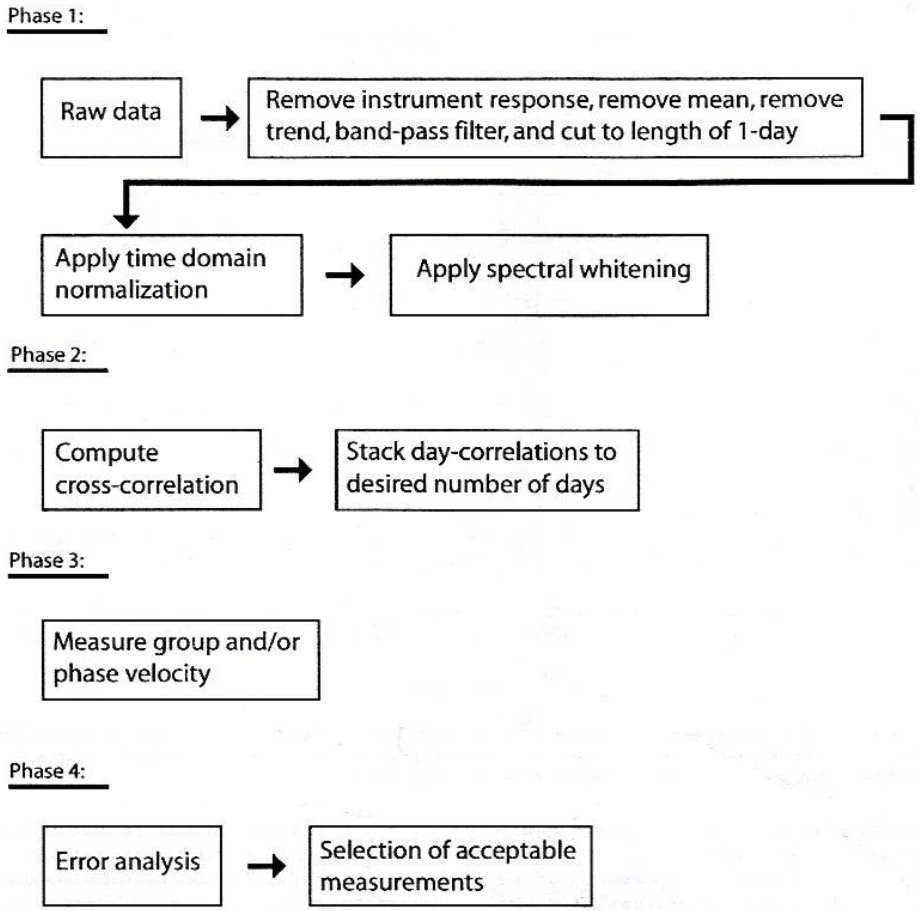

Figure 2. Schematic representation of the data processing scheme. Phase 1 (described in Section 2 of the paper) shows the steps involved in preparing single-station data prior to cross-correlation. Phase 2 (Section 3) outlines the cross-correlation procedure and stacking. Phase 3 (Section 4) includes dispersion measurement and Phase 4 (Section 5) is the error analysis and data selection process.

after Bensen et al. (2007)

The methods found many applications in the last years

-Surface-wave tomography at global and regional scale
-Estimation of building response
-Ground roll estimation and removal
-Retrieval of reflections
-Controlled Source Electromagnetic methods

Stefano Parolai

Green's functions from noise cross-correlation

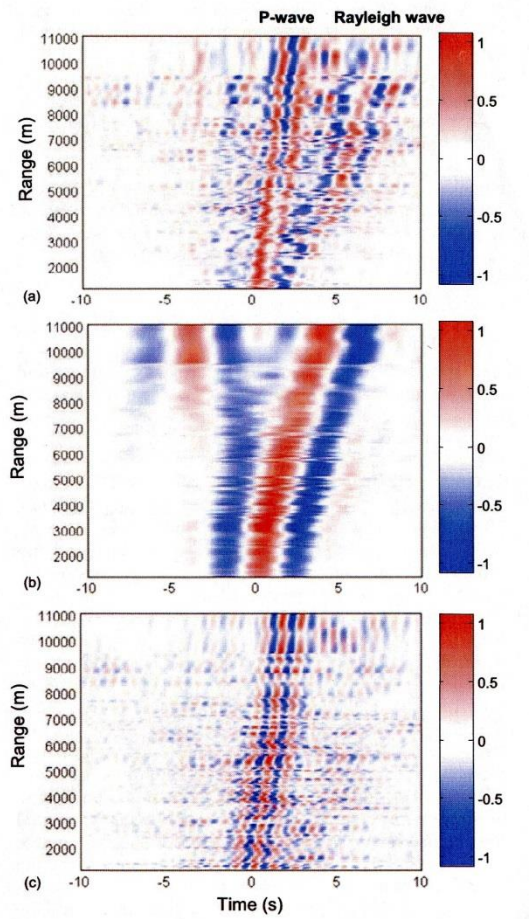

Figure 2. Range-time representation of the Z-Z component of the noise correlation tensor averaged over one month in three frequency bands (a) [0.1–1.3 Hz], (b) [0.1–0.45 Hz], and (c) [0.7–1.3 Hz]. Each plot has been normalized by its own maximum.

after Roux et al. (2005)

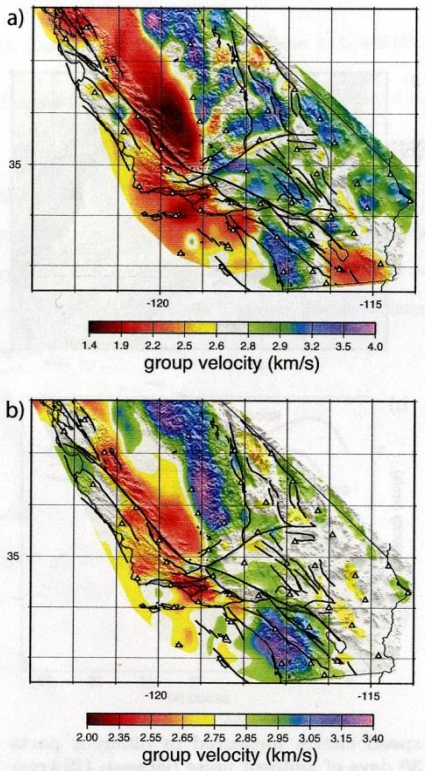

Figure 4: **Group speed maps constructed by cross-correlating 30 days of ambient noise between USArray stations.** (a) 7.5 s period Rayleigh waves. (b) 15 s period Rayleigh waves. Black solid lines show known active faults. White triangles show locations of USArray stations used in this study.

after Shapiro et al. (2005)

Stefano Parolai

Is an application for shallow geology investigations possible?

- Wavelengths are much larger than sensor distance

- Very strong attenuation

Stefano Parolai

Different scales

Europe

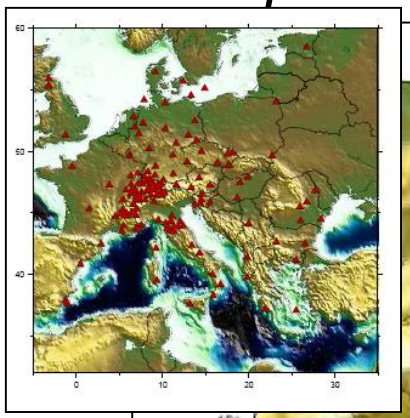

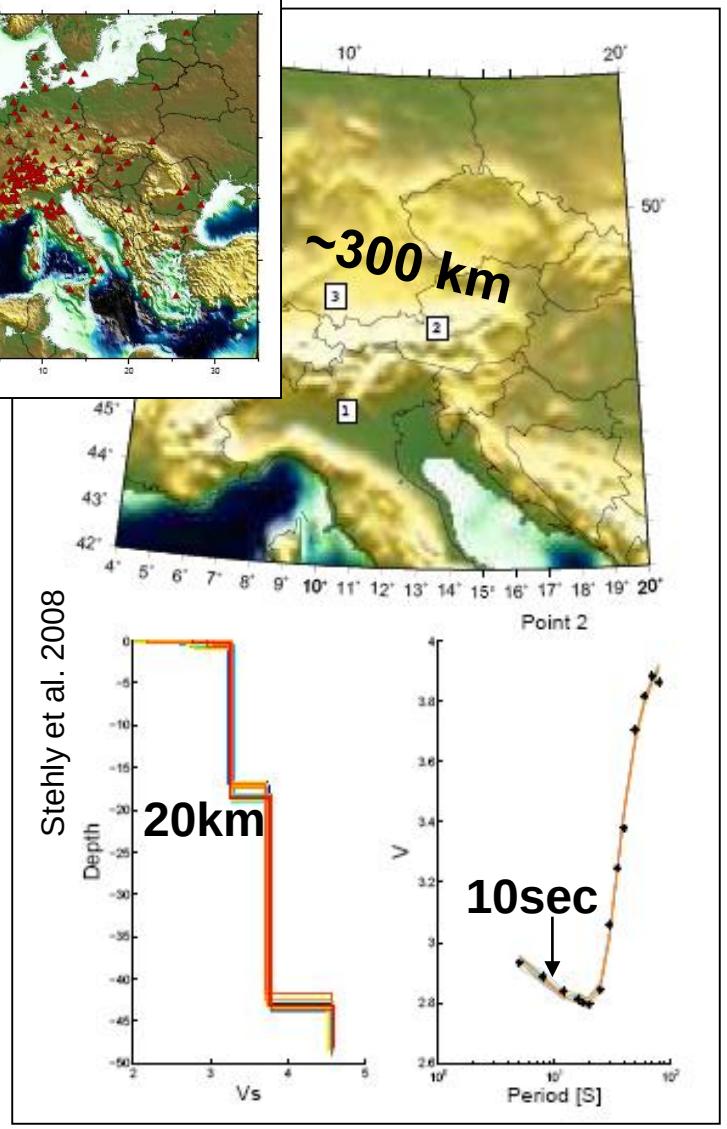

Broad-band sensor needed

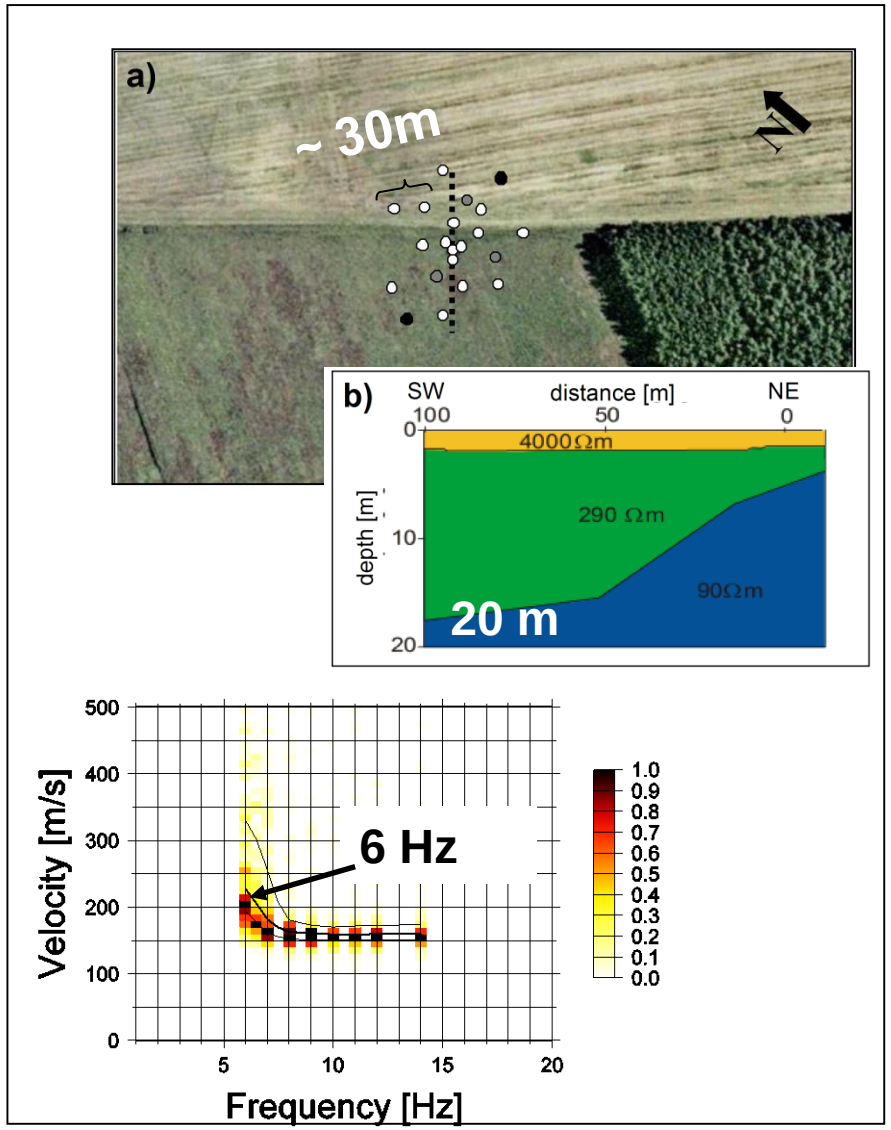

Short period sensor can be used

UNIVERSITÀ DEGLI STUDI DI TRIESTE

GFZ Helmholtz-Zentrum Potsdam

Stefano Parolai

Generally array methods assume that the structure below the array is 1D

Luo et al. 2008 showed that the velocity estimated between two stations is affected by lateral inhomogeneities between them

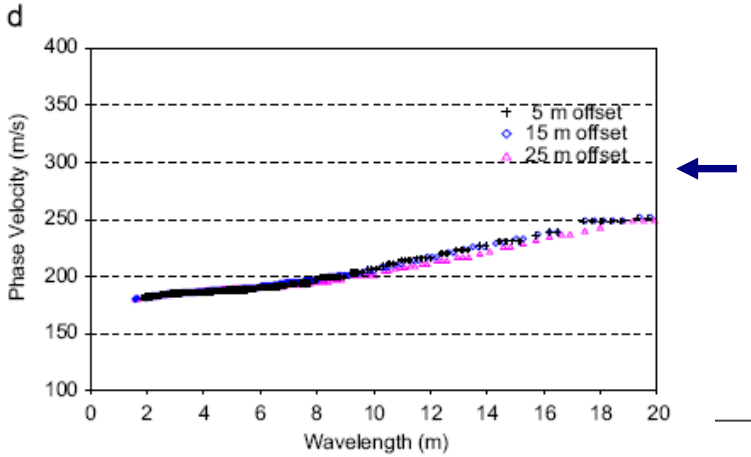

Using the whole spread

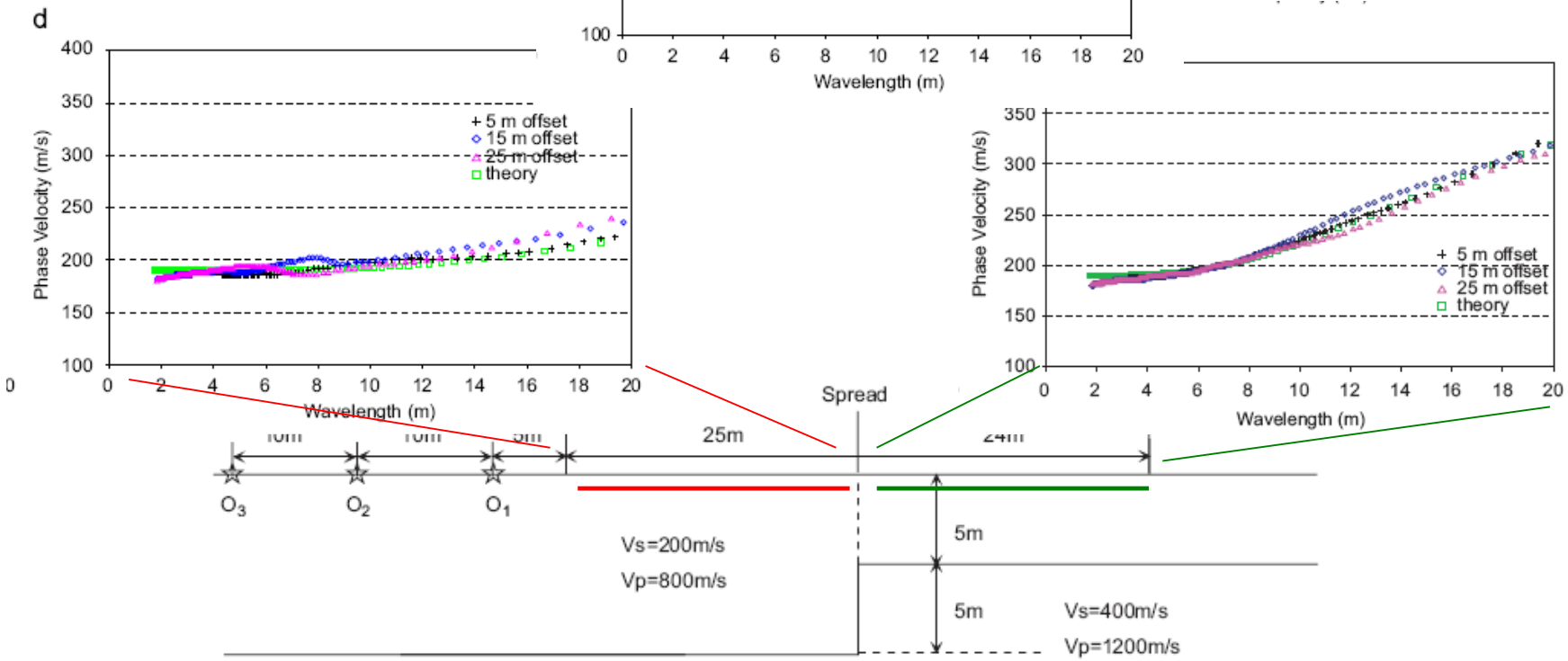

Fig. 2. The corner-edge model.

Stefano Parolai

The experiment

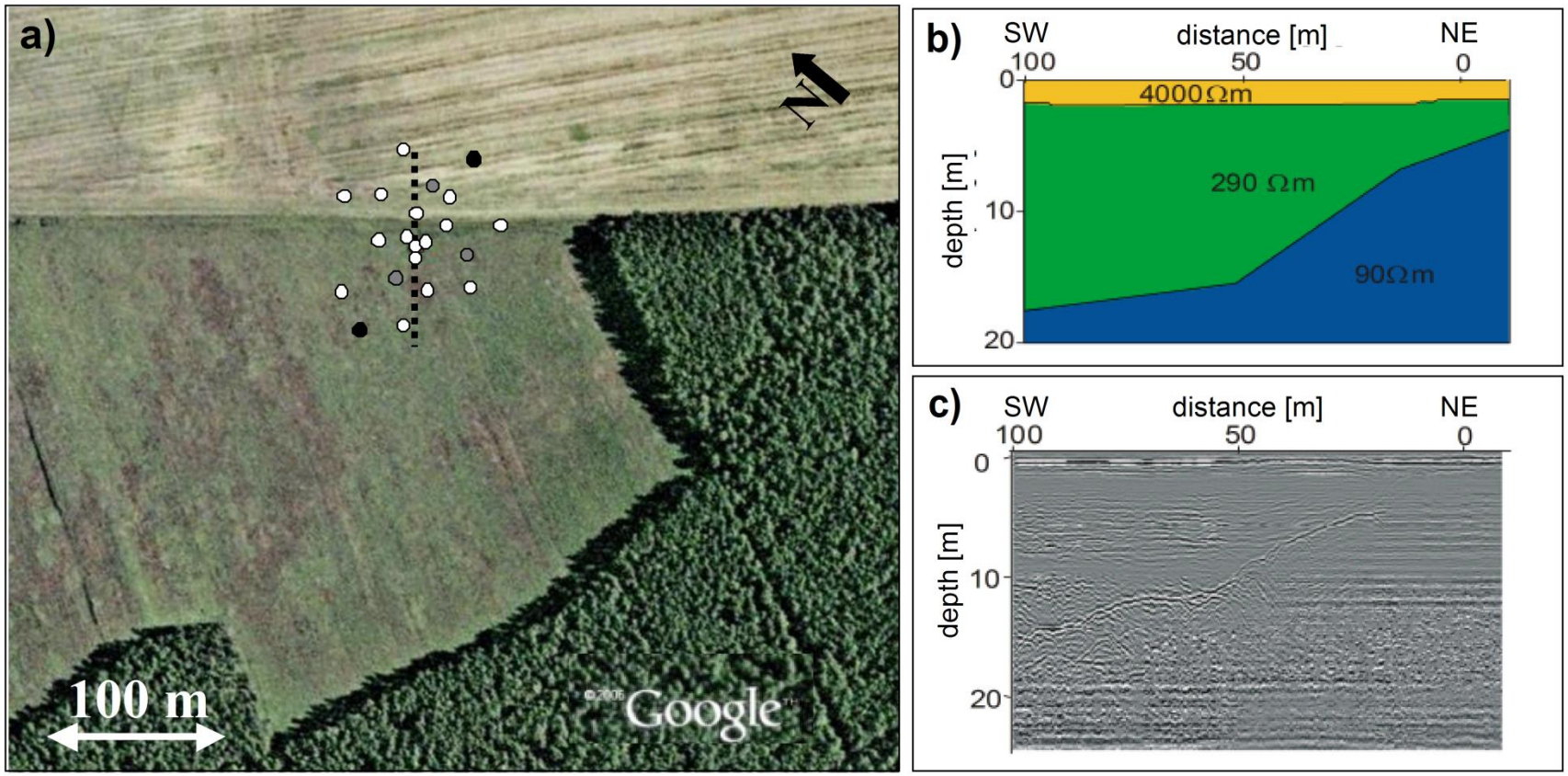

Figure 1: *a)* Nauen test site, showing the location of the EDL + 4.5Hz sensors (white dots), EDL + 1Hz Mark sensor (white square), EDL + broadband sensors (black dots), and Reftek + 4.5Hz sensors (grey dots), as well as the DC geoelectric and GP radar profiles (dotted line). *–b)* DC geoelectric profile. *c)* GP radar profile (*courtesy of the Department of Applied Geophysics, Technische Universität (TU) Berlin*).

Stefano Parolai

480 non-consecutive noise windows 30 s wide were extracted

The linear trend was removed from each window and a 5% cosine-taper was applied at both ends.

The cross-correlations were computed considering one-bit normalized data that yielded the highest signal-to-noise ratio for the data set at hand.

To estimate the group velocity at twelve different frequencies the cross-correlation functions were filtered by applying a Gaussian filter with a narrow band-width

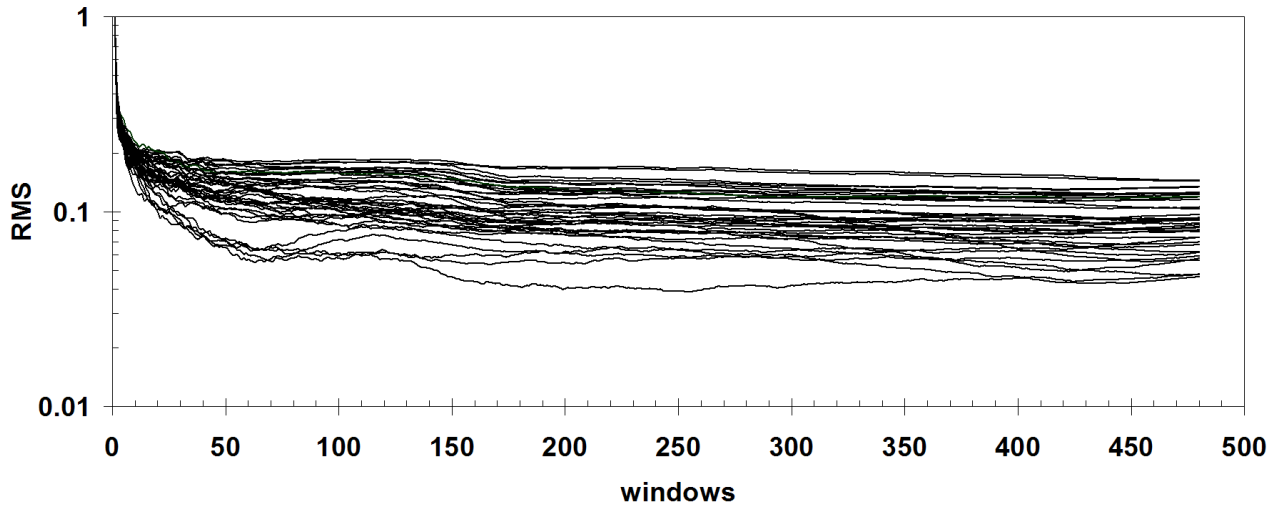

Figure 2: Stability (RMS - root mean square) of the estimated Green's functions with respect to the number of stacked windows for 14 Hz and 6 Hz.

Stefano Parolai

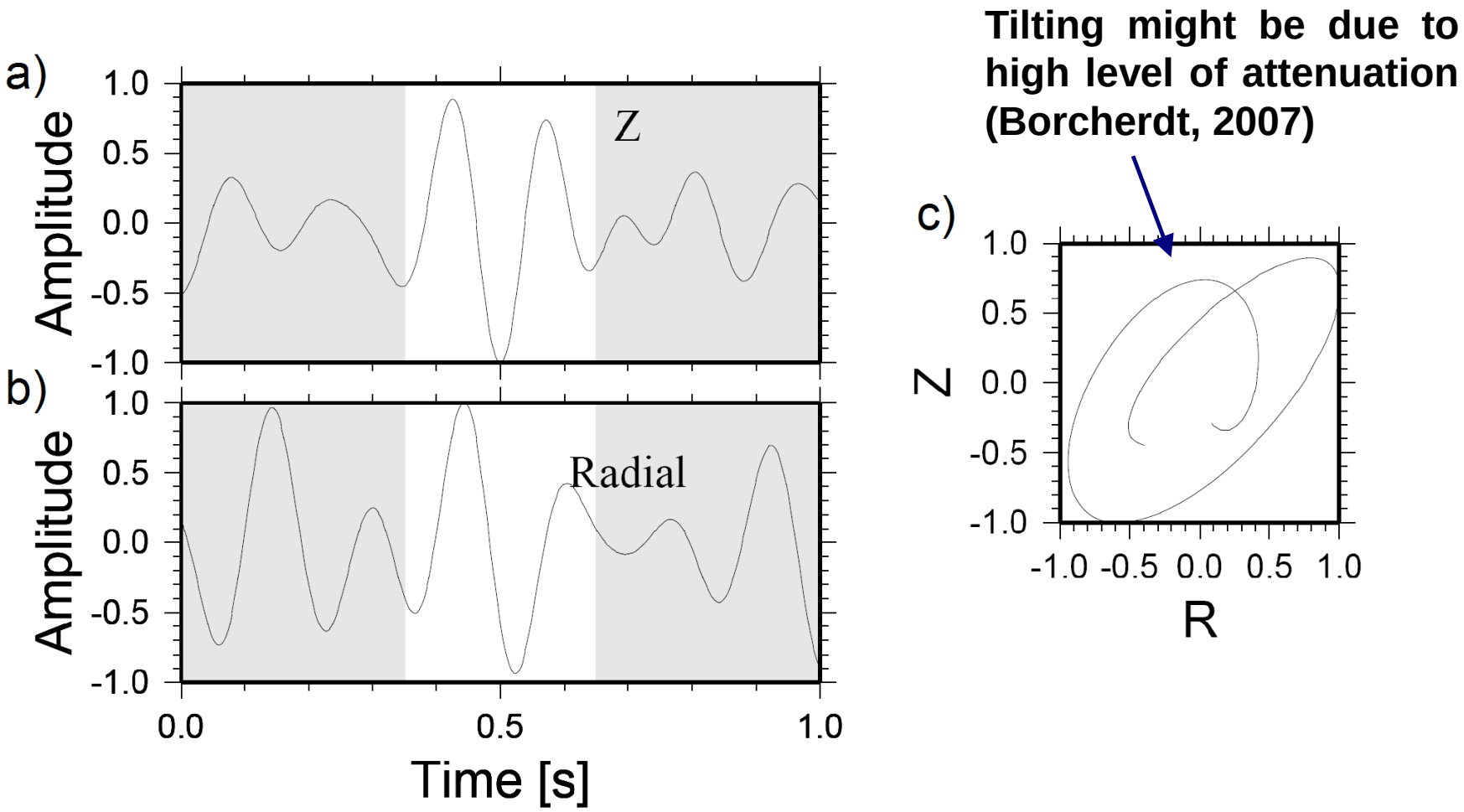

Figure 3: Vertical *(a)* and Radial *(b)* components of the Green's functions for a frequency of 6 Hz. The time window selected for estimating the group velocity is indicated by the white background. *c)* Particle motion in the selected time window of *a)* and *b)*.

Stefano Parolai

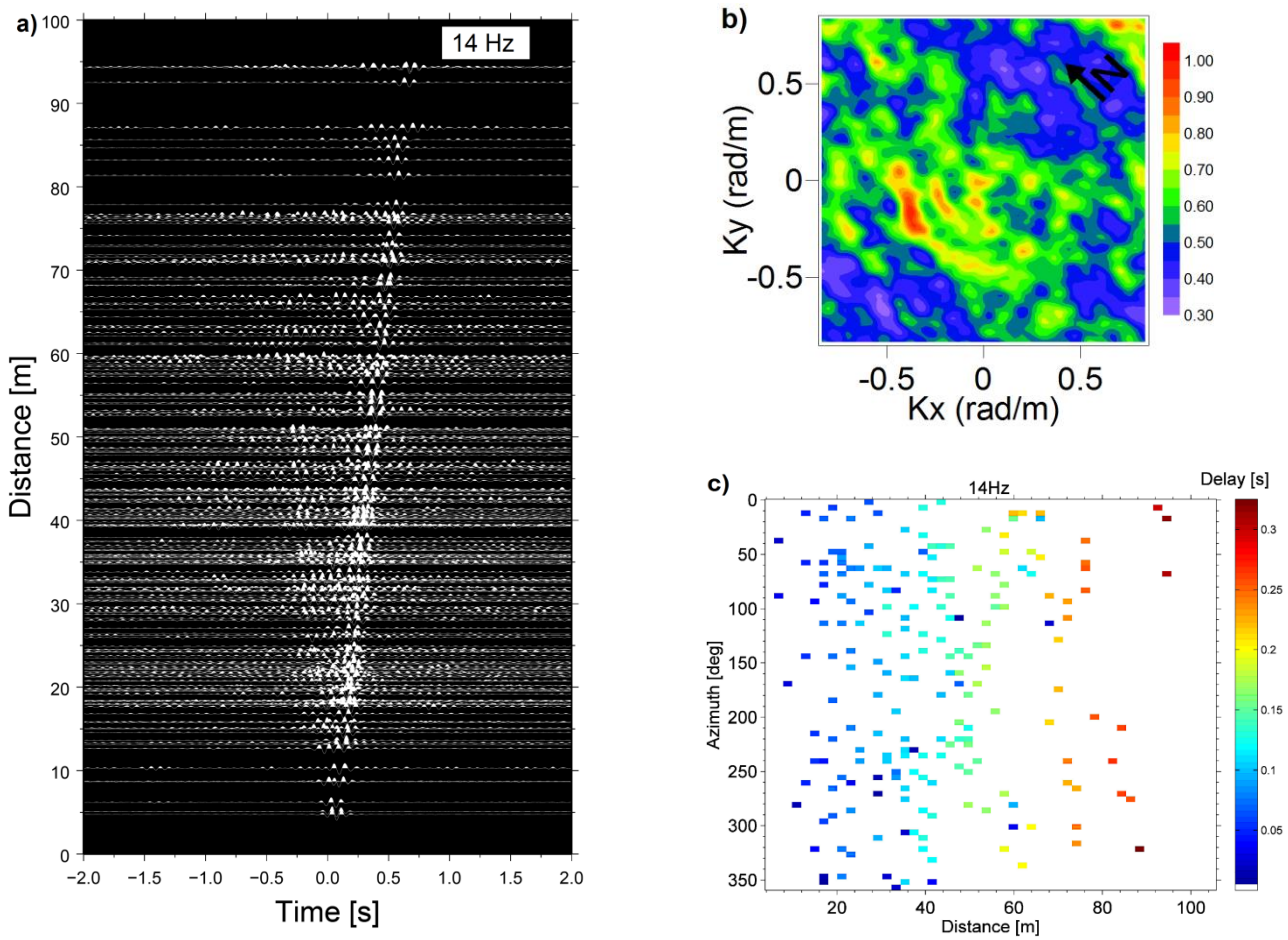

No-scattering as a function of azimuth

Figure 4: *–a)* Normalized cross-correlations computed for 14 Hz. *b)*– 2D-wavenumber plot showing the distribution of the noise sources as determined by F-K analysis results for 14 Hz. *c)* Time delays as a function of distance between each pair of stations and orientation of the pair with respect to north. The delay time is indicated by the colour of the symbol.

Stefano Parolai

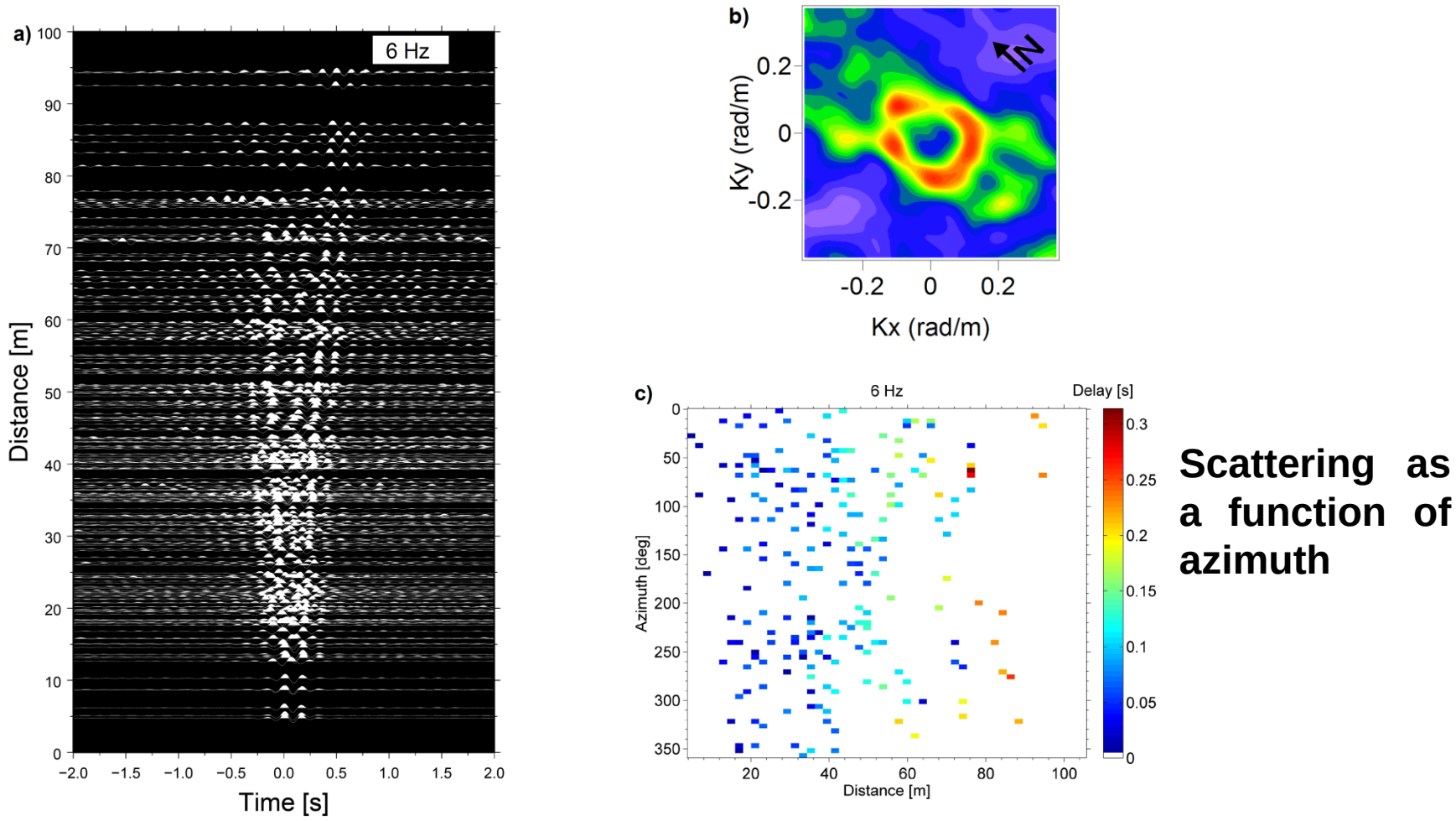

Scattering as a function of azimuth

Figure 5: Same as Figure (4) but for 6 Hz.

Stefano Parolai

Estimation of the initial average velocity for the inversion

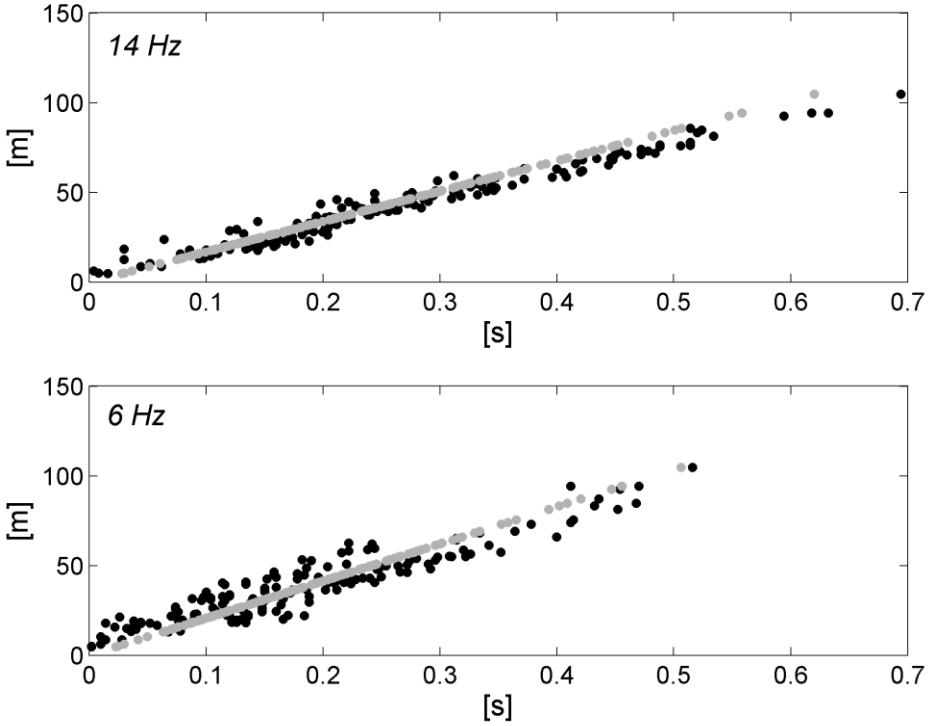

Figure 6: Observed (black dots) and theoretical (grey dots) travel times for frequencies 14 Hz and 6 Hz.

The linear tomography problem of computing the integral travel time (*t*) for a given slowness (*s*) along a raypath is given by

$$t = \int s \cdot dl \qquad (6)$$

where the *dl* is the line element along the raypath. Equation (1) can also be expressed in a simple discrete matrix form,

$$\mathbf{t} = \mathbf{L}_1\mathbf{s} \qquad (7)$$

.

In equation (7), **t** is the vector of observed travel times, **s** is the slowness of the cells, and $\mathbf{L}_1$ is an *MxN* matrix of ray-path segments, namely, *M* rays crossing the medium, divided into *N* cells.

This average slowness was the initial guess $s^{(k=1)}$ for the iterative scheme. Then, a new solution $s^{(k+1)}$ was determined by solving the following equation

$$\mathbf{W}\Delta\mathbf{t}^{(\mathbf{k})} = \mathbf{L}_2\Delta\mathbf{s}^{(\mathbf{k})} \qquad (8)$$

in which $\Delta\mathbf{t}$ is the vector of the normalized misfit between the observed and theoretical travel times, $[t_o - t_t]/ t_o$.
$\Delta\mathbf{s}$ is the vector of the normalized slowness modification $[s^{(k)} - s^{(k-1)}]/s^{(k)}$.
The diagonal matrix $\mathbf{W}_{(MxM)}$ is made up of weighting factor elements defined by the adaptive bi-weight estimation method, and was introduced to stabilize the iteration process.

Stefano Parolai

The design matrix $\mathbf{L_2}$ in equation (8) is derived from $\mathbf{L_1}$ in equation (7), after that some proper modification was included to account for *a priori* constraints on the solution. In particular, it is expressed as

$$\mathbf{L_2} = \begin{bmatrix} \mathbf{WL_1} \\ \mathbf{K}(\delta^2)\mathbf{M} \end{bmatrix} \qquad (9)$$

where the upper block is the ray-path segment matrix $\mathbf{L_1}$ properly weighted by the matrix **W**, while, the damping coefficient δ^2 and the matrices **K** and **M** describe the *a priori* constraints imposed on the solution.

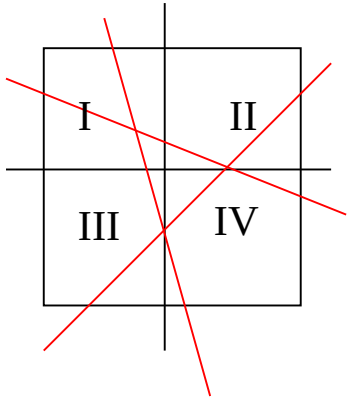

The matrix **K**(NxN) weights the data depending on the number, length, and orientation of each ray-path segment crossing each *Ni* cell.

Each cell *Ni* is first divided into four quadrants. Then, the length of the rays passing through each sector is summed, resulting in a 2x2 ray density matrix. The ray density matrix was factorized by performing the singular value decomposition (SVD).

The singular values ($\lambda 1$, $\lambda 2$) were used to compute the ellipticity ($\lambda min/\lambda MAX$) of the ray density matrix.
Ellipticity close to 1, means that a good resolution for a given cell is achieved

The elements of the matrix **K** in equation (9) were computed by multiplying the ellipticity for the number of rays crossing each cell.

Stefano Parolai

Matrix **M** constrains the solution to vary smoothly over the 2D domain. It increases the stability of the inverse problem by reducing of the influence of travel time errors.
The implementation of that smoothness constraint consists in adding a system of equations to the original travel time inversion problem,

$$s_{x,y} - \sum_{i=1}^{R} a_i s_{x-dx_i, y-dy_i} = 0 \qquad (10)$$

where R is the number of cells surrounding the selected one, $s_{x,y}$, and a_i are the normalized weights.

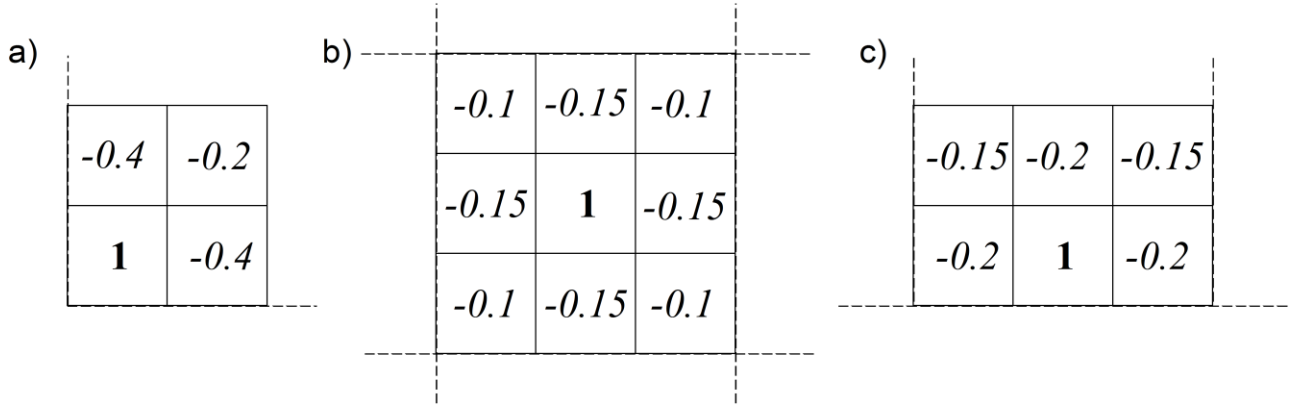

Figure 7: Examples of M matrix normalized weights for cells (*bold number*) located at the corner (a), the inner part (b), and along the model edges (c) and the surrounding cells (*italic numbers*).

Stefano Parolai

$$\mathbf{L}_2 = \begin{bmatrix} \mathbf{W}\mathbf{L}_1 \\ \mathbf{K}(\delta^2)\mathbf{M} \end{bmatrix} \qquad (9)$$

The term δ^2 in equation (9) is a damping coefficient introduced to balance resolution and instability in the inversion analysis

After some trial and error tests, $\delta 2$ was fixed to 0.5

Equation (8) was solved using the SVD method

$$\Delta \mathbf{s}^{(k)} = \mathbf{V} \Lambda^{\varepsilon} \mathbf{U}^{T} \mathbf{W} \Delta \mathbf{t}^{(k)} \qquad (11)$$

where the factorization of $\mathbf{L}_2$ is $\mathbf{ULV}^T$ and the non-zero elements of the diagonal matrix Λ^{ε} are equal to $(\lambda_{jj} / (\lambda_{jj}^{\,2} + \varepsilon^2))$

where l_{jj} are the singular values of **L,** and e^2 is a damping factor

After some trial-and-error tests, it was found that a value of ε^2=0.5 provides a satisfactory compromise between smoothness of solution and data misfit

Stefano Parolai

Inversion results (10 mX10 m cells)

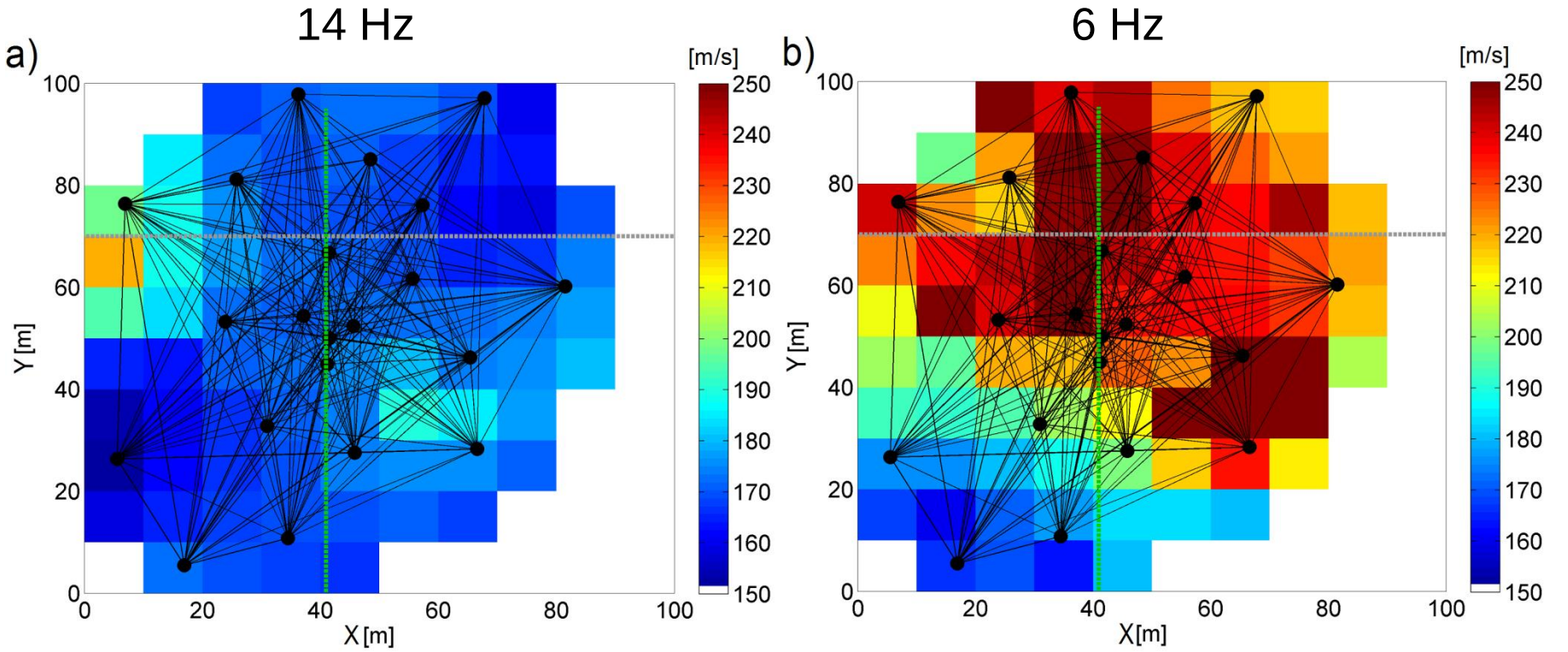

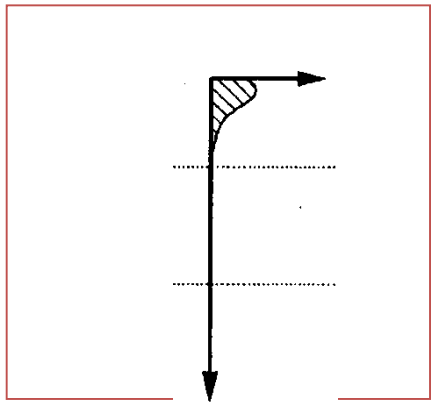

$$\lambda_R = V_R / f$$

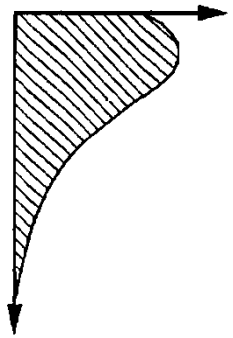

Inversion results *a)* Frequency 14 Hz. *b)* Frequency 6 Hz.. Locations of the DC geoelectric and GP radar profiles (green dotted line), and the field track (grey dotted line) are also shown.

Stefano Parolai

Validation with synthetic data (6 Hz)

Input models

Output models

Checkerboard

Real data model

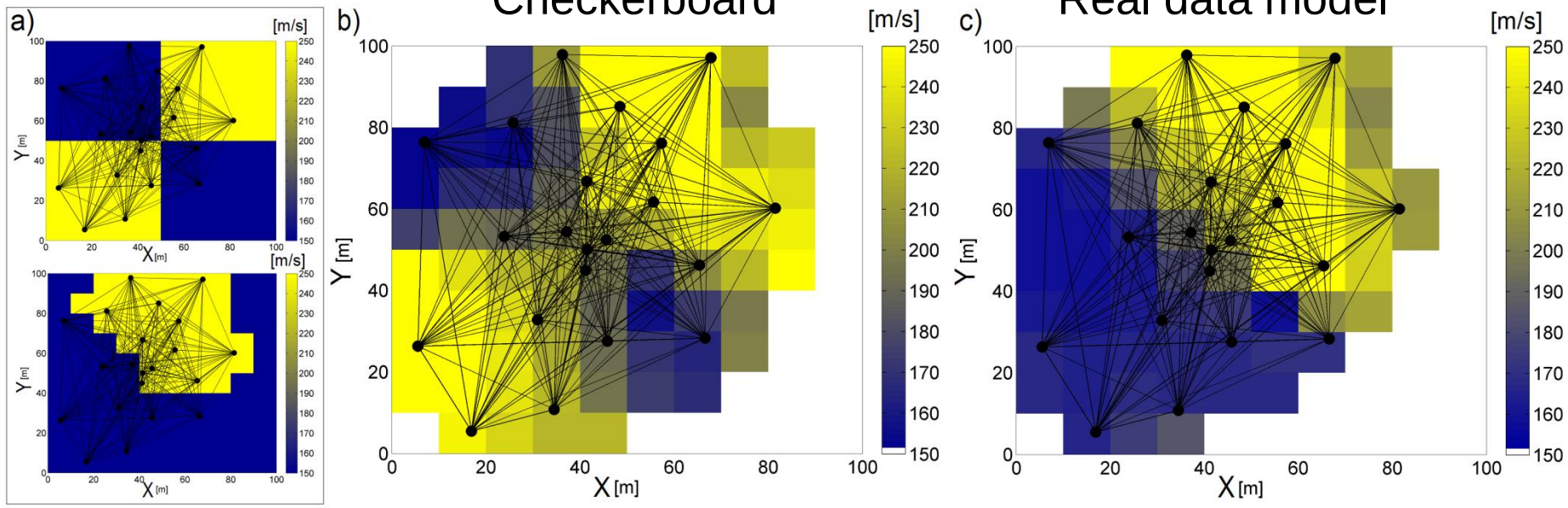

Figure 9: *a)* Input models for the validation tests. *b)* Inversion results for the checker-board model. *c)* Inversion results for the Nauen test site structure.

Stefano Parolai

Bootstrap analysis results

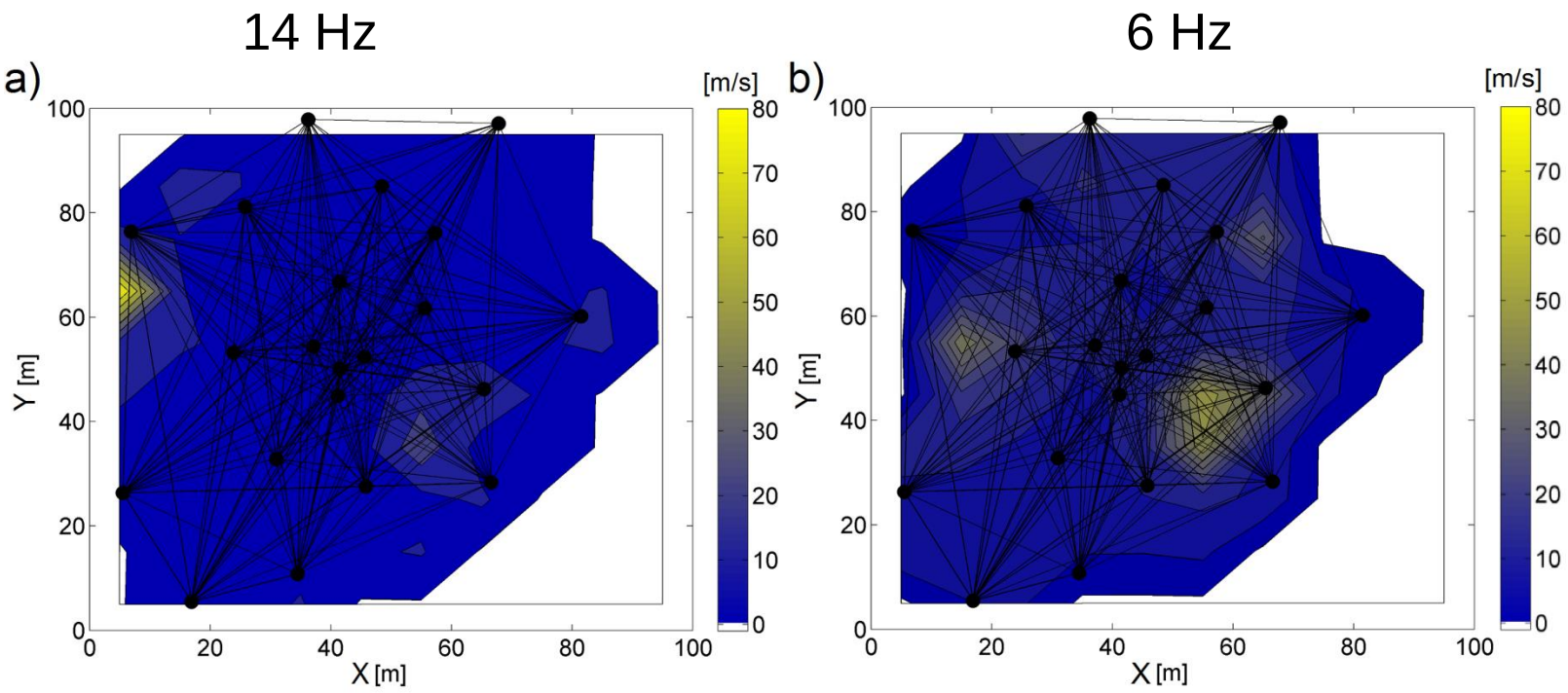

Figure 10: Standard deviation of velocity computed after 1000 repeated bootstrap inversions. *a)* Frequency 14 Hz. *b)* Frequency 6 Hz.

For each cell along the profile a dispersion curve is obtained

The inversion of the dispersion curves lead to 1D S-waves velocity profiles that allow a generation of a pseudo 2D velocity cross-section

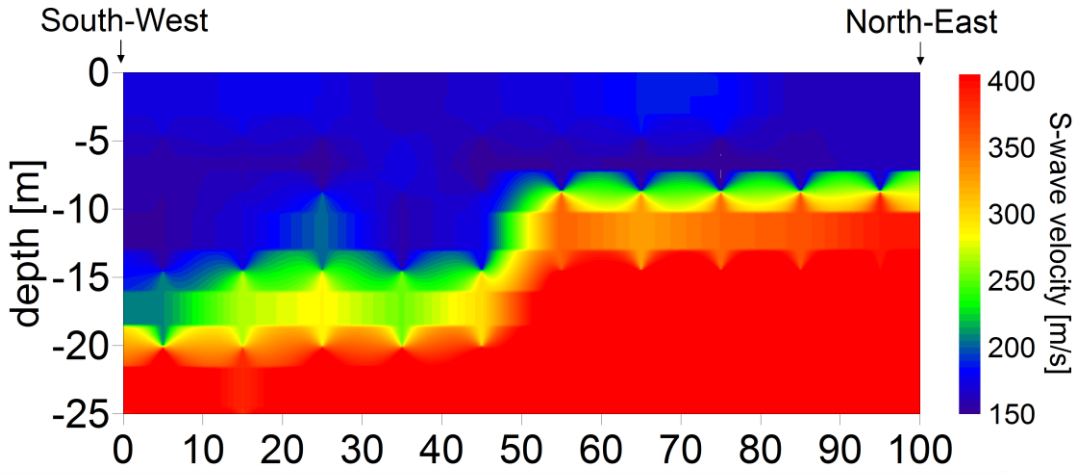

Picozzi et al. (2008)

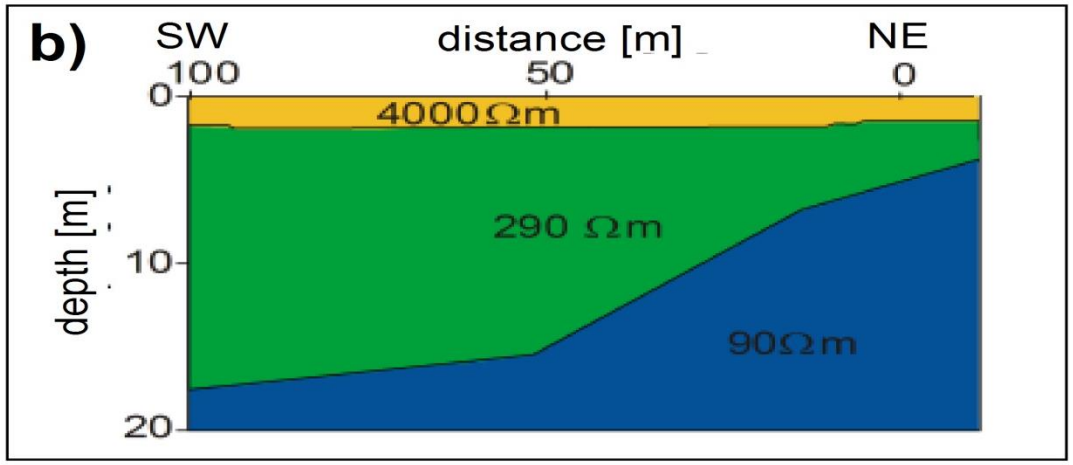

Stefano Parolai

From Pseudo 2D to full 3D with seismic noise: Including also topography!

$$u_3(|\mathbf{z}|) = \mathrm{l}e^{\mathrm{l}\mathbf{k}\mathbf{z}\cdot\mathbf{e}_z} - \mathrm{s}e^{\mathrm{p}\mathbf{k}\mathbf{z}\cdot\mathbf{e}_z}$$

$$f_1 \geq f_2 \geq f_3$$

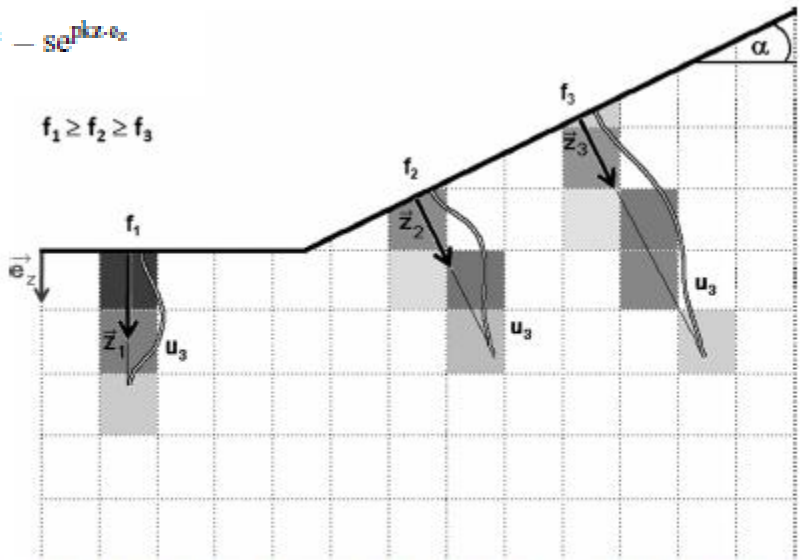

Figure 1. Calculation of the vertical weights for different frequencies for the block's cells, based on the displacement component u_3 for Rayleigh waves. The darker the individual cell's colour, the higher the weight. Note that the weight is calculated perpendicular to the slope of topography.

Stefano Parolai

Validation with Synthetics

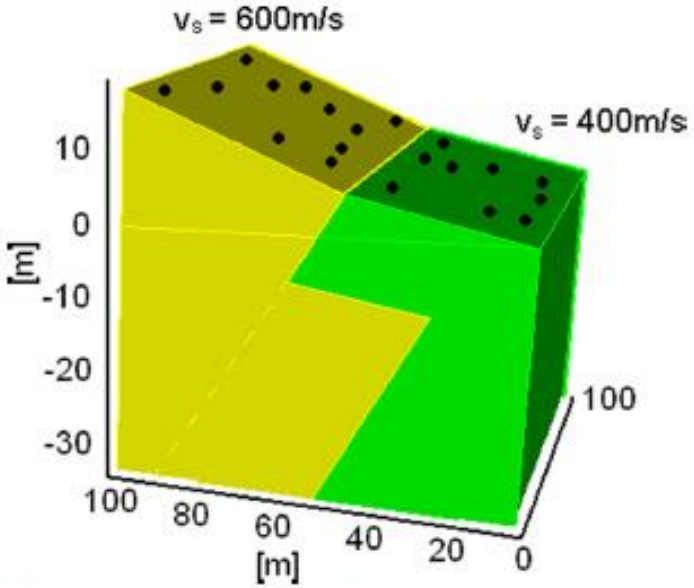

Figure 2. Simple 3-D structure used for the calculation of the noise synthetics. The two blocks are characterized by different shear-wave velocities. The black dots show the location of the receivers on the surface of the block.

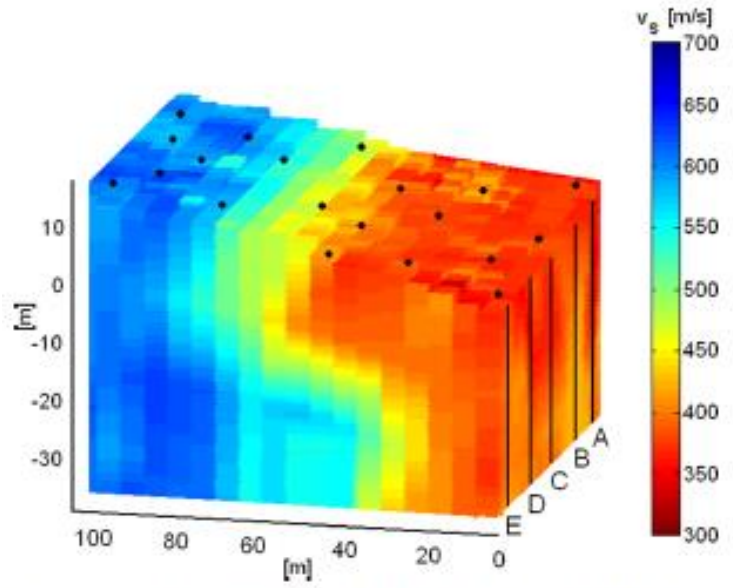

Figure 3. Inversion results for the model shown in Fig. 2 using noise synthetics. The images were obtained after 500 iterations. Black dots represent the receivers. Vertical black lines indicate cross-sections parallel to the topographic gradient for the resolution tests shown in Fig. 5.

Stefano Parolai

Validation with Synthetics

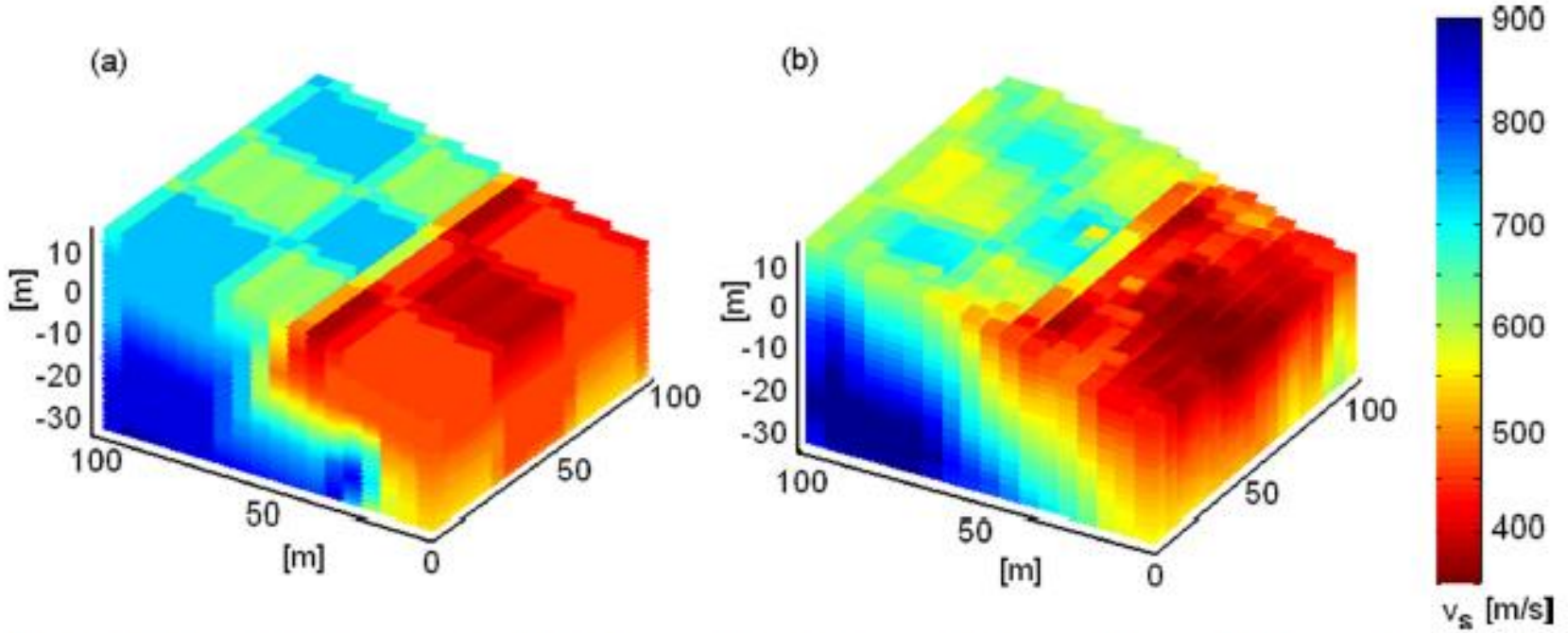

Figure 4. 3-D tomography with checkerboard. (a) The perturbed velocity model, generated by adding 20 per cent perturbation for every 20 m of depth below the surface on the initial model shown in Fig. 2. (b) The reconstructed model from the 3-D tomography.

Stefano Parolai

Application to the Issik Ata fault in Kyrgyzstan

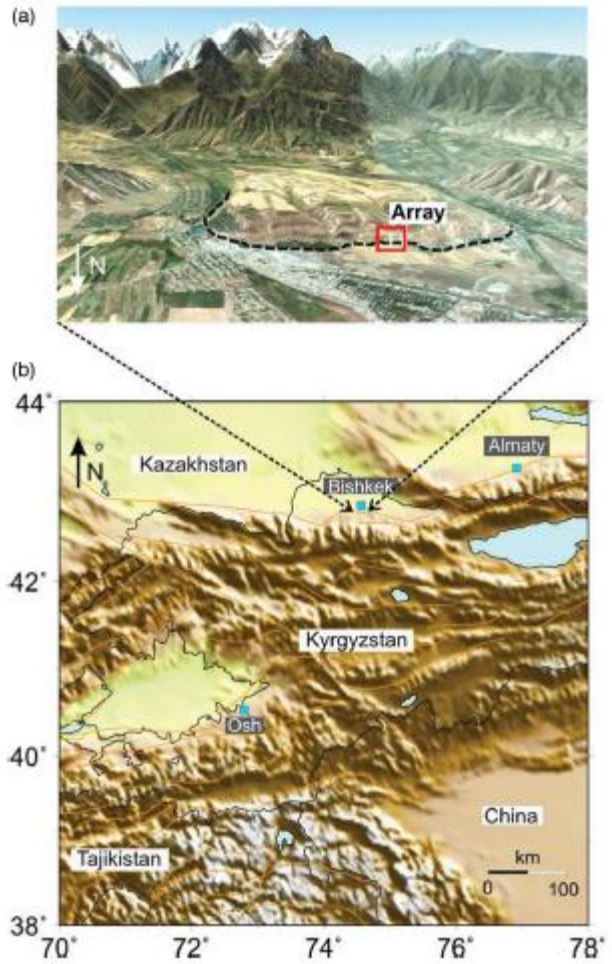

Figure 6. (a) Satellite image showing the southern outskirts of Bishkek facing the Ala-Too range. The topography is exaggerated by two times. Location of the array measurement is indicated. The dotted line shows the Issyk-Ata fault following Chediya *et al.* (2000). Google Earth, © 2012, CNS Spot Image © 2012, Digital Globe © 2012. (b) Map of Central Asia. Major faults are mapped in orange.

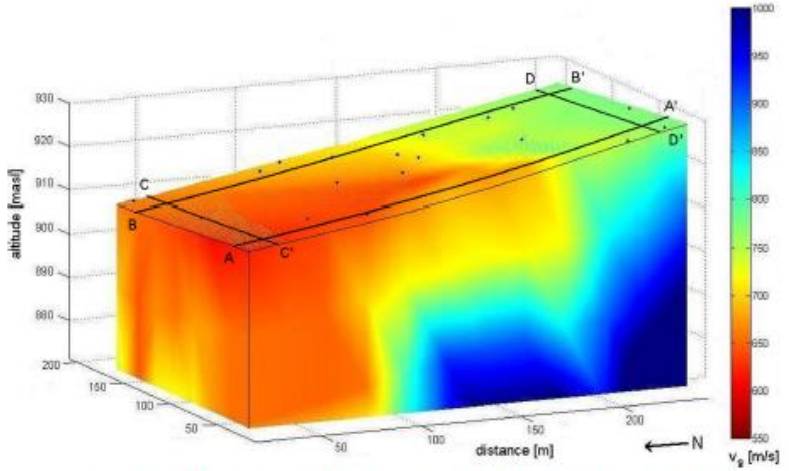

Figure 7. Inversion results of measurements on the Issyk-Ata fault obtained after 500 iterations. Topography is exaggerated about three times. The dots represent locations of the sensors. Locations of cross-sections shown in Fig. 8 are indicated by straight black lines.

Stefano Parolai

Application to the Issik Ata fault in Kyrgyzstan

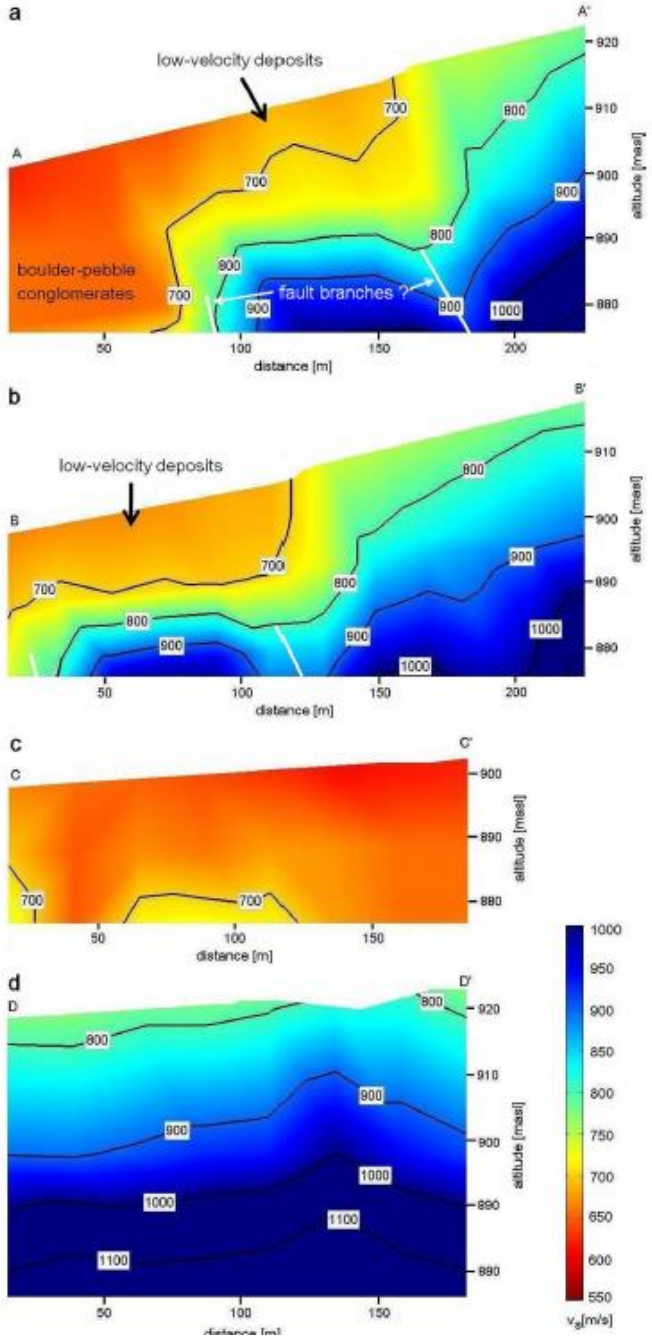

Stefano Parolai

Potential for landslide monitoring!!!!

Papan landslide

Installations of wireless seismic networks on the landslide for recording of seismic noise to be used for structural model and real-time monitoring

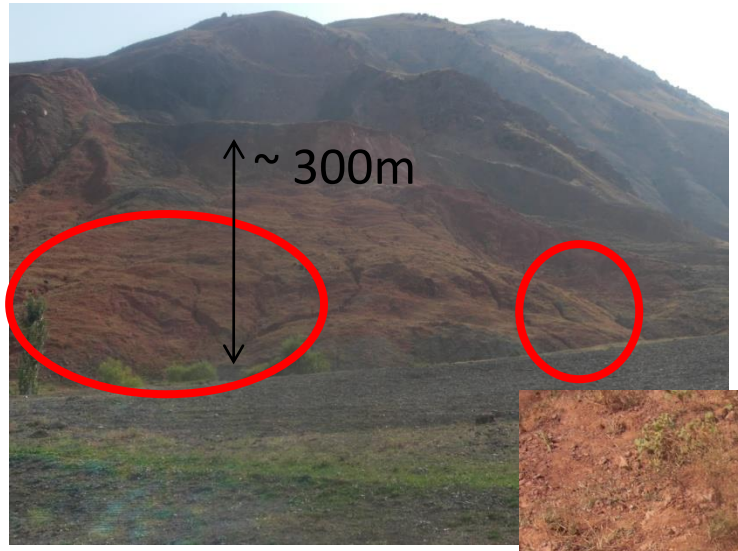

Stefano Parolai

Papan landslide

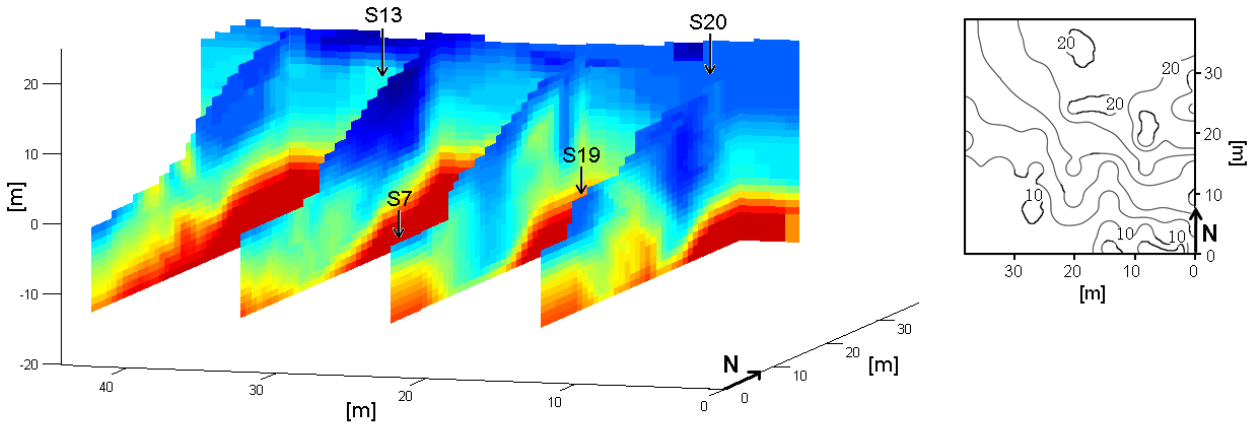

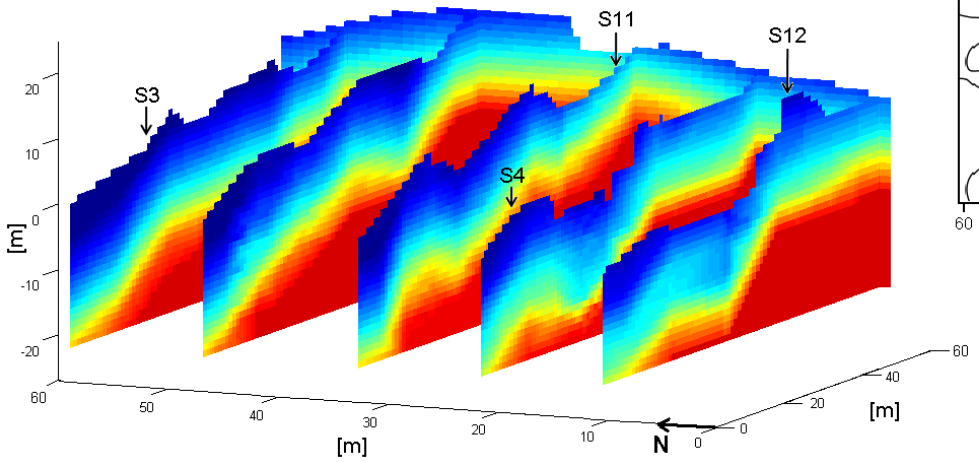

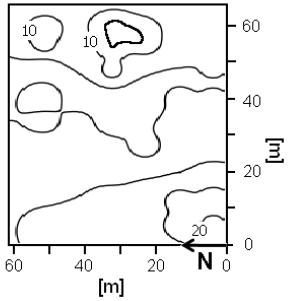

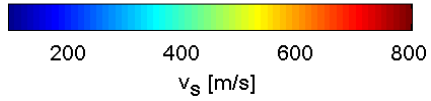

UNIVERSITÀ DEGLI STUDI DI TRIESTE

For each cell along the profile a dispersion curve is obtained

The inversion of the dispersion curves lead to 1D S-waves velocity profiles that allow a generation of a pseudo 2D velocity cross-section

Picozzi et al. (2008)

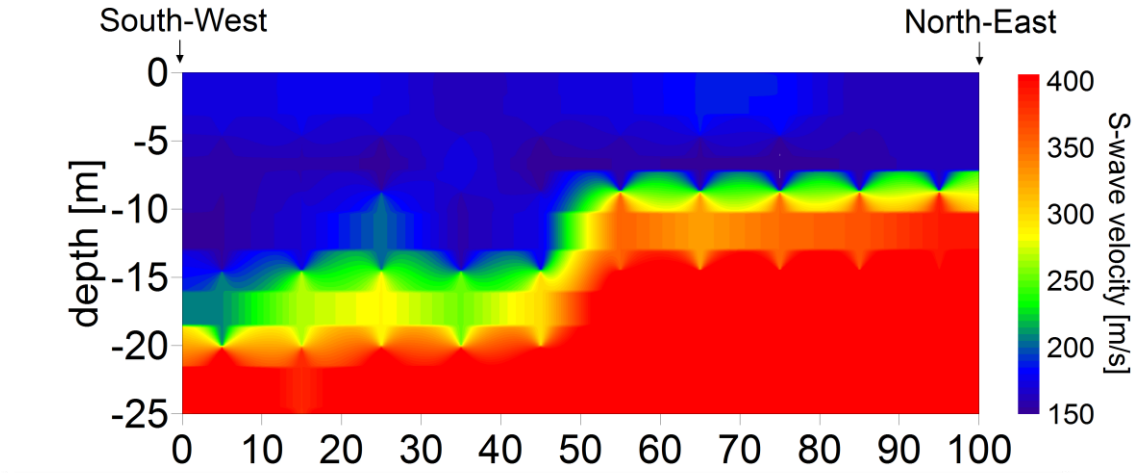

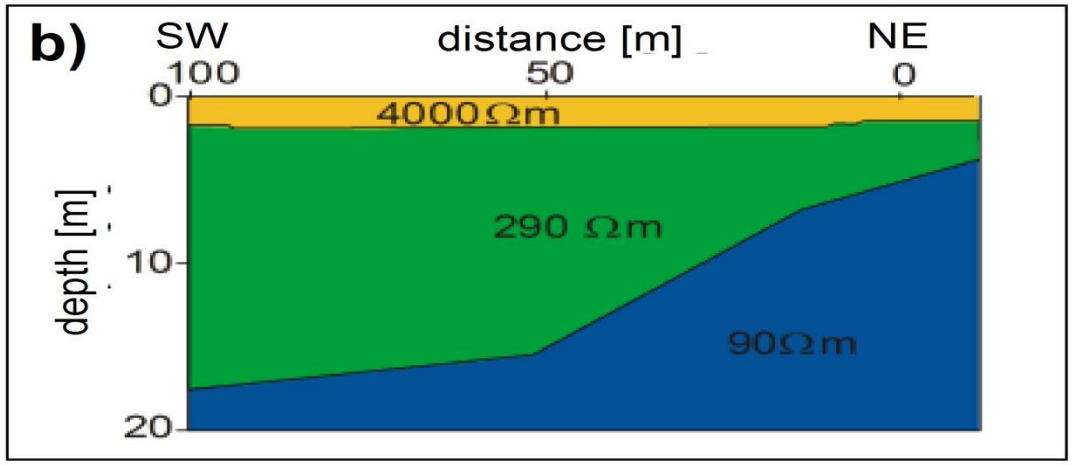

Site response

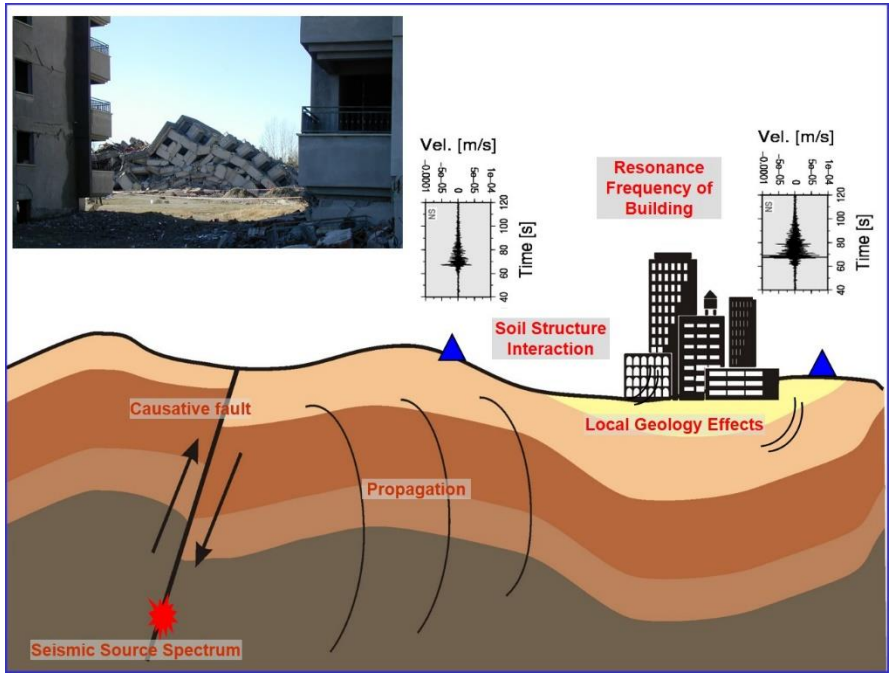

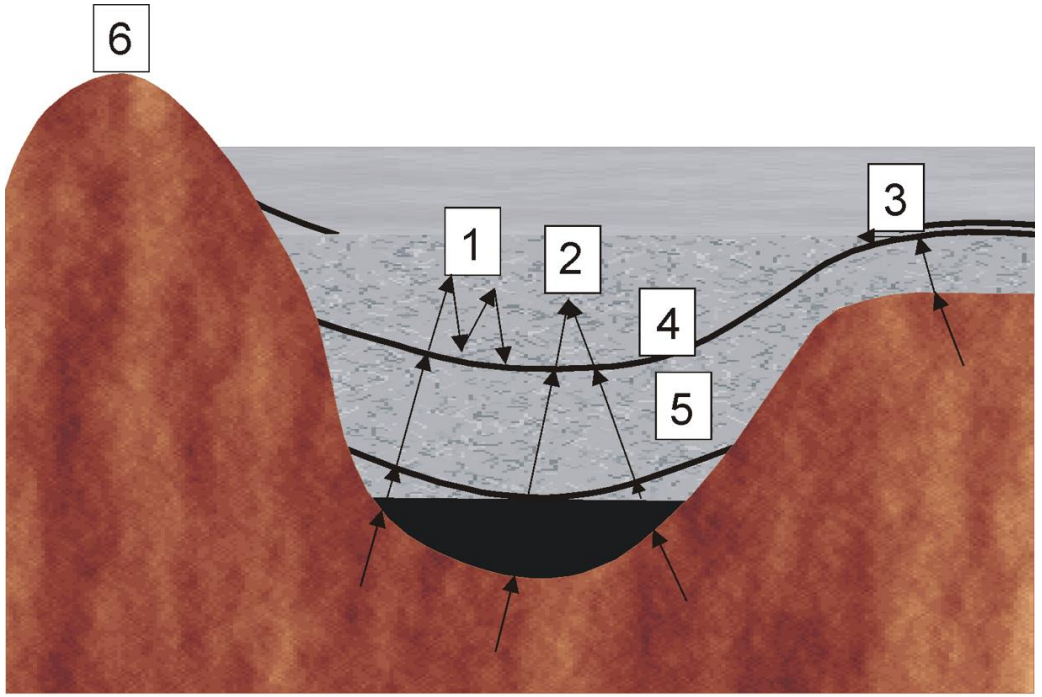

1 - Resonance due to impedance contrasts, 2 - Focusing due to subsurface topography, 3 - Body waves converted to surface waves, 4 - Water content, 5 - Randomness of the medium and 6 - Surface topography

Modified after Safak (2001)

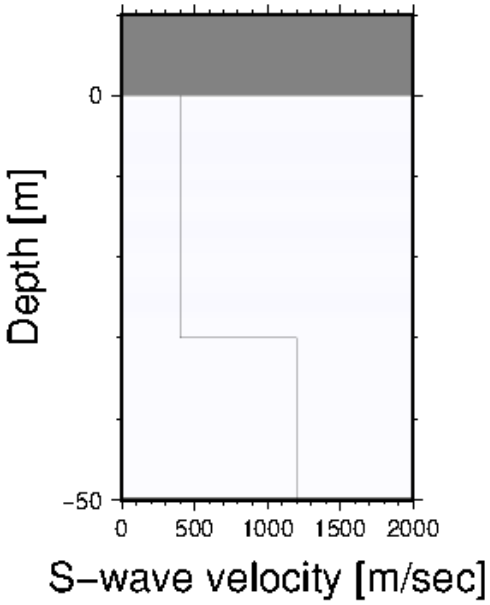

Cross-coupling effects

The Effects of Surface Geology on Seismic Motion, Irikura, Kudo, Okada & Sasatani (eds)
© 1998 Balkema, Rotterdam, ISBN 90 5809 030 2

Site response analysis in 3D

A.G.Tumarkin
Institute for Crustal Studies, University of California at Santa Barbara, Calif., USA

ABSTRACT: We study a three-dimensional seismic radiation field instead of treating each component of ground shaking individually. A 3D transfer function between all three components of motions at two sites helps in understanding and accounting for complex propagation effects such as conversions of different types of seismic waves, differences in incidence angles, etc. After combining two horizontal components into one complex time series we arrived at an efficient method of studying site amplification and polarization properties of planar ground motions (Tumarkin and Archuleta, 1997). For each frequency we are calculating the maximum amplitude and the corresponding azimuth of particle motion in the horizontal plane, as well as the eccentricity of this motion. We show the performance of these methods on data from the Garner Valley Downhole Array and from the Hyogo-Ken Nanbu earthquake.

Bulletin of the Seismological Society of America, 89, 4, pp. 877–887, August 1999

Numerical Evaluation of the Effect of Cross-Coupling of Different Components of Ground Motion in Site Response Analyses

by Roberto Paolucci

Abstract The effect of cross-coupling between the three components of ground motion in the evaluation of site-response functions, such as standard spectral ratios (SSRs) and horizontal-to-vertical spectral ratios (HVSRs), is analyzed in this article. Numerical analyses of the seismic response of fully 3D geological structures, namely, a real topographic irregularity and an ideal stratigraphic inclusion, have been carried out to obtain a 3D transfer function in the form of a 3×3 matrix. Each element of this matrix contains the frequency response in the *i*th direction due to an input motion in the *j*th direction. A synthetic set of acceleration time histories at the surface of the geological irregularity has been created by convolution with the 3D transfer function, using as input motion different real multicomponent strong-motion accelerograms recorded at stiff-soil or rock sites. The SSRs and HVSRs are calculated and compared with the theoretical 3D transfer function in order to highlight the effect of cross-coupling terms. These are found to generate a rather large dispersion in the site-response functions, as well as response peaks that could be misleading in the interpretation of both numerical and observed spectral ratios.

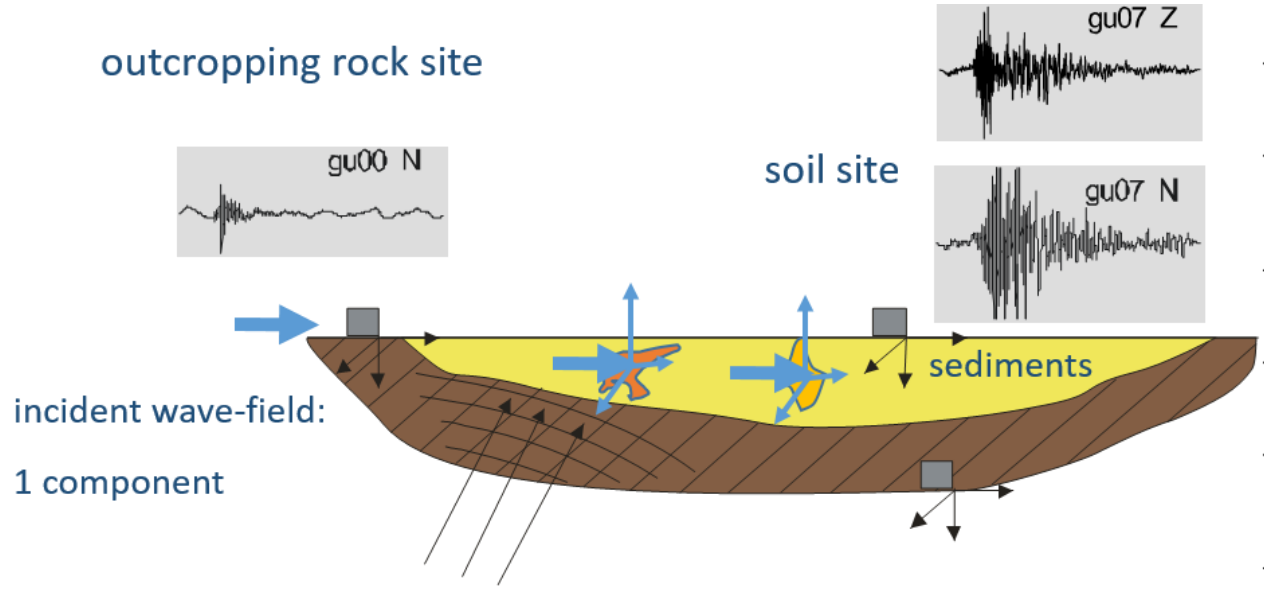

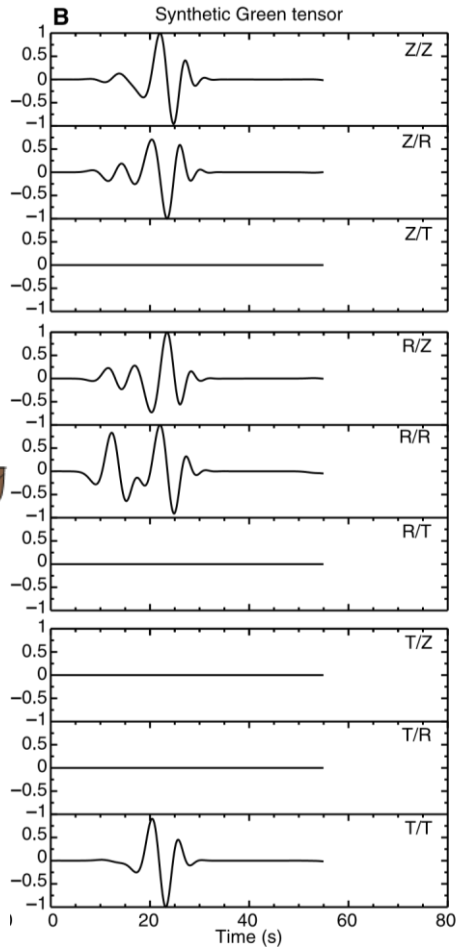

At least 3 simultaneously recorded earthquakes are required

$$
\begin{aligned}
Y_1^{(k)}(f) &= H_{11}^{(k)}(f) \cdot U_1(f) + H_{12}^{(k)}(f) \cdot U_2(f) + H_{13}^{(k)}(f) \cdot U_3(f) \\
Y_2^{(k)}(f) &= H_{21}^{(k)}(f) \cdot U_1(f) + H_{22}^{(k)}(f) \cdot U_2(f) + H_{23}^{(k)}(f) \cdot U_3(f) \\
Y_3^{(k)}(f) &= H_{31}^{(k)}(f) \cdot U_1(f) + H_{32}^{(k)}(f) \cdot U_2(f) + H_{33}^{(k)}(f) \cdot U_3(f),
\end{aligned}
\qquad (1)
$$

Proposed method

Using seismic noise

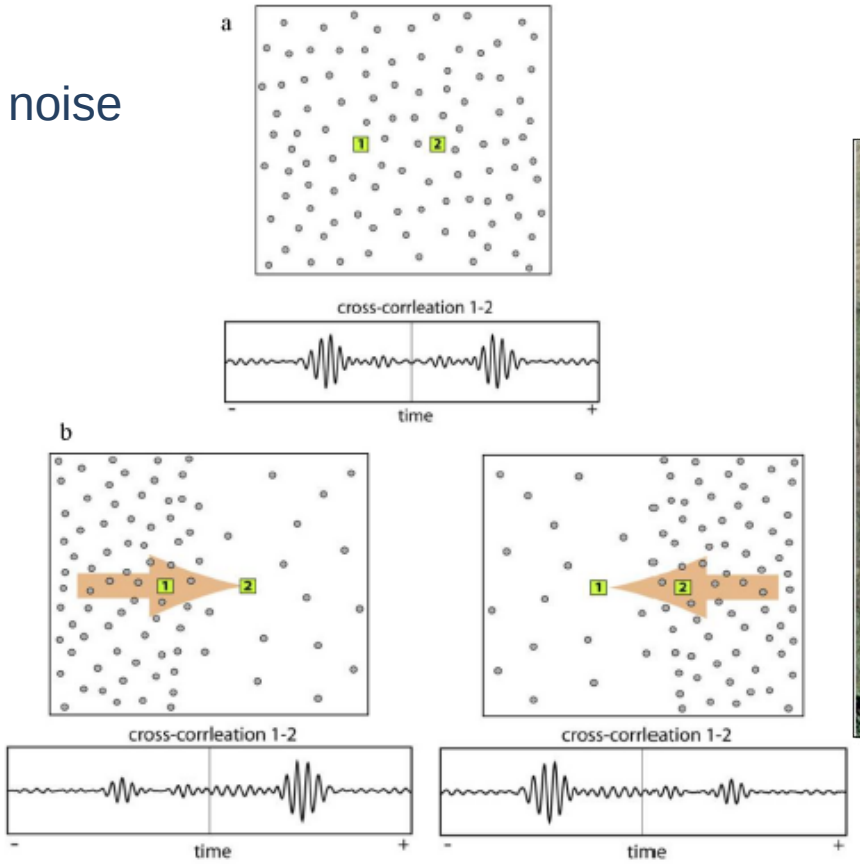

Figure 1. Schematic illustration of the effect of inhomogeneous noise sources distribution on the degree of symmetry of cross correlation. (a) Symmetric cross correlation between 1 and 2 obtained when the sources of noise are evenly distributed. (b) Asymmetric cross correlation (but symmetric travel times) associated with a nonisotropic distribution of sources.

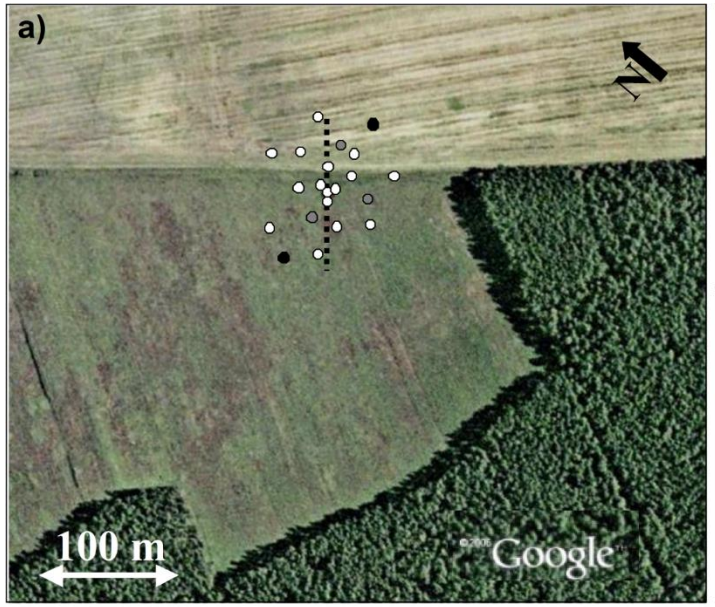

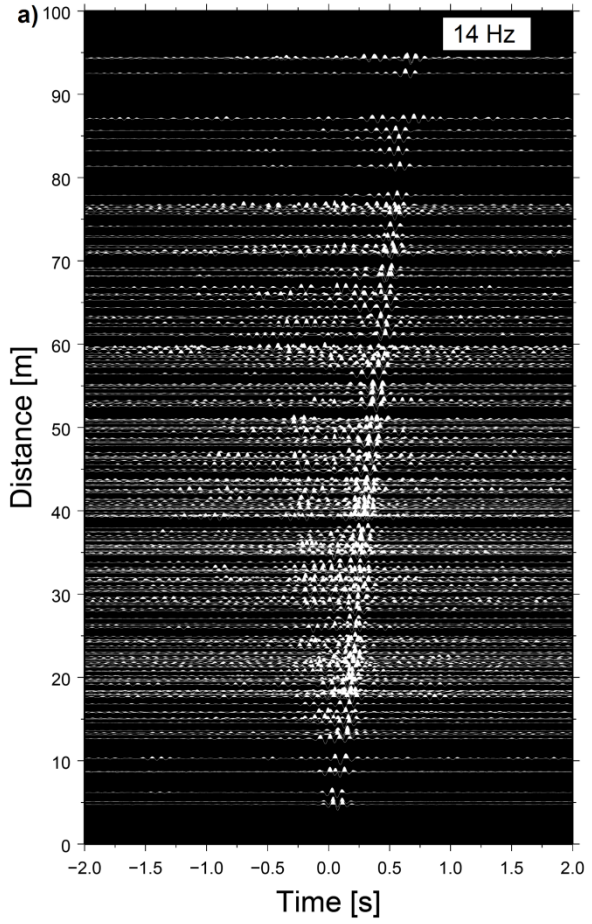

Picozzi et al (2009).

Proposed method

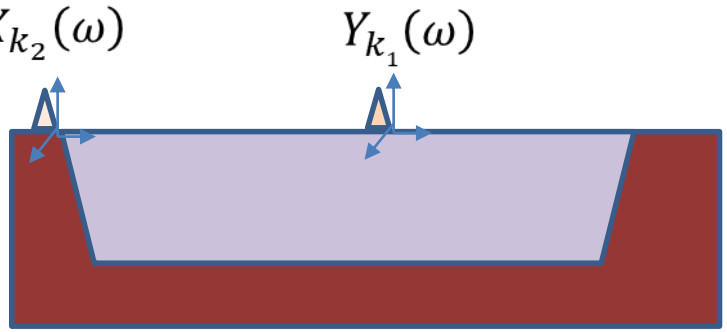

$$Y_Z(\omega) = X_Z(\omega)H_{ZZ}(\omega) + X_L(\omega)H_{LZ}(\omega) + X_T(\omega)H_{TZ}(\omega)$$

$$Y_L(\omega) = X_Z(\omega)H_{ZL}(\omega) + X_L(\omega)H_{LL}(\omega) + X_T(\omega)H_{TL}(\omega)$$

$$Y_T(\omega) = X_Z(\omega)H_{ZT}(\omega) + X_L(\omega)H_{LT}(\omega) + X_T(\omega)H_{TT}(\omega)$$

Z= Vertical
T= Transverse
L= Longitudinal

Data **d** and **A** elements

$$S_{k_1,k_2}(\omega) = W_\varepsilon(\omega)\frac{Y_{k_1}(\omega)}{X_{k_2}(\omega)}$$

$$W_\varepsilon(\omega) = \frac{|X_{k_2}(\omega)|^2}{|X_{k_2}(\omega)|^2 + \varepsilon}$$

$$\frac{Y_Z(\omega)}{X_Z(\omega)} = H_{ZZ}(\omega) + \frac{X_L(\omega)}{X_Z(\omega)}H_{LZ}(\omega) + \frac{X_T(\omega)}{X_Z(\omega)}H_{TZ}(\omega)$$

$$\frac{Y_Z(\omega)}{X_L(\omega)} = \frac{X_Z(\omega)}{X_L(\omega)}H_{ZZ}(\omega) + H_{LZ}(\omega) + \frac{X_T(\omega)}{X_L(\omega)}H_{TZ}(\omega)$$

$$\frac{Y_Z(\omega)}{X_T(\omega)} = \frac{X_Z(\omega)}{X_T(\omega)}H_{ZZ}(\omega) + \frac{X_L(\omega)}{X_T(\omega)}H_{LZ}(\omega) + H_{TZ}(\omega)$$

.....

.....

.....

.....

.....

$$\frac{Y_T(\omega)}{X_T(\omega)} = \frac{X_Z(\omega)}{X_T(\omega)}H_{ZT}(\omega) + \frac{X_L(\omega)}{X_T(\omega)}H_{LT}(\omega) + H_{TT}(\omega)$$

$$\mathbf{d} = \mathbf{A}\mathbf{x}$$

Solution via Gauss-Jordan algorithm with elimination

Parolai et al (2022),

Example: the Sarca Valley

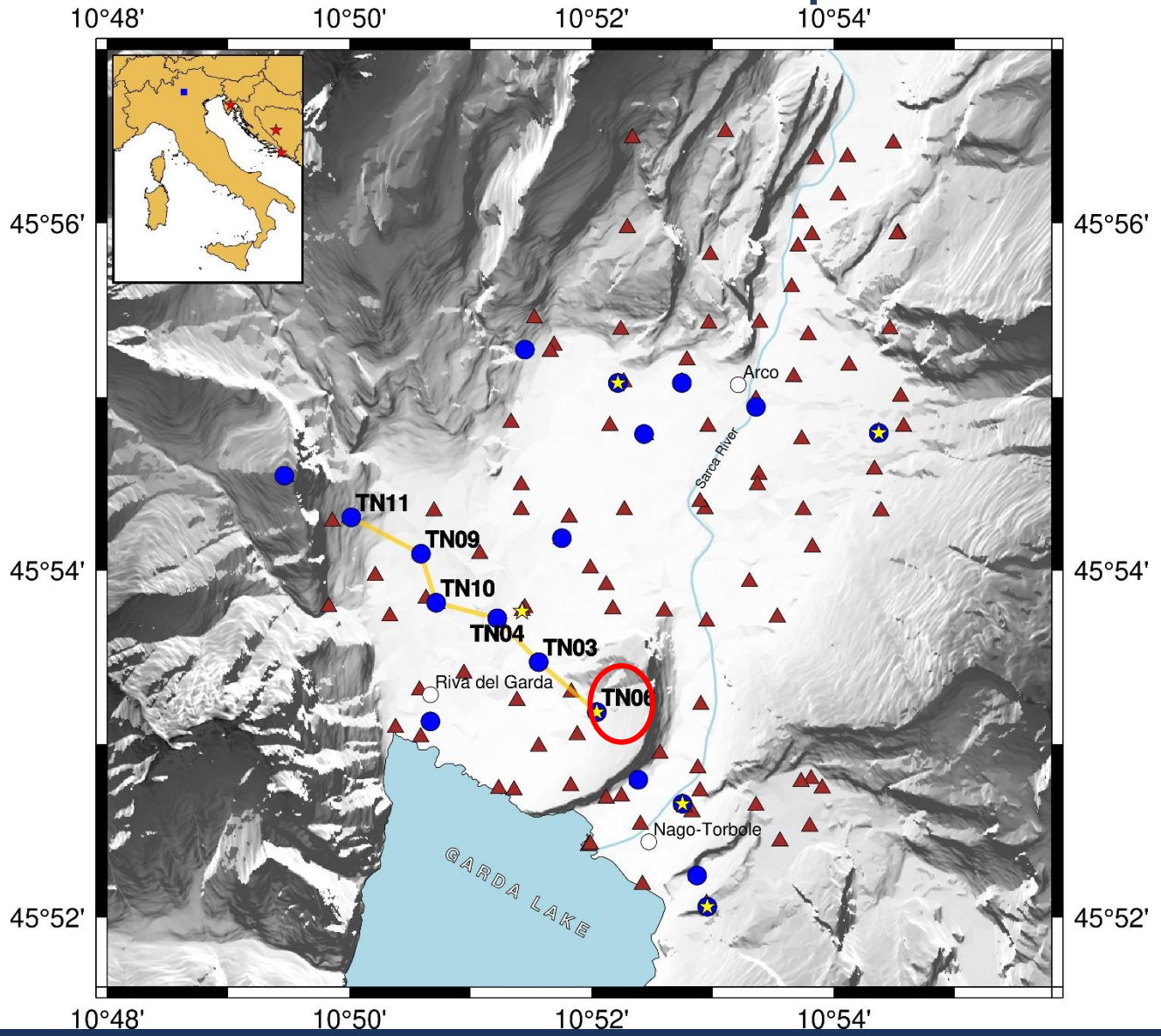

Installation of a temporary seismic network (blue circles)

110 single station noise measurements

Station TN06 selected as reference for the analyzed profile (yellow line)

Paoletti et al (2022), submitted

OGS

UNIVERSITÀ DEGLI STUDI DI TRIESTE

Example: the Sarca Valley

Noise sources distribution

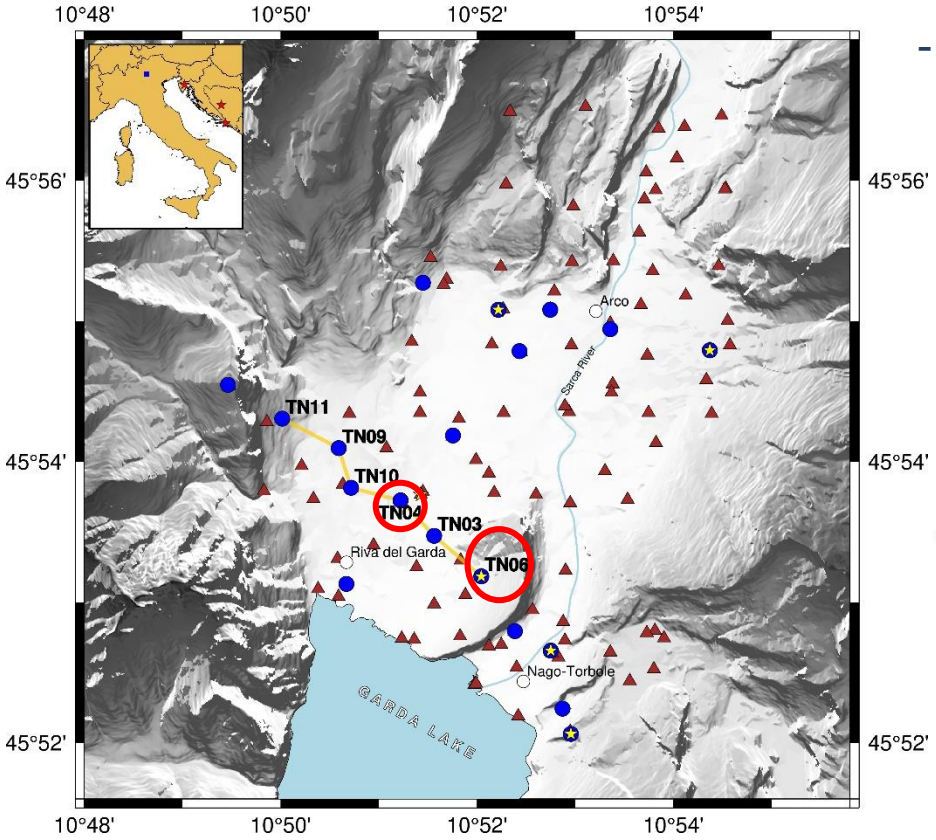

- Low-pass filtering (zero phase) with with corner frequency of 1 Hz
- Stacking of one hundred 60-second windows of the horizontal component after rotation for different azimuths

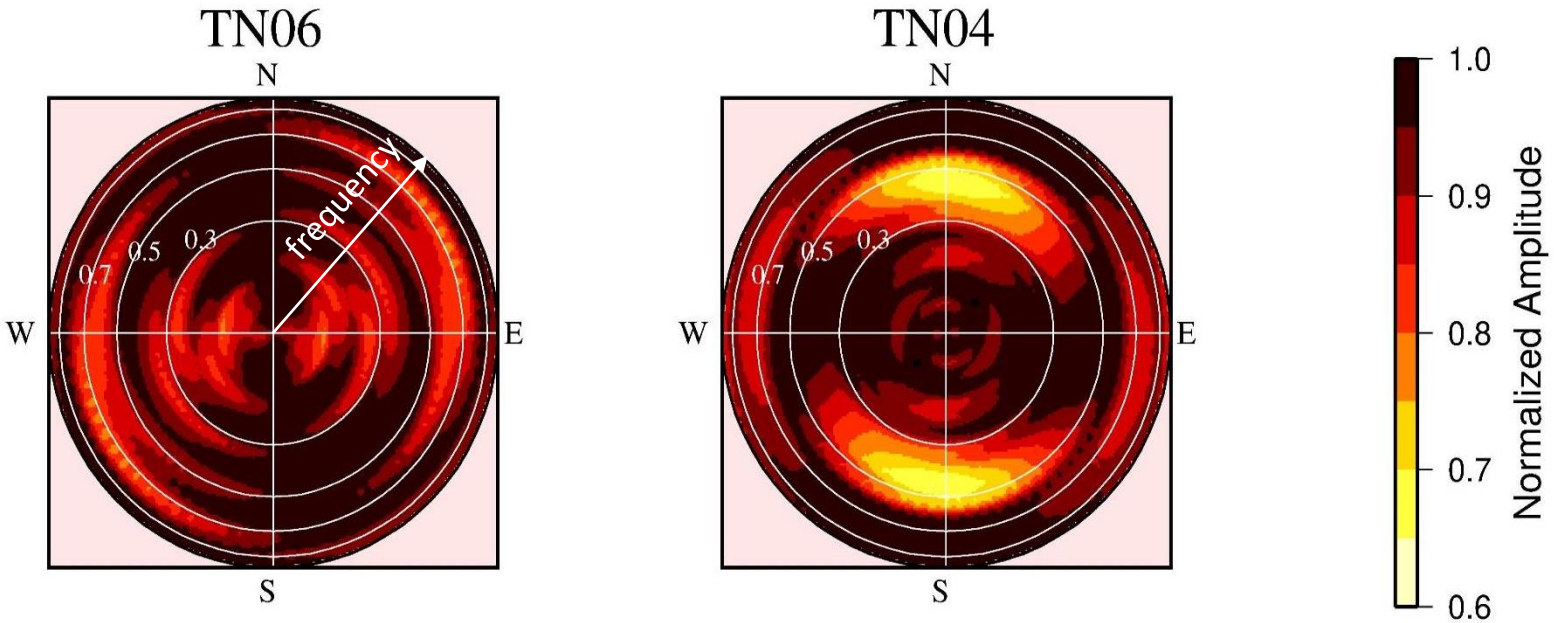

Parolai et al (2022)

Example: the Sarca Valley

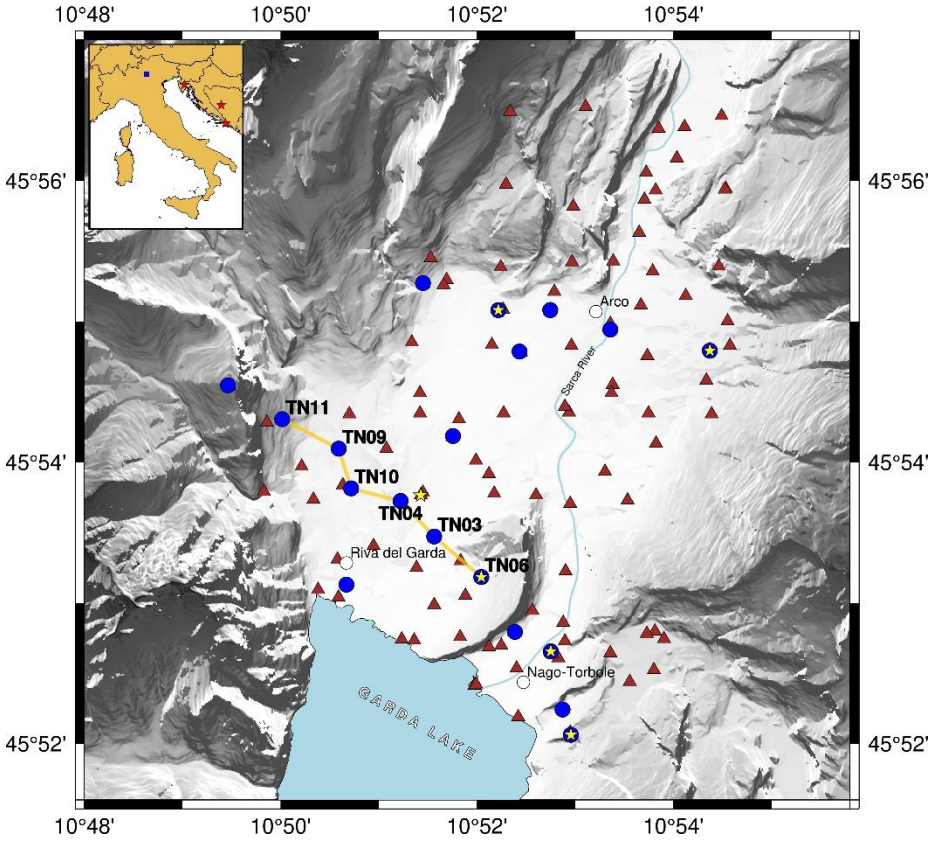

Frequency-responses in the time domain

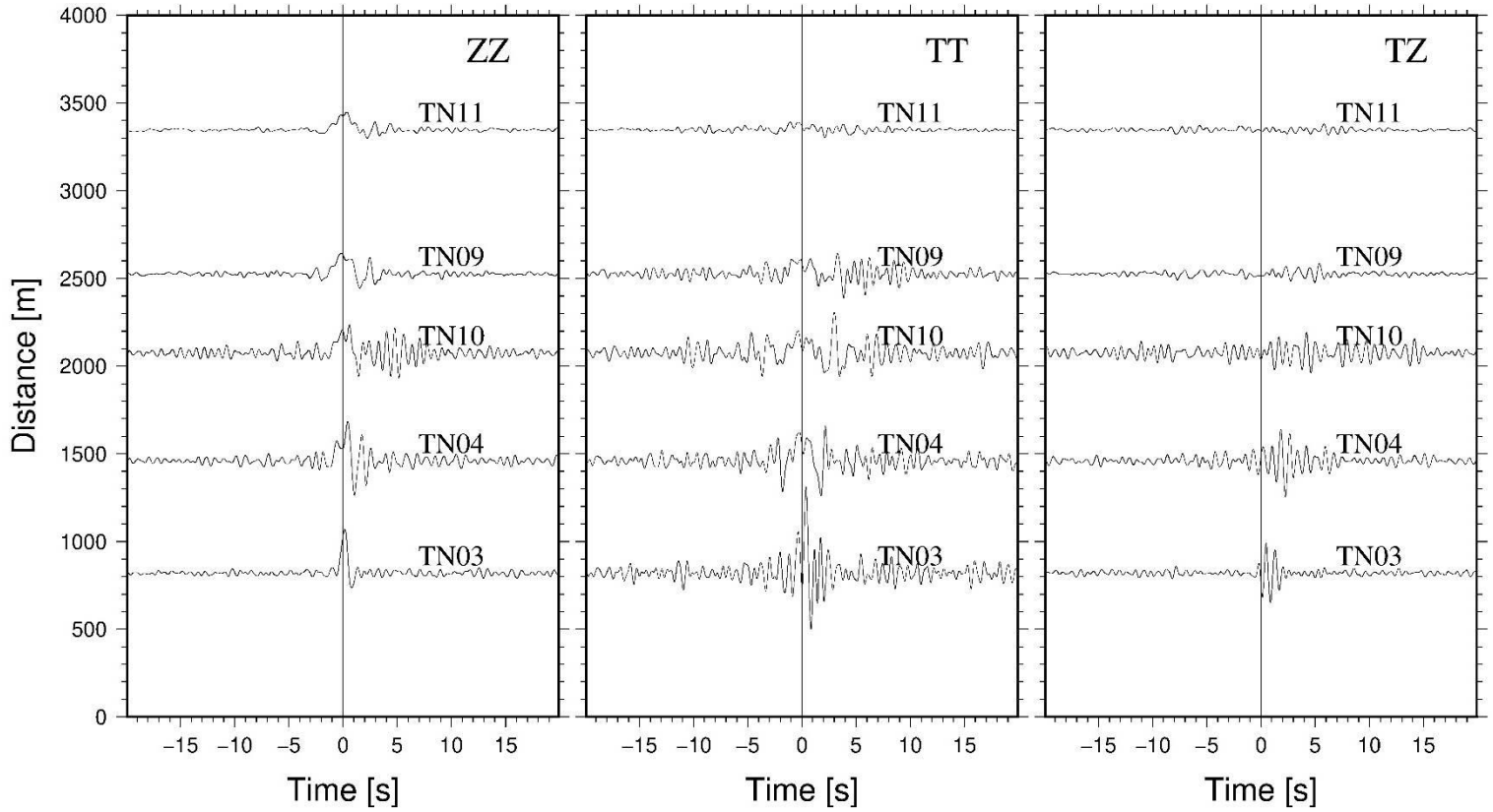

Parolai et al (2022)

Example: the Sarca Valley

Frequency-responses in the time domain: TN04

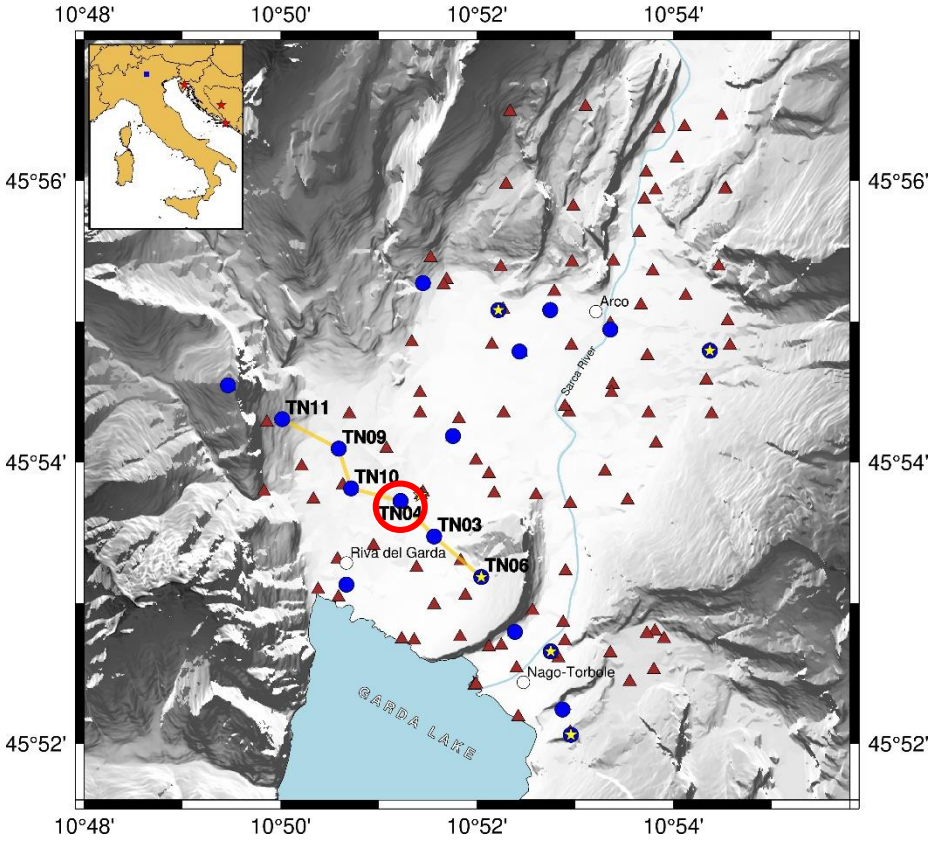

Parolai et al (2022)

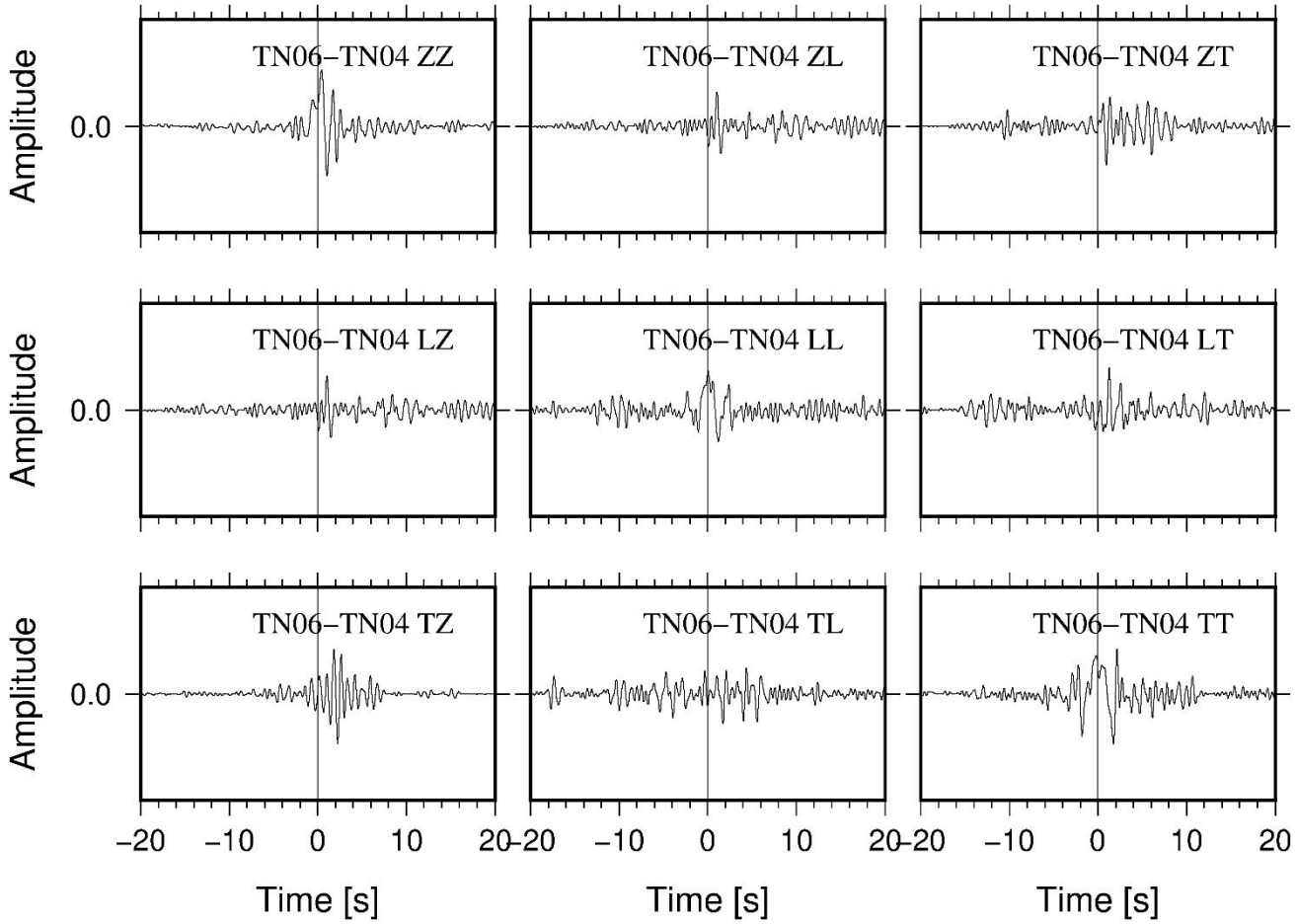

Example: the Sarca Valley

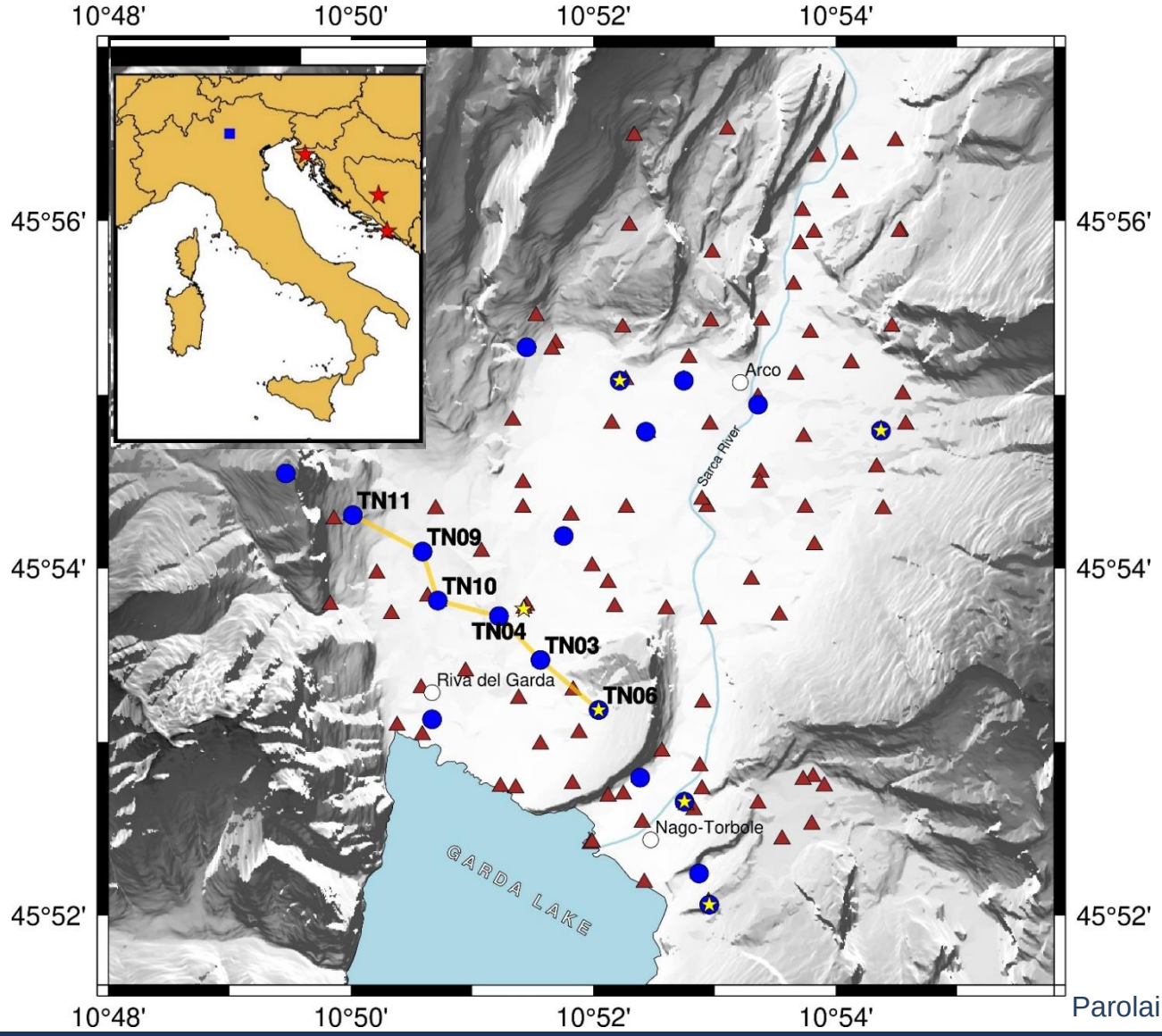

Comparison

Earthquake M=4.7 02/11/2019 14:11:33 Bosnia

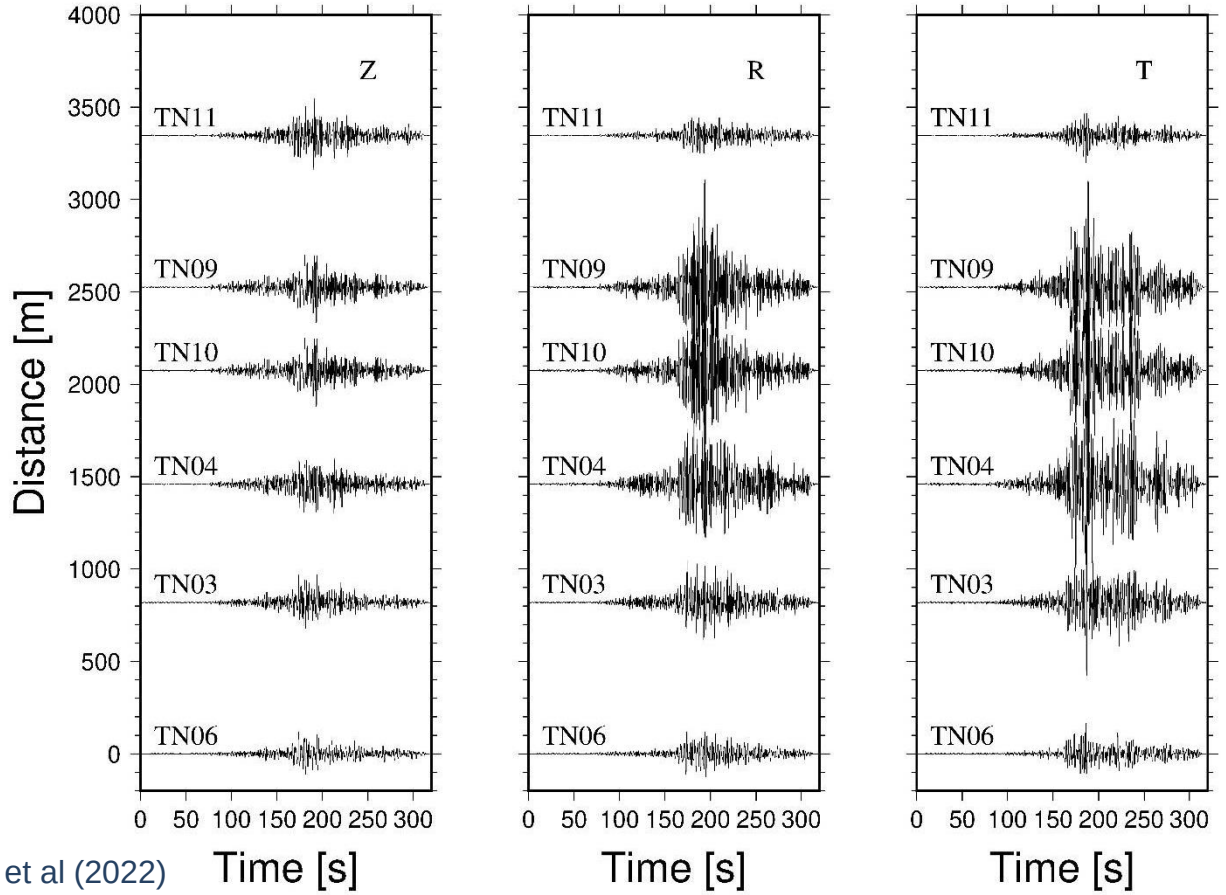

Parolai et al (2022)

Example: the Sarca Valley

Comparison

Earthquake | Noise | Earthquake | Noise

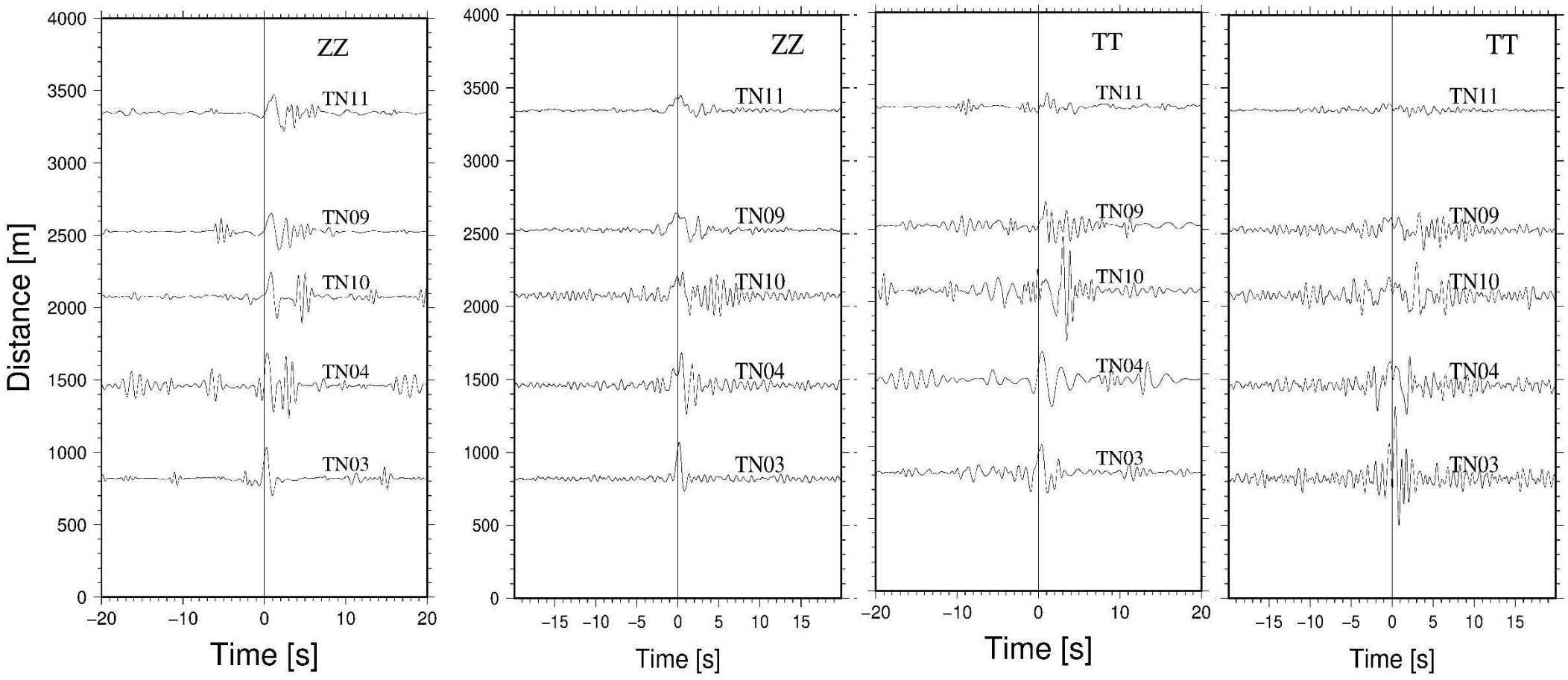

Paglai et al (2022) submitted

Example: the Sarca Valley

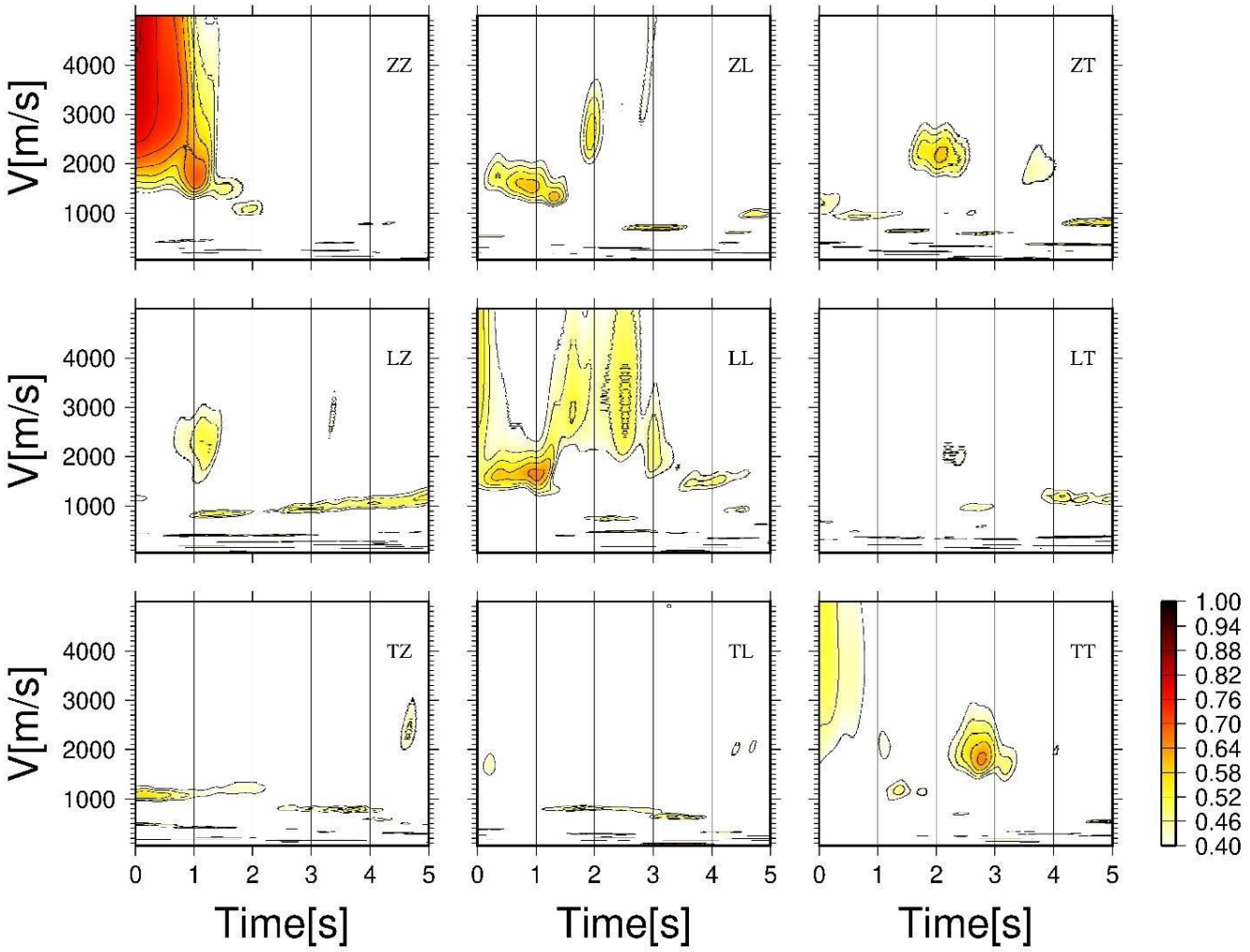

Semblance

$$S_T = \sum_{t=t_0}^{t_0+m\Delta} \left(\sum_{i=1}^{N} g_{ti} \right)^2 / N \left[\sum_{t=t_0}^{t_0+m\Delta} \sum_{i=1}^{N} (g_{ti})^2 \right].$$

gti= trace

N= number of traces

Reference station TN03

Parolai et al (2022)

Example: the Sarca Valley

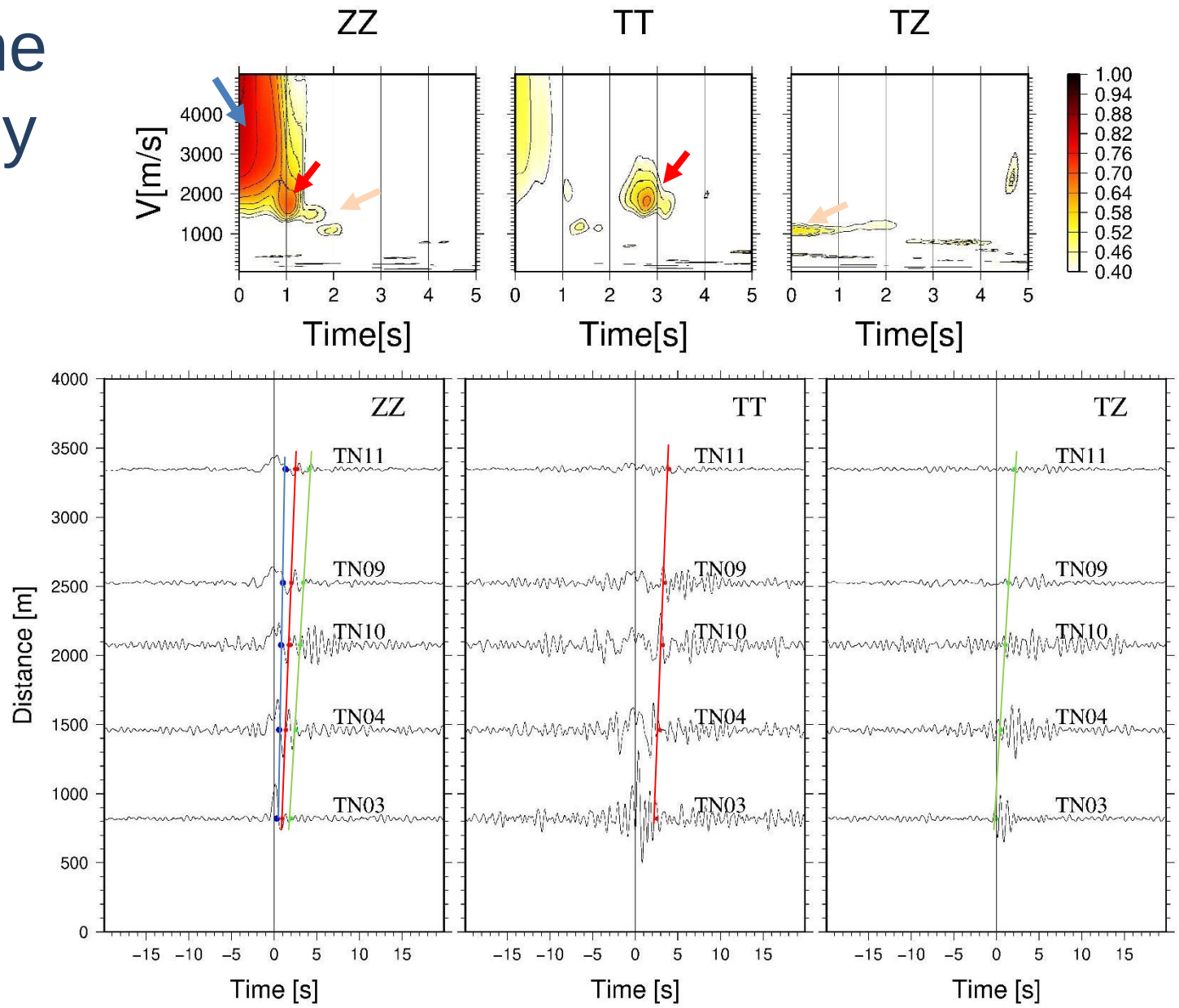

Parolai et al (2022)

Example: the Sarca Valley

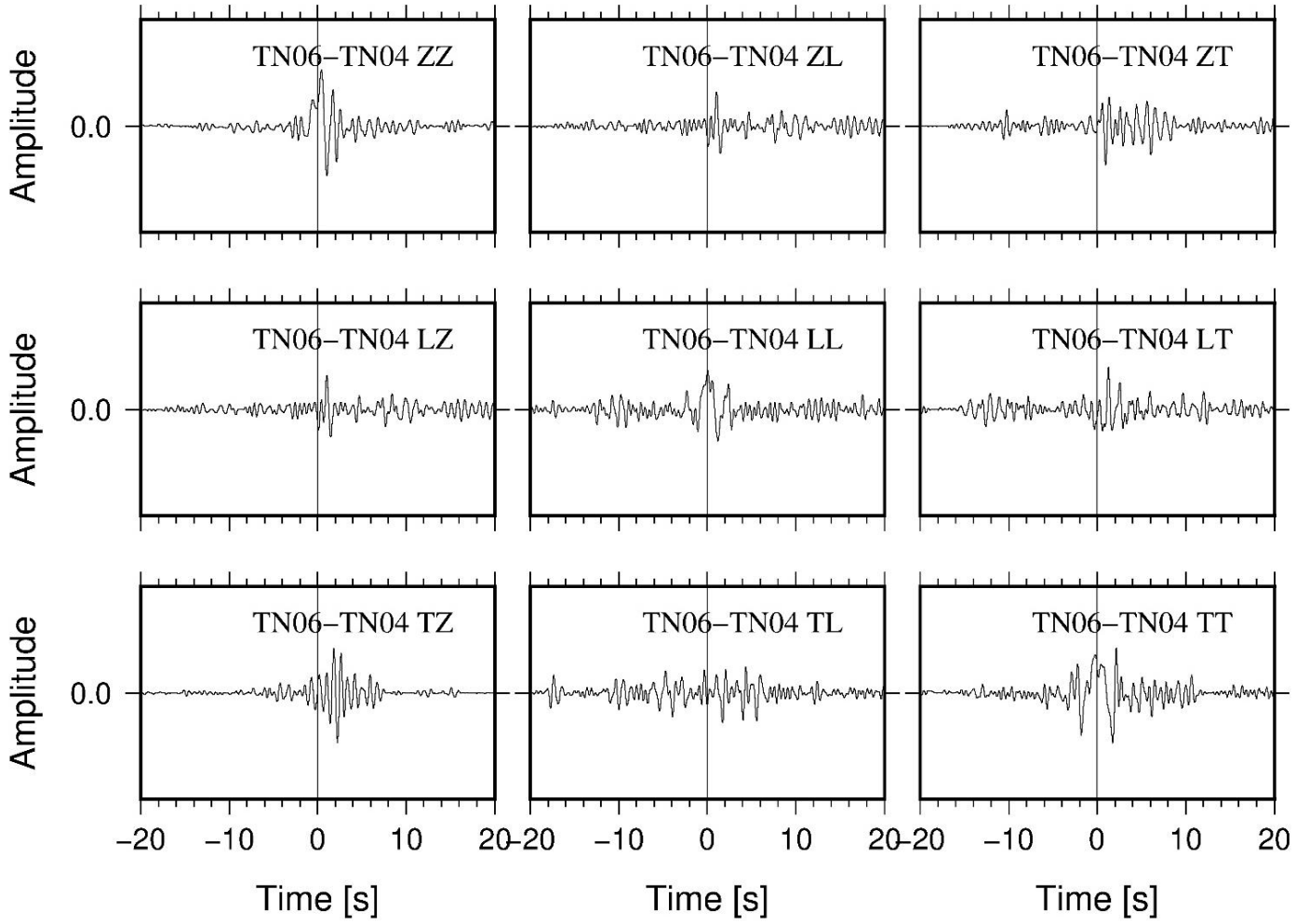

The total input energy for a **vertical** ground motion input will be distributed for **38.4%**, **27.3%**, and **34.3%** in the **ZZ**, **ZL**, and **ZT**

The total input energy for a **radial** ground motion input will be distributed for **44.5%**, **13.2%**, and **42.3%** in the **LL**, **LZ**, and **LT**

The total input energy for a transverse ground motion input will be distributed for **44%**, **23.8%**, and **32.2%** in the **TT**, **TZ**, and **TL**

Parolai et al (2022)

Seismic and strong motion networks

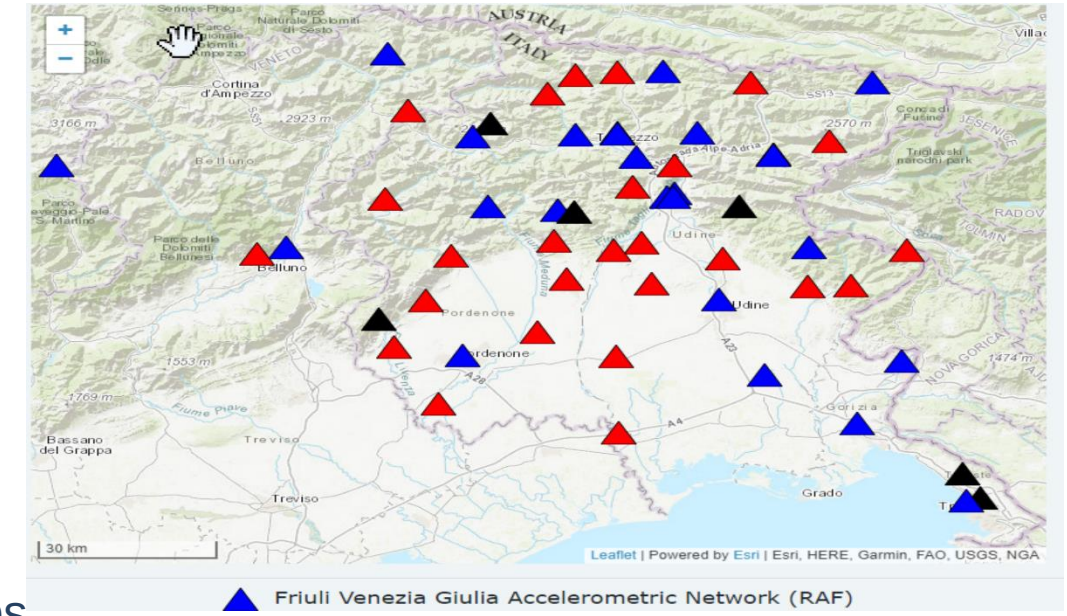

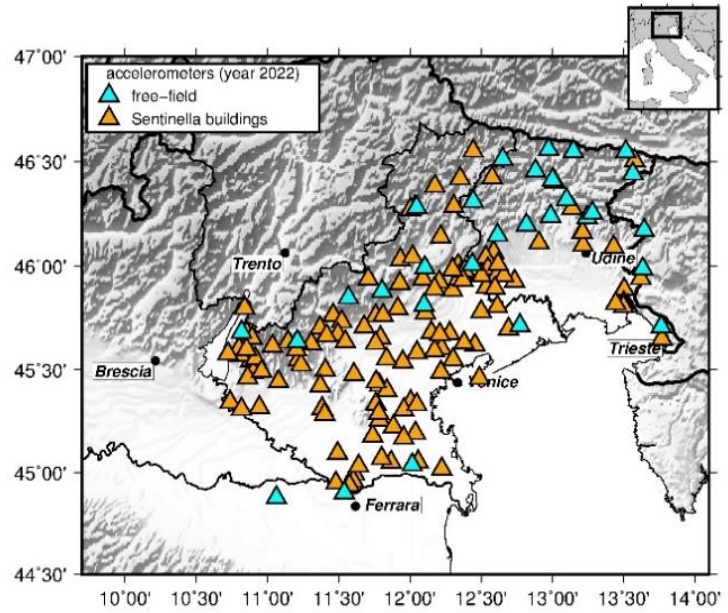

Shakemaps

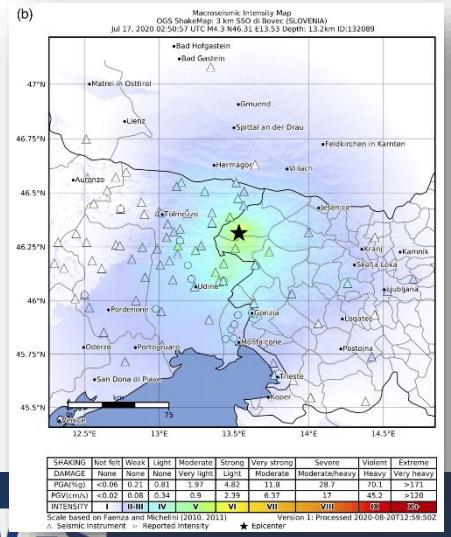

Impact assessment

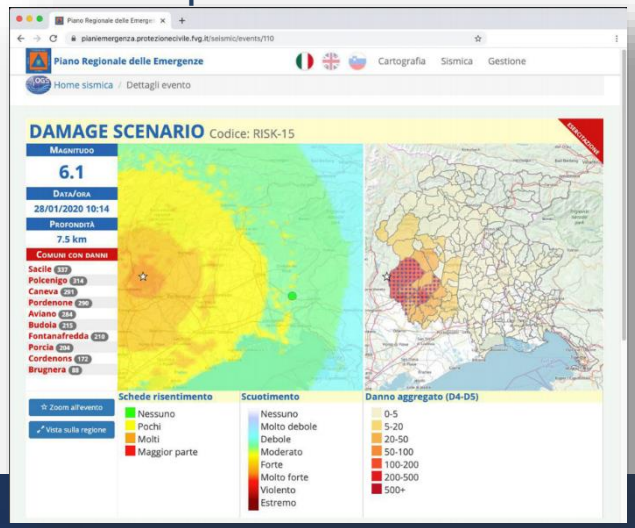

Numerical simulations